

December, 2019

Phenomenology of SMEFT Flavor Changing Operators

Daiki Ueda

*The Graduate University for Advanced Studies, SOKENDAI, Tsukuba, Ibaraki 305-0801,
Japan.*

*Ph.D thesis submitted to
Department of Particle and Nuclear Physics, The Graduate University for Advanced
Studies, SOKENDAI
December 2019*

Phenomenology of SMEFT Flavor Changing Operators

Daiki Ueda

*Department of Particle and Nuclear Physics
The Graduate University for Advanced Studies, SOKENDAI*

A thesis submitted for the degree of Doctor of Philosophy in 2019

Abstract

We establish a systematic way to estimate flavor and CP violating observables within the Standard Model Effective Field Theory (SMEFT), which describes high energy phenomena beyond the electroweak symmetry breaking (EWSB) scale. Based on the established SMEFT approach, we investigate the SMEFT effects on low-scale observables such as $\Delta F = 2$ observables and nucleon electric dipole moments (EDMs). For that purpose, we provide one-loop matching formulae at the EWSB scale for $\Delta F = 2$ transitions, and discuss $\Delta F = 2$ observables of down-type quark within the framework of the SMEFT. In addition, we study new physics (NP) contributions to the nucleon EDMs in the SMEFT. Similar to the case for $\Delta F = 2$, we provide the one-loop formulae for $\Delta F = 0$ transitions relevant for the nucleon EDMs and discuss correlations of these effects with $\Delta F = 2$ observables such as ϵ_K and ΔM_{B_d} . As the result, we conclude that the SMEFT approach is quantitatively and qualitatively essential to evaluate the NP effects on the low-scale observables when the NP scale is much higher than the EWSB one.

Contents

1	Introduction	1
1.1	Overview	1
1.2	Organization of this thesis	4
2	An Introduction to SMEFT Operator	5
2.1	The Standard Model	5
2.2	The Standard Model Effective Field Theory	8
2.3	Relevant operator in $\Delta F = 2$ and 0 process	10
3	Matching Formula	13
3.1	Introduction of one-loop matching formula	13
3.2	Formula for $\Delta F = 2$ process	14
3.3	Formula for $\Delta F = 0$ process	17
3.4	Discussions	18
3.5	Conclusion of matching formula	18
4	Observables	19
4.1	ϵ_K	19
4.2	ΔM_{B_d}	20
4.3	Nucleon EDMs	20
4.4	Flavor changing observable in Z mediated correction	21
4.4.1	ϵ'/ϵ_K	21
4.4.2	$K \rightarrow \pi\nu\bar{\nu}$	22
4.4.3	$K_L \rightarrow \mu^+\mu^-$	23
4.4.4	$K_S \rightarrow \mu^+\mu^-$	24
5	SMEFT top-quark effects on $\Delta F = 2$ observables	27
5.1	Scale Uncertainty	27
5.2	Scale Uncertainty in General Model	29
5.3	Scale Uncertainty in the Left-Right Symmetric Models	30
5.3.1	Left-Right Symmetric Models	30
5.3.2	Matching Scale Uncertainty	34
5.4	Conclusion of Matching Scale Uncertainty	39

6	<i>Z</i> mediated correction to flavor changing observable	41
6.1	<i>Z</i> mediated SMEFT correction	41
6.2	SMEFT correction in general <i>Z</i> model	42
6.3	<i>Z</i> mediated correction in the Minimal Supersymmetric Standard Model	43
6.3.1	MSSM	44
6.3.2	<i>Z</i> mediated SUSY corrections	48
6.4	Conclusion of <i>Z</i> mediated correction to $\Delta F = 2$ observable	53
7	Nucleon EDM from SMEFT flavor-changing operator	55
7.1	Flavor conserving process by flavor changing operators	55
7.2	Numerical analysis of EDM	56
7.3	Conclusion of nucleon EDM from SMEFT flavor-changing operator	59
8	Conclusion	63
A	Quantum Corrections	67
A.1	Renormalization group equations of SMEFT	67
A.2	QCD RGEs for EDMs	70
B	Left-right symmetric models	73
B.1	Higgs sector in left-right symmetric models	73
B.2	Loop functions	75
C	Double penguin contributions	79
D	$b \rightarrow d\gamma$ and $b \rightarrow s\gamma$	85
E	Vacuum stability	87
F	Neutron and proton EDM with chiral Lagrangian technique	91

List of Figures

3.1	Feynman diagrams for the one-loop matchings onto the $\Delta F = 2$ operators ($i \neq j$).	15
5.1	For $(C_{qd}^{(8)})_{1113}$ and $(C_{qd}^{(8)})_{1213}$, $(C_4)_{ij}(M_W)$ are shown.	31
5.2	For $(C_{qd}^{(8)})_{1313}$ and $(C_{qd}^{(8)})_{2313}$, $(C_4)_{ij}(M_W)$ are shown.	32
5.3	For $(C_{qd}^{(8)})_{3313}$ and $(C_{ud}^{(8)})_{3313}$, $(C_4)_{ij}(M_W)$ are shown.	33
5.4	Schematic figure for the SMEFT framework in the left-right symmetric model.	35
5.5	$C_4(M_{W_L})$ and $C_5(M_{W_L})$ for ΔM_{B_s} in comparison with the conventional results.	37
5.6	ΔM_{B_s} in comparison with the conventional results at $\mu = M_{W_R}$ and m_t .	38
6.1	The correlations of observables through the Z boson in $(C_{Hq}^{(1)})_{12}$ and $(C_{Hq}^{(3)})_{12}$.	44
6.2	The correlations of observables through the Z boson in $(C_{Hd})_{12}$.	45
6.3	Feynman diagrams relevant for the matchings onto the operators $(O_{Hd})_{12}$.	49
6.4	Contour plots of ϵ_K on the $M_{\text{SUSY}} - T_D$ plane.	50
6.5	Correlations between ϵ_K , ϵ'/ϵ_K , $\mathcal{B}(K \rightarrow \pi\nu\bar{\nu})$ and $\mathcal{B}(\bar{B} \rightarrow X_{d,s}\gamma)$.	51
6.6	The maximal gluino contributions to ϵ'/ϵ_K , as a function of $m_{\tilde{Q}}$.	53
7.1	The neutron and proton EDMs for the SMEFT $\Delta F = 1$ operators.	57
7.2	Contours of the EDMs and ϵ_K and ΔM_{B_d} for $(C_{qd}^{(1)})$.	58
7.3	For $C_{qd}^{(8)}$, which is same as Fig. 7.2.	59
7.4	For $C_{qd}^{(1)}$, which is same as Fig. 7.2.	60
7.5	For $C_{ud}^{(1)}$, which is same as Fig. 7.2.	61
7.6	For $C_{ud}^{(8)}$, which is same as Fig. 7.2.	61
C.1	The one-loop contribution to $\Delta F = 2$ operators at the NP scale.	81
E.1	The upper bound on $ (T_D)_{i3} $ for $i = 1, 2$ from the vacuum stability condition.	88
E.2	The vacuum stability condition of $ (T_D)_{i3} $ for $i = 1, 2$ as a function of m_A .	89

1.1 Overview

The standard model (SM) of the particle physics is a theory which describes nature very well. In 2012, the last missing piece of the SM, the Higgs boson was observed by the Large Hadron Collider (LHC) experiments [1, 2]. This great discovery was a culmination of the success of the SM. However, some unsolved problems, such as the hierarchy problem and an identity of the dark matter are remained in the SM. Thus, the discovery is also a beginning of searching for new physics (NP).

Without a fine-tuning between the observed Higgs mass and the bare mass of the Higgs boson, a mass of NP particle coupling to the Higgs boson is implied as $\sim 100 \text{ GeV} - 1 \text{ TeV}$. In addition, if weakly interacting massive particles (WIMPs) dominate a energy density of cold non-baryonic matter in the universe, $\Omega h^2 \simeq 0.1 (\langle\sigma v\rangle/10^{-26} \text{ cm}^2/\text{s})^{-1}$ [3], it is expected that the mass of the WIMPs is around $\sim 100 \text{ GeV} - 1 \text{ TeV}$. In particular, these unsolved problems indicate that the NP scale is not far from the electroweak symmetry breaking (EWSB) scale and give us a guideline for the energy scale at which the human race must aim.

However, by the LHC experiment, the NP particles with a few TeV mass have not been detected yet [4]. At this stage, the experimental facts indicate that the NP consists either very weakly coupled particles or heavy ones well above the EWSB scale. In particular, in the second scenario which we focus in this thesis, indirect searches for the NP become important, because FCNCs and CP violating observables are sensitive to physics at the high energy scale. Many observable quantities in the flavor-changing processes are precisely determined in both of theoretical calculations and experimental data. In the near future, the precisions in the flavor experiments will be further improved, and theoretical precise calculations become more important [5, 6]. Besides, in the flavor-conserving processes, several experiments are proposed to measure nucleon EDMs, whose sensitivities would be improved by 2 – 3 orders of magnitudes in near future [7–9]. Although EDMs are flavor-conserving processes, they have a sensitivity to flavor violations through the W -boson interactions. Thus, NP effects on quark flavor-changing neutral currents can contribute to quark EDMs simultaneously by exchanging the W boson.

Since the EDMs are very sensitive to NP, they can also probe flavor-changing contributions to NP.

In conventional evaluations of CP and flavor violating observables, heavy degree of freedom, such as NP particles and the heavy SM particles including the top quark and the EW gauge boson (W, Z, H), are simultaneously decoupled. Then, the NP model is matched onto the low energy effective field theory (LEFT), which is described by the light SM particles without the top quark and EW gauge boson. For example, the kaon $\Delta S = 2$ observables are described by following effective Hamiltonian only including the down and strange quarks:

$$\begin{aligned}
 \mathcal{H}_{\text{eff}}^{\Delta S=2} = & (C_1)_{12}(\bar{d}\gamma^\mu P_L s)(\bar{d}\gamma_\mu P_L s) \\
 & + (C_2)_{12}(\bar{d}P_L s)(\bar{d}P_L s) + (C_3)_{12}(\bar{d}^\alpha P_L s^\beta)(\bar{d}^\beta P_L s^\alpha) \\
 & + (C_4)_{12}(\bar{d}P_L s)(\bar{d}P_R s) + (C_5)_{12}(\bar{d}^\alpha P_L s^\beta)(\bar{d}^\beta P_R s^\alpha) \\
 & + (C'_1)_{12}(\bar{d}\gamma^\mu P_R s)(\bar{d}\gamma_\mu P_R s) \\
 & + (C'_2)_{12}(\bar{d}P_R s)(\bar{d}P_R s) + (C'_3)_{12}(\bar{d}^\alpha P_R s^\beta)(\bar{d}^\beta P_R s^\alpha), \tag{1.1}
 \end{aligned}$$

where α, β are color indices. The LEFT are eventually compared with experimental data. However, in the current perspective, this procedure for the evaluations of the CP and flavor violating observables is broken down. A class of the NP models where both of NP and SM particles appear simultaneously in a loop diagram, makes this point clear. As mentioned before, the NP particles are likely to be much heavier than the SM ones. When there is a large mass hierarchy among the particles in a loop diagram, higher order corrections of the perturbation cannot be negligible. Then, corrections of the dynamical top quark to the low-scale effective operators can be relevant, because the top quark has a large Yukawa coupling and mass. In particular, in the conventional evaluations, it is not clear that “in which energy scale the top quark mass (or the top Yukawa coupling) is evaluated.” We call this problem as “matching scale uncertainty” in this thesis. In addition, since the LEFT does not include the W boson as a dynamical degree of freedom, it is difficult to analyze correlations between observables with the FCNC observables and the EDMs through a model independent way. In evaluation of CP and flavor violating observables, integrating out both of NP and SM particles is no longer appropriate because of the much high NP scale, and the conventional evaluations based on the LEFT must be improved by an instead effective field theory in which the heavy SM degree of freedoms are retained.

The Standard Model Effective Field Theory (SMEFT) [10–12] is one of the candidates for the effective field theory above the EWSB scale. In the SMEFT, the higher dimensional operators are invariant under the SM gauge symmetries, $SU(3)_C \times SU(2)_L \times U(1)_Y$, and all the SM particles, particularly the electroweak bosons (W, Z, H) and the top quark (t), are dynamical degrees of freedom. The NP diagrams are matched onto the SMEFT, and the renormalization group

equations (RGEs) in the SMEFT [13–15] are solved. At the EWSB scale, the SMEFT are also matched onto the LEFT. By this procedure, we can escape the matching scale uncertainty. In addition, we can analyze the correlations between the FCNC observables and the EDMs without specifying a NP model because of the dynamical W boson in the SMEFT. In the SMEFT procedure, the NP contributions are encoded at the NP scale, and evaluated at the EWSB scale by solving the SMEFT RGEs. Concerning the Yukawa, gauge couplings and so on, the anomalous dimensions of the SMEFT dimension six operators have already been calculated at the one-loop level. On the other hand, the matching at the EWSB scale had not been calculated at the one-loop level, which is needed to analyze the NP effects with the same order perturbation calculations^{#1}. In Chapter 5, the effects of one-loop matching formulae are also discussed qualitatively.

Stimulated by the current situation in the evaluations of the low-scale observables, in this thesis, we provide the one-loop matching formulae relevant to the low-scale $\Delta F = 2$ and 0 operators with the top Yukawa couplings, and we establish a systematic way to estimate flavor and CP violating observables in the SMEFT, which are based on the works by the author [16, 17]. By using the one-loop matching formulae and solving the RGEs in the SMEFT, we investigate whether the SMEFT effects are negligible or not. In the $\Delta F = 2$ processes, we discuss the scale uncertainty, which is reduced by the one-loop matching formulae and the SMEFT RGEs. In addition, the one-loop matching formulae mediated by the Z boson contributes to $\Delta F = 1$ processes, such as $K \rightarrow \pi\nu\bar{\nu}$ which is theoretical clean and sensitive to physics at high energy scale. By using our matching formulae including the Z mediated corrections, we discuss correlations between the $\Delta F = 2$ observables and $\Delta F = 1$ ones with particular emphasis on the kaon system. We show that the constraint from ϵ_K is drastically changed by the right-handed NP contributions in the Z mediated corrections. Besides, through the one-loop matching formulae for $\Delta F = 0$ processes, the SMEFT $\Delta F = 1$ operators contribute to low-scale $\Delta F = 0$ observables, such as the nucleon electric dipole moments (EDM). We discuss the nucleon EDMs within the framework of the SMEFT.

By these investigations, it becomes clear that the SMEFT is essential to reduce the scale uncertainty, the right-handed NP effects are tightly constrained in the Z mediated SMEFT corrections, and the nucleon EDMs can provide an complementary information on the $\Delta F = 1$ effective operators in future. As a result, we will conclude that the SMEFT effects are quantitatively and qualitatively essential in evaluations of the NP contributions to the low-scale observables when the NP scale is much higher than the EWSB one.

^{#1}A part of the one-loop matching formula is shown in Ref. [18]. We found that its result is inadequate because the left-handed top quark contributions are missing, and thus, inconsistent with the SMEFT RGEs [19]. In addition, the logarithmic scale dependence in Eqs. (4.24)-(4.26) of the journal version of Ref. [18] is inconsistent with that from the RGEs, which are fixed in our result, Eqs. (3.16)-(3.18). The formula related to the SMEFT quark-Higgs operators are given in Ref. [20] (see also Ref. [21]); the result is included in this paper.

1.2 Organization of this thesis

This thesis is organized as following.

In Chapter 2, we briefly review the SM and the standard model effective field theory (SMEFT). In Section 2.1, in order to clarify an importance of indirect search of the NP, we discuss flavor and CP violating effects in the SM. In Section 2.2, we briefly review the SMEFT and we summarize the dimension-six operators in the SMEFT. In Section 2.3, we summarize the flavor changing operators in the SMEFT relevant to $\Delta F = 2$ and 0 processes at the one-loop level.

In Chapter 3, we provide tree and one-loop matching formulae for the SMEFT $\Delta F = 1$ operators, which contribute to the $\Delta F = 0$ and 2 processes in a low scale. In Section 3.2, we provide matching formulae contributing to the $\Delta F = 2$ operators in the LEFT. Besides, in Section 3.3, we provide matching formulae for the $\Delta F = 0$ process. In Section 3.4, we discuss that the SMEFT $\Delta F = 1$ operators are mainly divided into two type, and we summarize relations between the each operator and observables. Section 3.5 are devoted to the conclusion in this chapter.

In Chapter 4, we briefly summarize $\Delta F = 0, 1$ and 2 observables, which are used in this thesis. Section 4.1 is devoted to the indirect CP violation in $K^0 - \bar{K}^0$ oscillation, Section 4.2 the mass difference in B_d meson, Section 4.3 the nucleon EDMs, Section 4.4.1 the direct CP violation of the $K \rightarrow \pi\pi$ decays, Section 4.4.2 the decay processes, $K^+ \rightarrow \pi^+\nu\bar{\nu}$ and $K_L \rightarrow \pi^0\nu\bar{\nu}$ and Section 4.4.3 the decay processes, $K_L \rightarrow \mu^+\mu^-$.

In Chapter 5, focusing on $\Delta F = 2$ observables, we study the SMEFT corrections above the EWSB scale, paying particular attention to the dynamical top quark. In Section 5.1, we explain the matching scale uncertainty in conventional evaluations and show our strategy for reducing the scale uncertainty. In Section 5.2, we numerically analyze the scale uncertainty by a model independent way. In Section 5.3, we focus on the left-right symmetric model and investigate the effects of the scale uncertainty. Section 5.4 are devoted to the conclusion in this chapter.

In Chapter 6, we evaluate the SMEFT correction to $\Delta F = 2$ observables, paying particular attention to the Z mediated corrections. In Section 6.1, we discuss the scenario, the Z mediated SMEFT corrections. In Section 6.2, we investigate the correlations between the $\Delta F = 2$ observables and the $\Delta F = 1$ ones by a model independent way. In Section 6.3, we focus on a gluino mediated penguin in the MSSM and investigate the effects of the Z mediated SMEFT corrections to the $\Delta F = 2$ observables. Section 6.4 is devoted to the conclusion in this chapter.

In Chapter 7, we study the SMEFT $\Delta F = 1$ operators effects on nucleon EDMs. In Section 7.1, we briefly explain the flavor conserving processes induced by the $\Delta F = 1$ SMEFT operators. In Section 7.2, we numerically analyze the nucleon EDMs by a model independent way within the framework of the SMEFT. Section 7.3 is devoted to the conclusion in this chapter.

Chapter 8 is devoted to the conclusion of this thesis.

An Introduction to SMEFT Operator

In this chapter, we review the standard model (SM) of particles physics and the standard model effective field theory (SMEFT) with particular emphasis on flavor changing operators. In Section 2.1, in order to clarify an importance of indirect searches of the NP, we discuss flavor and CP violating effects in the SM. In Section 2.2, we review the SMEFT operators. In Section 2.3, $\Delta F = 2$ and 0 SMEFT operators are summarized.

2.1 The Standard Model

The Standard Model (SM) of particle physics as the gauge theory consists of the electroweak (EW), and strong interactions, which has been tested for a long time. In the SM, the gauge group $SU(3)_C \times SU(2)_L \times U(1)_Y$ is imposed. The particle contents in the SM are listed in Table 2.1. The Lagrangian of the SM is given as

Table 2.1: Particle contents in the SM.

Component fields	Gauge quantum numbers		
	$SU(3)_C$	$SU(2)_L$	$U(1)_Y$
$\begin{pmatrix} u_{iL} \\ d_{iL} \end{pmatrix}$	3	2	1/6
u_{iR}	3	1	2/3
d_{iR}	3	1	-1/3
$\begin{pmatrix} \nu_{iL} \\ e_{iL} \end{pmatrix}$	1	2	-1/2
e_{iR}	1	1	-1
g_μ^X	8	1	0
W_μ^A	1	3	0
B_μ	1	1	0
$H = \begin{pmatrix} H^+ \\ H^0 \end{pmatrix}$	1	2	1/2

$$\mathcal{L}_{\text{SM}} = -\frac{1}{4}G_{\mu\nu}^A G^{A\mu\nu} - \frac{1}{4}W_{\mu\nu}^I W^{I\mu\nu} - \frac{1}{4}B_{\mu\nu} B^{\mu\nu} \\ + (D_\mu H)^\dagger (D^\mu H) + m^2 H^\dagger H - \frac{1}{2}\lambda(H^\dagger H)^2$$

$$+ i (\bar{l}\gamma^\mu D_\mu l + \bar{e}\gamma^\mu D_\mu e + \bar{q}\gamma^\mu D_\mu q + \bar{u}\gamma^\mu D_\mu u + \bar{d}\gamma^\mu D_\mu d) - (\bar{l}Y_e e H + \bar{q}Y_u u \tilde{H} + \bar{q}Y_d d H + \text{h.c.}), \quad (2.1)$$

where l , q and H are the left-handed lepton, quark and Higgs $SU(2)_L$ doublets, respectively, while the right-handed lepton and quark are denoted by e , u and d . Besides, $\tilde{H}^i = \epsilon_{ij}(H^j)^*$, where ϵ_{ij} is the totally antisymmetric tensor satisfying $\epsilon_{12} = +1$. Flavor indices i, j, k, l run 1, 2, 3. Covariant derivatives are defined as

$$D_\mu = \partial_\mu - ig_1 Y B_\mu - ig_2 \frac{\tau^a}{2} W_\mu^a - ig_s G_\mu^A T^A, \quad (2.2)$$

where Y is the hypercharge, τ^a are the Pauli matrices and $T^A = \lambda^A/2$ with the Gell-Mann matrices. The gauge field strength tensors are also defined as

$$G_{\mu\nu}^A = \partial_\mu G_\nu^A - \partial_\nu G_\mu^A + g_s f^{ABC} G_\mu^B G_\nu^C, \quad (2.3)$$

$$W_{\mu\nu}^I = \partial_\mu W_\nu^I - \partial_\nu W_\mu^I + g_2 \epsilon^{IJK} W_\mu^J W_\nu^K, \quad (2.4)$$

$$B_{\mu\nu} = \partial_\mu B_\nu - \partial_\nu B_\mu, \quad (2.5)$$

where f^{ABC} is the structure constant.

After the electroweak symmetry breaking, the Higgs doublet takes the vacuum expectation value (VEV) v . Because of the freedom of $SU(2)_L$ rotations, the Higgs doublet can be expressed as

$$H = \begin{pmatrix} G^+ \\ (v + h^0 + iG^0)/\sqrt{2} \end{pmatrix}. \quad (2.6)$$

Then, the mass of the SM Higgs and gauge bosons are obtained as

$$m_h^2 = \lambda v^2, \quad (2.7)$$

$$m_Z^2 = \frac{1}{4}(g_1^2 + g_2^2)v^2, \quad (2.8)$$

$$m_W^2 = \frac{1}{2}g_2^2 v^2. \quad (2.9)$$

Besides, the covariant derivative after the EWSB is obtained as

$$D_\mu = \partial_\mu - i \frac{g_2}{\sqrt{2}} (W_\mu^+ I_+ + W_\mu^- I_-) - ig_Z (I_3 - Q \sin^2 \theta_W) Z_\mu - ie Q A_\mu - ig_s G_\mu^A T^A, \quad (2.10)$$

where the charges, couplings and gauge bosons are defined as

$$I^a = \tau^a/2, \quad I_\pm = I_1 \pm iI_2, \quad (2.11)$$

$$Q = I_3 + Y, \quad (2.12)$$

$$g_Z = (g_1^2 + g_2^2)^{1/2} = g_2/\cos \theta_W = g_1/\sin \theta_W, \quad (2.13)$$

$$e = g_1 g_2 / g_Z = g_2 \sin \theta_W = g_1 \cos \theta_W, \quad (2.14)$$

$$Z_\mu = W_\mu^3 \cos \theta_W - B_\mu \sin \theta_W, \quad (2.15)$$

$$A_\mu = W_\mu^3 \sin \theta_W + B_\mu \cos \theta_W, \quad (2.16)$$

$$W_\mu^\pm = (W_\mu^1 \mp iW_\mu^2) / \sqrt{2}, \quad (2.17)$$

For convenience, we show the Pauli matrices:

$$\tau^1 = \begin{pmatrix} 0 & 1 \\ 1 & 0 \end{pmatrix}, \quad \tau^2 = \begin{pmatrix} 0 & -i \\ i & 0 \end{pmatrix}, \quad \tau^3 = \begin{pmatrix} 1 & 0 \\ 0 & -1 \end{pmatrix}. \quad (2.18)$$

The fermion field in the Lagrangian 2.1 are in the interaction eigenstates, where

$$q_1 = \begin{pmatrix} u_L \\ d'_L \end{pmatrix}, \quad q_2 = \begin{pmatrix} c_L \\ s'_L \end{pmatrix}, \quad q_3 = \begin{pmatrix} t_L \\ b'_L \end{pmatrix}, \quad l_1 = \begin{pmatrix} \nu_L^{e'} \\ e_L \end{pmatrix}, \quad l_2 = \begin{pmatrix} \nu_L^{\mu'} \\ \mu_L \end{pmatrix}, \quad l_3 = \begin{pmatrix} \nu_L^{\tau'} \\ \tau_L \end{pmatrix}, \quad (2.19)$$

$$\begin{pmatrix} d'_L \\ s'_L \\ b'_L \end{pmatrix} = V \begin{pmatrix} d_L \\ s_L \\ b_L \end{pmatrix}, \quad \begin{pmatrix} \nu_L^{e'} \\ \nu_L^{\mu'} \\ \nu_L^{\tau'} \end{pmatrix} = U_{\text{PMNS}} \begin{pmatrix} \nu_1 \\ \nu_2 \\ \nu_3 \end{pmatrix}. \quad (2.20)$$

Flavor changing interaction and GIM mechanism

Here, we focus on flavor changing interactions in the quark sector. In the SM, the flavor changing interactions in the Feynman-'t Hooft gauge are obtained as

$$\begin{aligned} \mathcal{L}_{\text{SM}} \supset & \frac{g_2}{\sqrt{2}} [(V^*)_{ij} \bar{d}_j \gamma^\mu P_L u_i W_\mu^- + V_{ij} \bar{u}_i \gamma^\mu P_L d_j W_\mu^+] \\ & + \frac{\sqrt{2}}{v} m_{u_i} [(V^*)_{ij} \bar{d}_j L u_i R G^- + V_{ij} \bar{u}_i R d_j L G^+] \\ & - \frac{\sqrt{2}}{v} m_{d_j} [(V^*)_{ij} \bar{d}_j R u_i L G^- + V_{ij} \bar{u}_i L d_j R G^+], \end{aligned} \quad (2.21)$$

where the quark fields are the mass eigenstates. V is the CKM matrix, which is experimentally determined unitary matrix [22]. In the Wolfenstein parametrization, the CKM matrix is expressed by

$$V = \begin{pmatrix} 1 - \frac{1}{2}\lambda^2 & \lambda & A\lambda^3(\rho - i\eta) \\ -\lambda & 1 - \frac{1}{2}\lambda^2 & A\lambda^2 \\ A\lambda^3(1 - \rho - i\eta) & -A\lambda^2 & 1 \end{pmatrix} + \mathcal{O}(\lambda^4), \quad (2.22)$$

where $\lambda \simeq 0.23$ is an expansion parameter and η corresponds to a CP violating phase. Focusing the matrix elements, it is clear that

$$V^\dagger V = 1, \quad (2.23)$$

$$\text{Im} V_{ci} \simeq 0, \quad \text{for } i = d, s, b, \quad (2.24)$$

$$|V_{td}| \ll |V_{ts}| \ll |V_{tb}|. \quad (2.25)$$

In particular, these properties are important to understand flavor changing processes. As the results of Eq. (2.23), the GIM mechanism [23] occurs. Let us roughly estimate a following flavor changing amplitude:

$$\mathcal{A} = \sum_{j=1,2,3} V_{ji}^* V_{jk} F(x_j) \text{ for } i \neq j, \quad (2.26)$$

where $F(x)$ is a some loop function of $x_j \equiv m_{u_j}^2/m_W^2$ with the up type quark mass m_{u_j} . In the quark sector of the SM, there exists a large mass hierarchy, and except for a quark of the third generation, x_j takes a small value. Thus, $F(x_j) \simeq F(0) + \Delta F(x_3)\delta_{j3}$ is approximately satisfied, and \mathcal{A} is roughly obtained as

$$\mathcal{A} \sim V_{ti}^* V_{tk} \cdot \Delta F(x_t). \quad (2.27)$$

This mechanism that flavor changing processes are suppressed because of the unitarity of the CKM matrix is called as the GIM mechanism. In particular, the suppression is often called as the GIM suppression, and light quarks contributions in loop diagrams are suppressed. Since, the bottom quark is much lighter than the top quark, the effect of the GIM suppression in the D meson systems becomes large. Thus, light quarks contributions are suppressed by the GIM mechanism. However, for the K meson systems, it is noticed that the charm quark contributions can become large because of small values of $|V_{td}|$ and $|V_{ts}|$. Actually, in CP conserving processes, the charm contributions dominate, and uncertainties in the SM prediction, such as in ΔM_K becomes large. On the other hand, in CP violating processes, the charm contributions are not large because of Eq. (2.24).

For the B meson systems, the top quark contributions dominate by the GIM mechanism. As the results, the SM contributions in the meson mixing processes become much small, and a sensitivity to new physics becomes high. In the K , B_d and B_s meson systems, meson mixing amplitudes are roughly proportional to $|V_{td}^* V_{ts}|^2 \simeq \lambda^{10}$, $|V_{td}^* V_{tb}|^2 \simeq \lambda^6$ and $|V_{ts}^* V_{tb}|^2 \simeq \lambda^4$, respectively. Thus, the sensitivity in the kaon system to the NP scale is roughly higher than B_d and B_s systems by almost 10^2 TeV and 10^3 TeV, respectively.

2.2 The Standard Model Effective Field Theory

The SM describes nature very well. However, some unsolved problems, such as the hierarchy problem and the identity of the dark matter, are remained in the SM. Thus, an existence of NP which solves remained problems has been believed. In this sense, the SM is an effective field theory valid up to the NP scale Λ , where new particles appear as dynamical degrees of freedom. The effective field theory above the NP scale, Λ , must satisfies the following conditions [11, 18]:

1. Its gauge group contains the SM gauge $SU(3)_C \times SU(2)_L \times U(1)_Y$,
2. All SM degrees of freedom are included as dynamical fields.

In addition to above conditions, it is often assumed that undiscovered weakly coupled *light* particles, such as axions or sterile neutrinos do not exist [11, 18]. However, the existence of weakly coupled *light* particles is not important, unless we are interested in experiments at the resonance energy of the new particles [24]. Below the NP scale, heavy new particles are decoupled, and the NP contributions are encoded in higher-dimensional operators as

$$\mathcal{L}_{\text{SMEFT}} = \mathcal{L}_{\text{SM}} + \frac{1}{\Lambda^2} \sum_k C_k^{(6)} \mathcal{O}_k^{(6)} + \mathcal{O}\left(\frac{1}{\Lambda^3}\right), \quad (2.28)$$

where the first term is the SM Lagrangian at the renormalizable level, and the remaining terms are higher dimensional operators^{#1}. Because of the above conditions, the higher dimensional operators are constructed by $\text{SU}(3)_C \times \text{SU}(2)_L \times \text{U}(1)_Y$ invariant operators consisting of the SM fields. The non-redundant operator basis for the dimension-six are determined in [11], which is called as the ‘‘Warsaw basis’’^{#2}. The independent operators $\mathcal{O}_n^{(6)}$ are listed in Table 2.2 and 2.3. The independence means that there does not exist linear combinations of the operators and they are not equation of motion (EOM)-vanishing up to total derivatives.

Table 2.2: Dimension-six operators other than the four-fermion ones.

X^3		H^6 and $H^4 D^2$		$\psi^2 H^3$	
\mathcal{O}_G	$f^{ABC} G_\mu^{A\nu} G_\nu^{B\rho} G_\rho^{C\mu}$	\mathcal{O}_H	$(H^\dagger H)^3$	\mathcal{O}_{eH}	$(H^\dagger H)(\bar{l}_p e_r \tilde{H})$
$\mathcal{O}_{\tilde{G}}$	$f^{ABC} \tilde{G}_\mu^{A\nu} G_\nu^{B\rho} G_\rho^{C\mu}$	$\mathcal{O}_{H\Box}$	$(H^\dagger H)\Box(H^\dagger H)$	\mathcal{O}_{uH}	$(H^\dagger H)(\bar{q}_p u_r \tilde{H})$
\mathcal{O}_W	$\epsilon^{IJK} W_\mu^{I\nu} W_\nu^{J\rho} W_\rho^{K\mu}$	\mathcal{O}_{HD}	$(H^\dagger D^\mu H)^*(H^\dagger D_\mu H)$	\mathcal{O}_{dH}	$(H^\dagger H)(\bar{q}_p d_r H)$
$\mathcal{O}_{\tilde{W}}$	$\epsilon^{IJK} \tilde{W}_\mu^{I\nu} W_\nu^{J\rho} W_\rho^{K\mu}$				
$X^2 H^2$		$\psi^2 XH$		$\psi^2 H^2 D$	
\mathcal{O}_{HG}	$H^\dagger H G_{\mu\nu}^A G^{A\mu\nu}$	\mathcal{O}_{eW}	$(\bar{l}_p \sigma^{\mu\nu} e_r) \tau^I H W_{\mu\nu}^I$	$\mathcal{O}_{Hl}^{(1)}$	$(H^\dagger i \overleftrightarrow{D}_\mu H)(\bar{l}_p \gamma^\mu l_r)$
$\mathcal{O}_{H\tilde{G}}$	$H^\dagger H \tilde{G}_{\mu\nu}^A G^{A\mu\nu}$	\mathcal{O}_{eB}	$(\bar{l}_p \sigma^{\mu\nu} e_r) H B_{\mu\nu}$	$\mathcal{Q}_{Hl}^{(3)}$	$(H^\dagger i \overleftrightarrow{D}_\mu^I H)(\bar{l}_p \tau^I \gamma^\mu l_r)$
\mathcal{O}_{HW}	$H^\dagger H W_{\mu\nu}^I W^{I\mu\nu}$	\mathcal{O}_{uG}	$(\bar{q}_p \sigma^{\mu\nu} T^A u_r) \tilde{H} G_{\mu\nu}^A$	\mathcal{O}_{He}	$(H^\dagger i \overleftrightarrow{D}_\mu H)(\bar{e}_p \gamma^\mu e_r)$
$\mathcal{O}_{H\tilde{W}}$	$H^\dagger H \tilde{W}_{\mu\nu}^I W^{I\mu\nu}$	\mathcal{O}_{uW}	$(\bar{q}_p \sigma^{\mu\nu} u_r) \tau^I \tilde{H} W_{\mu\nu}^I$	$\mathcal{O}_{Hq}^{(1)}$	$(H^\dagger i \overleftrightarrow{D}_\mu H)(\bar{q}_p \gamma^\mu q_r)$
\mathcal{O}_{HB}	$H^\dagger H B_{\mu\nu} B^{\mu\nu}$	\mathcal{O}_{uB}	$(\bar{q}_p \sigma^{\mu\nu} u_r) \tilde{H} B_{\mu\nu}$	$\mathcal{O}_{Hq}^{(3)}$	$(H^\dagger i \overleftrightarrow{D}_\mu^I H)(\bar{q}_p \tau^I \gamma^\mu q_r)$
$\mathcal{O}_{H\tilde{B}}$	$H^\dagger H \tilde{B}_{\mu\nu} B^{\mu\nu}$	\mathcal{O}_{dG}	$(\bar{q}_p \sigma^{\mu\nu} T^A d_r) H G_{\mu\nu}^A$	\mathcal{O}_{Hu}	$(H^\dagger i \overleftrightarrow{D}_\mu H)(\bar{u}_p \gamma^\mu u_r)$
\mathcal{O}_{HWB}	$H^\dagger \tau^I H W_{\mu\nu}^I B^{\mu\nu}$	\mathcal{O}_{dW}	$(\bar{q}_p \sigma^{\mu\nu} d_r) \tau^I H W_{\mu\nu}^I$	\mathcal{O}_{Hd}	$(H^\dagger i \overleftrightarrow{D}_\mu H)(\bar{d}_p \gamma^\mu d_r)$
$\mathcal{O}_{H\tilde{W}B}$	$H^\dagger \tau^I H \tilde{W}_{\mu\nu}^I B^{\mu\nu}$	\mathcal{O}_{dB}	$(\bar{q}_p \sigma^{\mu\nu} d_r) H B_{\mu\nu}$	\mathcal{O}_{Hud}	$i(\tilde{H}^\dagger \overleftrightarrow{D}_\mu H)(\bar{u}_p \gamma^\mu d_r)$

The derivatives are defined as

$$H^\dagger \overleftrightarrow{D}_\mu^I H = H^\dagger \tau^I D_\mu H - (D_\mu H)^\dagger \tau^I H, \quad (2.29)$$

where τ^I is the $\text{SU}(2)_L$ generator.

^{#1}The dimension-five Weinberg operator [25] related to neutrino masse, and we do not discuss in this thesis.

^{#2}In [10], dimension-six terms have been listed. However, some of the operators include redundance. It took almost twenty four years to reduce the redundance.

Table 2.3: Four-fermion operators.

$(\bar{L}L)(\bar{L}L)$		$(\bar{R}R)(\bar{R}R)$		$(\bar{L}L)(\bar{R}R)$	
\mathcal{O}_{ll}	$(\bar{l}_p \gamma_\mu l_r)(\bar{l}_s \gamma^\mu l_t)$	\mathcal{O}_{ee}	$(\bar{e}_p \gamma_\mu e_r)(\bar{e}_s \gamma^\mu e_t)$	\mathcal{O}_{le}	$(\bar{l}_p \gamma_\mu l_r)(\bar{e}_s \gamma^\mu e_t)$
$\mathcal{O}_{qq}^{(1)}$	$(\bar{q}_p \gamma_\mu q_r)(\bar{q}_s \gamma^\mu q_t)$	\mathcal{O}_{uu}	$(\bar{u}_p \gamma_\mu u_r)(\bar{u}_s \gamma^\mu u_t)$	\mathcal{O}_{lu}	$(\bar{l}_p \gamma_\mu l_r)(\bar{u}_s \gamma^\mu u_t)$
$\mathcal{O}_{qq}^{(3)}$	$(\bar{q}_p \gamma_\mu \tau^I q_r)(\bar{q}_s \gamma^\mu \tau^I q_t)$	\mathcal{O}_{dd}	$(\bar{d}_p \gamma_\mu d_r)(\bar{d}_s \gamma^\mu d_t)$	\mathcal{O}_{ld}	$(\bar{l}_p \gamma_\mu l_r)(\bar{d}_s \gamma^\mu d_t)$
$\mathcal{O}_{lq}^{(1)}$	$(\bar{l}_p \gamma_\mu l_r)(\bar{q}_s \gamma^\mu q_t)$	\mathcal{O}_{eu}	$(\bar{e}_p \gamma_\mu e_r)(\bar{u}_s \gamma^\mu u_t)$	\mathcal{O}_{qe}	$(\bar{q}_p \gamma_\mu q_r)(\bar{e}_s \gamma^\mu e_t)$
$\mathcal{O}_{lq}^{(3)}$	$(\bar{l}_p \gamma_\mu \tau^I l_r)(\bar{q}_s \gamma^\mu \tau^I q_t)$	\mathcal{O}_{ed}	$(\bar{e}_p \gamma_\mu e_r)(\bar{d}_s \gamma^\mu d_t)$	$\mathcal{O}_{qu}^{(1)}$	$(\bar{q}_p \gamma_\mu q_r)(\bar{u}_s \gamma^\mu u_t)$
		$\mathcal{O}_{ud}^{(1)}$	$(\bar{u}_p \gamma_\mu u_r)(\bar{d}_s \gamma^\mu d_t)$	$\mathcal{O}_{qu}^{(8)}$	$(\bar{q}_p \gamma_\mu T^A q_r)(\bar{u}_s \gamma^\mu T^A u_t)$
		$\mathcal{O}_{ud}^{(8)}$	$(\bar{u}_p \gamma_\mu T^A u_r)(\bar{d}_s \gamma^\mu T^A d_t)$	$\mathcal{O}_{qd}^{(1)}$	$(\bar{q}_p \gamma_\mu q_r)(\bar{d}_s \gamma^\mu d_t)$
				$\mathcal{O}_{qd}^{(8)}$	$(\bar{q}_p \gamma_\mu T^A q_r)(\bar{d}_s \gamma^\mu T^A d_t)$
$(\bar{L}R)(\bar{R}L)$ and $(\bar{L}R)(\bar{L}R)$		B -violating			
\mathcal{O}_{ledq}	$(\bar{l}_p^j e_r)(\bar{d}_s^k q_t^j)$	\mathcal{O}_{duq}	$\epsilon^{\alpha\beta\gamma} \epsilon_{jk} [(d_p^\alpha)^T C u_r^\beta] [(q_s^j)^T C l_t^k]$		
$\mathcal{O}_{quqd}^{(1)}$	$(\bar{q}_p^j u_r) \epsilon_{jk} (\bar{q}_s^k d_t)$	\mathcal{O}_{qqu}	$\epsilon^{\alpha\beta\gamma} \epsilon_{jk} [(q_p^{\alpha j})^T C q_r^{\beta k}] [(u_s^\gamma)^T C e_t]$		
$\mathcal{O}_{quqd}^{(8)}$	$(\bar{q}_p^j T^A u_r) \epsilon_{jk} (\bar{q}_s^k T^A d_t)$	\mathcal{O}_{qqq}	$\epsilon^{\alpha\beta\gamma} \epsilon_{jn} \epsilon_{km} [(q_p^{\alpha j})^T C q_r^{\beta k}] [(q_s^m)^T C l_t^n]$		
$\mathcal{O}_{lequ}^{(1)}$	$(\bar{l}_p^j e_r) \epsilon_{jk} (\bar{q}_s^k u_t)$	\mathcal{O}_{duu}	$\epsilon^{\alpha\beta\gamma} [(d_p^\alpha)^T C u_r^\beta] [(u_s^\gamma)^T C e_t]$		
$\mathcal{O}_{lequ}^{(3)}$	$(\bar{l}_p^j \sigma_{\mu\nu} e_r) \epsilon_{jk} (\bar{q}_s^k \sigma^{\mu\nu} u_t)$				

Within the above dimension-six operators, the one-loop anomalous dimension matrix for the SM Higgs self coupling, gauge coupling and Yukawa coupling corrections were completely calculated [13–15]. Since, in this thesis, we focus on the top quark corrections above the EWSB scale, the anomalous dimension terms which depend on the top Yukawa and QCD couplings are listed in Appendix A.1.

2.3 Relevant operator in $\Delta F = 2$ and 0 process

In the previous section, we have summarized the SMEFT dimension-six operators. In this thesis, we mainly focus on the $\Delta F = 1$ SMEFT dimension-six operators, which contribute to $\Delta F = 2$ and 0 processes. In particular, we investigate the flavor changing of down type quark induced by the top quark corrections. For convenience, we summarize the $\Delta F = 1$ SMEFT dimension-six operators relevant for the low-scale $\Delta F = 2$ and 0 processes of down type quark.

First, the dimension-six operators relevant for the low-scale $\Delta F = 2$ processes are shown as

$$(\mathcal{O}_{qq}^{(1)})_{ijkl} = (\bar{q}^i \gamma_\mu q^j)(\bar{q}^k \gamma_\mu q^l), \quad (2.30)$$

$$(\mathcal{O}_{qq}^{(3)})_{ijkl} = (\bar{q}^i \gamma_\mu \tau^I q^j)(\bar{q}^k \gamma_\mu \tau^I q^l), \quad (2.31)$$

$$(\mathcal{O}_{qd}^{(1)})_{ijkl} = (\bar{q}^i \gamma_\mu q^j)(\bar{d}^k \gamma_\mu d^l), \quad (2.32)$$

$$(\mathcal{O}_{qd}^{(8)})_{ijkl} = (\bar{q}^i \gamma_\mu T^A q^j)(\bar{d}^k \gamma_\mu T^A d^l), \quad (2.33)$$

$$(\mathcal{O}_{dd})_{ijkl} = (\bar{d}^i \gamma_\mu d^j)(\bar{d}^k \gamma_\mu d^l), \quad (2.34)$$

$$(\mathcal{O}_{Hq}^{(1)})_{ij} = (H^\dagger i \overleftrightarrow{D}_\mu H)(\bar{q}^i \gamma^\mu q^j), \quad (2.35)$$

$$(\mathcal{O}_{Hq}^{(3)})_{ij} = (H^\dagger i \overleftrightarrow{D}_\mu^I H)(\bar{q}^i \gamma^\mu \tau^I q^j), \quad (2.36)$$

$$(\mathcal{O}_{Hd})_{ij} = (H^\dagger i \overleftrightarrow{D}_\mu H)(\bar{d}^i \gamma^\mu d^j). \quad (2.37)$$

The above operators are relevant at the one-loop level. In order to study NP effects at the higher energy scales, the following dimension-six operators have to be additionally included:

$$(\mathcal{O}_{qu}^{(1)})_{ijkl} = (\bar{q}^i \gamma_\mu q^j)(\bar{u}^k \gamma^\mu u^l), \quad (2.38)$$

$$(\mathcal{O}_{qu}^{(8)})_{ijkl} = (\bar{q}^i \gamma_\mu T^A q^j)(\bar{u}^k \gamma^\mu T^A u^l), \quad (2.39)$$

$$(\mathcal{O}_{uu})_{ijkl} = (\bar{u}^i \gamma_\mu u^j)(\bar{u}^k \gamma^\mu u^l), \quad (2.40)$$

$$(\mathcal{O}_{ud}^{(1)})_{ijkl} = (\bar{u}^i \gamma_\mu u^j)(\bar{d}^k \gamma^\mu d^l), \quad (2.41)$$

$$(\mathcal{O}_{ud}^{(8)})_{ijkl} = (\bar{u}^i \gamma_\mu T^A u^j)(\bar{d}^k \gamma^\mu T^A d^l), \quad (2.42)$$

$$(\mathcal{O}_{Hu})_{ij} = (H^\dagger i \overleftrightarrow{D}_\mu H)(\bar{u}^i \gamma^\mu u^j), \quad (2.43)$$

$$(\mathcal{O}_{H\Box})_{ij} = (H^\dagger H)\Box(H^\dagger H), \quad (2.44)$$

$$(\mathcal{O}_{HD})_{ij} = (H^\dagger D_\mu H)^*(H^\dagger D^\mu H), \quad (2.45)$$

These operators contribute to the $\Delta F = 2$ observables through the operator mixings during the RG evolutions and the matching conditions at the EWSB scale (see Chapter 3).

Next, the dimension-six $\Delta F = 1$ operators relevant for the low-scale $\Delta F = 0$ processes are shown as

$$(\mathcal{O}_{qq}^{(1)})_{ijkl} = (\bar{q}^i \gamma_\mu q^j)(\bar{q}^k \gamma_\mu q^l), \quad (2.46)$$

$$(\mathcal{O}_{qq}^{(3)})_{ijkl} = (\bar{q}^i \gamma_\mu \tau^I q^j)(\bar{q}^k \gamma_\mu \tau^I q^l), \quad (2.47)$$

$$(\mathcal{O}_{qd}^{(1)})_{ijkl} = (\bar{q}^i \gamma_\mu q^j)(\bar{d}^k \gamma^\mu d^l), \quad (2.48)$$

$$(\mathcal{O}_{qd}^{(8)})_{ijkl} = (\bar{q}^i \gamma_\mu T^A q^j)(\bar{d}^k \gamma^\mu T^A d^l), \quad (2.49)$$

$$(\mathcal{O}_{dd})_{ijkl} = (\bar{d}^i \gamma_\mu d^j)(\bar{d}^k \gamma^\mu d^l), \quad (2.50)$$

$$(\mathcal{O}_{Hq}^{(1)})_{ij} = (H^\dagger i \overleftrightarrow{D}_\mu H)(\bar{q}^i \gamma^\mu q^j), \quad (2.51)$$

$$(\mathcal{O}_{Hq}^{(3)})_{ij} = (H^\dagger i \overleftrightarrow{D}_\mu^I H)(\bar{q}^i \gamma^\mu \tau^I q^j), \quad (2.52)$$

$$(\mathcal{O}_{Hd})_{ij} = (H^\dagger i \overleftrightarrow{D}_\mu H)(\bar{d}^i \gamma^\mu d^j), \quad (2.53)$$

$$(\mathcal{O}_{qu}^{(1)})_{ijkl} = (\bar{q}^i \gamma_\mu q^j)(\bar{u}^k \gamma^\mu u^l), \quad (2.54)$$

$$(\mathcal{O}_{qu}^{(8)})_{ijkl} = (\bar{q}^i \gamma_\mu T^A q^j)(\bar{u}^k \gamma^\mu T^A u^l), \quad (2.55)$$

$$(\mathcal{O}_{ud}^{(1)})_{ijkl} = (\bar{u}^i \gamma_\mu u^j)(\bar{d}^k \gamma^\mu d^l), \quad (2.56)$$

$$(\mathcal{O}_{ud}^{(8)})_{ijkl} = (\bar{u}^i \gamma_\mu T^A u^j)(\bar{d}^k \gamma^\mu T^A d^l). \quad (2.57)$$

These operators contribute to the $\Delta F = 0$ observables through the RGEs and matching conditions at the EWSB scale (see Chapter 3).

In Chapter 3, the matching conditions for the $\Delta F = 2$ and 0 processes at the EWSB scale are discussed. The SMEFT RGEs relevant for these operators are listed in Appendix A.1. Phenomenology of the $\Delta F = 2$ operators are discussed in Chapter 5 and 6, and that of the $\Delta F = 0$ processes are in Chapter 7. In Chapter 5, the $\Delta F = 2$ processes induced by \mathcal{O}_{Hd} and $\mathcal{O}_{Hq}^{(1,3)}$ are discussed with paying attention to correlations between $\Delta F = 2$ and 1 observables. Chapter 5 are devoted to phenomenology of the $\Delta F = 0$ operators.

Matching Formula

This chapter is based on the works by the author [16, 17]. In this chapter, we provide tree and one-loop matching formulae for the SMEFT which contribute to the $\Delta F = 2$ and 0 processes in a low-energy scale. At the electroweak symmetry breaking (EWSB) scale, the SMEFT $\Delta F = 1$ operators of down-type quark are matched onto the conventional low-scale $\Delta F = 2$ and 0 operators by the one-loop matching formulae.

3.1 Introduction of one-loop matching formula

The experimental data indicate that the NP scale is much higher than the EWSB scale. Then, the NP contributions are encoded in the SMEFT rather than the low-scale effective field theory (LEFT), which is described by the light SM particles. The LEFT for $\Delta F = 2$ processes are defined as [26]

$$\begin{aligned}
\mathcal{H}_{\text{eff}}^{\Delta F=2} = & (C_1)_{ij}(\bar{d}_i\gamma^\mu P_L d_j)(\bar{d}_i\gamma_\mu P_L d_j) \\
& + (C_2)_{ij}(\bar{d}_i P_L d_j)(\bar{d}_i P_L d_j) + (C_3)_{ij}(\bar{d}_i^\alpha P_L d_j^\beta)(\bar{d}_i^\beta P_L d_j^\alpha) \\
& + (C_4)_{ij}(\bar{d}_i P_L d_j)(\bar{d}_i P_R d_j) + (C_5)_{ij}(\bar{d}_i^\alpha P_L d_j^\beta)(\bar{d}_i^\beta P_R d_j^\alpha) \\
& + (C'_1)_{ij}(\bar{d}_i\gamma^\mu P_R d_j)(\bar{d}_i\gamma_\mu P_R d_j) \\
& + (C'_2)_{ij}(\bar{d}_i P_R d_j)(\bar{d}_i P_R d_j) + (C'_3)_{ij}(\bar{d}_i^\alpha P_R d_j^\beta)(\bar{d}_i^\beta P_R d_j^\alpha),
\end{aligned} \tag{3.1}$$

where i, j ($i \neq j$) are flavor indices, and α, β are color ones. Besides, the LEFT for EDMs are defined as

$$\mathcal{L}_{\text{CPV}} = \sum_{a=1,2,4,5} \sum_i C_a^i \mathcal{O}_a^i + C_3 \mathcal{O}_3 + \sum_{a=1,2} \sum_{i \neq j} \tilde{C}_a^{ij} \tilde{\mathcal{O}}_a^{ij} + \frac{1}{2} \sum_{a=3,4} \sum_{i \neq j} \tilde{C}_a^{ij} \tilde{\mathcal{O}}_a^{ij}, \tag{3.2}$$

where i, j are quark-flavor indices. The effective operators are defined as^{#1}

$$\mathcal{O}_1^i = -\frac{i}{2} m_{d_i} \bar{d}_i e Q_d (F \cdot \sigma) \gamma_5 d_i, \tag{3.3}$$

$$\mathcal{O}_2^i = -\frac{i}{2} m_{d_i} \bar{d}_i g_s (G \cdot \sigma) \gamma_5 d_i, \tag{3.4}$$

$$\mathcal{O}_3 = -\frac{1}{6} g_s f^{ABC} \epsilon^{\mu\nu\rho\sigma} G_{\mu\lambda}^A G_\nu^{B\lambda} G_{\rho\sigma}^C, \tag{3.5}$$

^{#1} Besides, there is a strong CP phase, $\bar{\theta}$. In this thesis, we assume $\bar{\theta} = 0$, for simplicity.

$$\mathcal{O}_4^i = (\bar{d}_i^\alpha d_i^\alpha)(\bar{d}_j^\beta i\gamma_5 d_j^\beta), \quad (3.6)$$

$$\mathcal{O}_5^i = (\bar{d}_i^\alpha \sigma^{\mu\nu} d_i^\alpha)(\bar{d}_j^\beta i\sigma_{\mu\nu} \gamma_5 d_j^\beta), \quad (3.7)$$

$$\tilde{\mathcal{O}}_1^{ij} = (\bar{d}_i^\alpha d_i^\alpha)(\bar{d}_j^\beta i\gamma_5 d_j^\beta), \quad (3.8)$$

$$\tilde{\mathcal{O}}_2^{ij} = (\bar{d}_i^\alpha d_i^\beta)(\bar{d}_j^\beta i\gamma_5 d_j^\alpha), \quad (3.9)$$

$$\tilde{\mathcal{O}}_3^{ij} = (\bar{d}_i^\alpha \sigma^{\mu\nu} d_i^\alpha)(\bar{d}_j^\beta i\sigma_{\mu\nu} \gamma_5 d_j^\beta), \quad (3.10)$$

$$\tilde{\mathcal{O}}_4^{ij} = (\bar{d}_i^\alpha \sigma^{\mu\nu} d_i^\beta)(\bar{d}_j^\beta i\sigma_{\mu\nu} \gamma_5 d_j^\alpha), \quad (3.11)$$

where α, β are color indices, and $F_{\mu\nu}$ ($G_{\mu\nu}^A$) is the electromagnetic (gluon) field strength. We define $F \cdot \sigma = F_{\mu\nu} \sigma^{\mu\nu}$, $G \cdot \sigma = G_{\mu\nu}^A \sigma^{\mu\nu} T^A$ and $\tilde{G}_{\mu\nu}^A = \frac{1}{2} \epsilon_{\mu\nu\rho\sigma} G^{A\rho\sigma}$ with $\sigma^{\mu\nu} = \frac{i}{2} [\gamma^\mu, \gamma^\nu]$ and $\epsilon^{0123} = +1$. Also, f^{ABC} is the structure constant, and m_q is a mass for quark q . At the EWSB scale, the SMEFT operators are matched onto the LEFT and they are eventually compared with experimental data.

In this chapter, we provide the one-loop matching formulae, which contribute to the $\Delta F = 2$ and 0 processes in a low-energy scale. In Section 3.2 and 3.3, it is found that the SMEFT $\Delta F = 1$ operators listed in Section 2.3 contribute to the operators in Eq. (3.1) and (3.11) by the one-loop correction with top quark. In Section 3.4, we discuss importances of the one-loop matching formulae. Section 3.5 is devoted to a conclusion of this chapter.

3.2 Formula for $\Delta F = 2$ process

In this section, we provide the formulae for the SMEFT corrections at the one-loop level which contribute to the $\Delta F = 2$ LEFT operators in Eq. (3.1).

At the tree level, they are related to the SMEFT operators as

$$(C_1)_{ij}^{\text{tree}} = - \left[(C_{qq}^{(1)})_{ijij} + (C_{qq}^{(3)})_{ijij} \right], \quad (3.12)$$

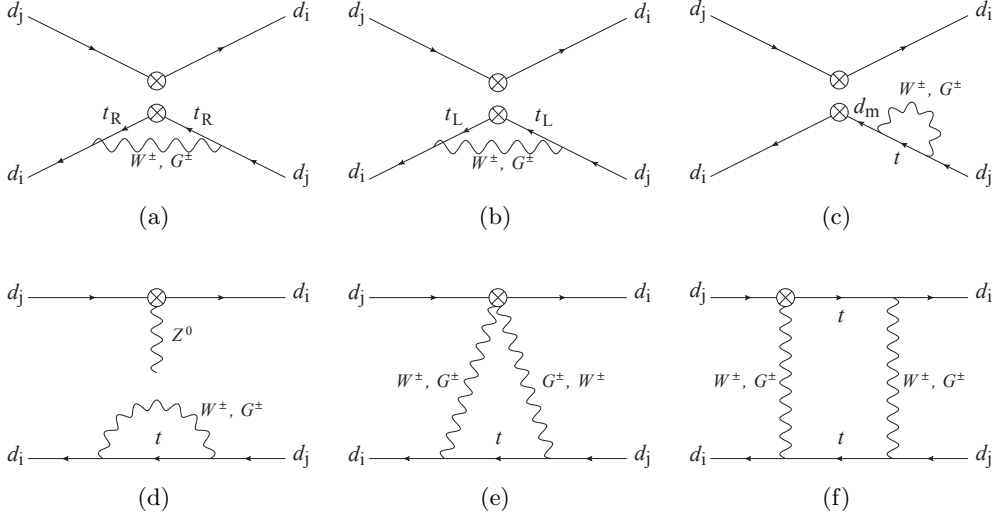
$$(C_1')_{ij}^{\text{tree}} = -(C_{dd})_{ijij}, \quad (3.13)$$

$$(C_4)_{ij}^{\text{tree}} = (C_{qd}^{(8)})_{ijij}, \quad (3.14)$$

$$(C_5)_{ij}^{\text{tree}} = 2(C_{qd}^{(1)})_{ijij} - \frac{1}{N_c} (C_{qd}^{(8)})_{ijij}, \quad (3.15)$$

where the Wilson coefficients in the left-handed side are defined in the low-scale basis, Eq. (3.1), and those in the right-handed side are defined in the SMEFT, Eq. (2.28). Both of them are evaluated as a weak scale, $\mu = \mu_W$. The other low-scale $\Delta F = 2$ coefficients are zero at this level.

Radiative corrections from the top quark can be sizable because of the large Yukawa coupling. Combined with the SM bosons, they contribute to flavor-changing transitions of the down-type quarks. In particular, the SMEFT $\Delta F = 1$ operators can induce the $\Delta F = 2$ amplitudes through the RGEs and the one-loop matchings at the weak scale, which are exhibited in Fig. 3.1. The


 Figure 3.1: Feynman diagrams for the one-loop matchings onto the $\Delta F = 2$ operators ($i \neq j$).

one-loop matching conditions in the Feynman-'t Hooft gauge are obtained as

$$\begin{aligned}
 (C_1)_{ij}^{1\text{-loop}} &= \frac{\alpha \lambda_t^{ij}}{4\pi s_W^2} \left[\left(-2 + \frac{2}{N_c} \right) (C_{qu}^{(8)})_{ij33} - 4(C_{qu}^{(1)})_{ij33} + 4(C_{Hq}^{(1)})_{ij} \right] I_1(x_t, \mu_W) \\
 &- \frac{2\alpha \lambda_t^{ij}}{\pi s_W^2} \left[(C_{qq}^{(1)})_{ij33} + (C_{qq}^{(1)})_{33ij} - (C_{qq}^{(3)})_{ij33} - (C_{qq}^{(3)})_{33ij} + 2(C_{qq}^{(3)})_{3ji3} + 2(C_{qq}^{(3)})_{i33j} \right] J(x_t) \\
 &+ \frac{\alpha}{2\pi s_W^2} \sum_{m=1}^3 \left[\lambda_t^{im} \left((C_{qq}^{(1)})_{mji} + (C_{qq}^{(1)})_{ijmj} + (C_{qq}^{(3)})_{mji} + (C_{qq}^{(3)})_{ijmj} \right) \right. \\
 &\quad \left. + \lambda_t^{mj} \left((C_{qq}^{(1)})_{imij} + (C_{qq}^{(1)})_{ijim} + (C_{qq}^{(3)})_{imij} + (C_{qq}^{(3)})_{ijim} \right) \right] K(x_t, \mu_W) \\
 &- \frac{\alpha \lambda_t^{ij}}{\pi s_W^2} (C_{Hq}^{(3)})_{ij} I_2(x_t, \mu_W) + \frac{\alpha \lambda_t^{ij}}{4\pi s_W^2} \sum_{m=1}^3 \left[\lambda_t^{im} (C_{Hq}^{(3)})_{mj} + (C_{Hq}^{(3)})_{im} \lambda_t^{mj} \right] S_0(x_t), \quad (3.16)
 \end{aligned}$$

$$\begin{aligned}
 (C_4)_{ij}^{1\text{-loop}} &= \frac{\alpha \lambda_t^{ij}}{\pi s_W^2} (C_{ud}^{(8)})_{33ij} I_1(x_t, \mu_W) + \frac{2\alpha \lambda_t^{ij}}{\pi s_W^2} (C_{qd}^{(8)})_{33ij} J(x_t) \\
 &- \frac{\alpha}{2\pi s_W^2} \sum_{m=1}^3 \left[\lambda_t^{im} (C_{qd}^{(8)})_{mji} + \lambda_t^{mj} (C_{qd}^{(8)})_{imij} \right] K(x_t, \mu_W), \quad (3.17)
 \end{aligned}$$

$$\begin{aligned}
 (C_5)_{ij}^{1\text{-loop}} &= \frac{2\alpha \lambda_t^{ij}}{\pi s_W^2} \left[(C_{ud}^{(1)})_{33ij} - \frac{1}{2N_c} (C_{ud}^{(8)})_{33ij} - (C_{Hd})_{ij} \right] I_1(x_t, \mu_W) \\
 &+ \frac{4\alpha \lambda_t^{ij}}{\pi s_W^2} \left[(C_{qd}^{(1)})_{33ij} - \frac{1}{2N_c} (C_{qd}^{(8)})_{33ij} \right] J(x_t) \\
 &- \frac{\alpha}{\pi s_W^2} \sum_{m=1}^3 \left[\lambda_t^{im} \left((C_{qd}^{(1)})_{mji} - \frac{1}{2N_c} (C_{qd}^{(8)})_{mji} \right) \right. \\
 &\quad \left. + \lambda_t^{mj} \left((C_{qd}^{(1)})_{imij} - \frac{1}{2N_c} (C_{qd}^{(8)})_{imij} \right) \right] K(x_t, \mu_W), \quad (3.18)
 \end{aligned}$$

where the parameters are defined as

$$x_t \equiv \frac{m_t^2}{M_W^2}, \quad \lambda_t^{ij} \equiv V_{ti}^* V_{tj}. \quad (3.19)$$

Here, V_{ij} is the CKM matrix, and $s_W = \sin \theta_W$ with the Weinberg angle θ_W . The loop functions are given as

$$I_1(x, \mu) = \frac{x}{8} \left[\ln \frac{\mu}{M_W} - \frac{x-7}{4(x-1)} - \frac{x^2-2x+4}{2(x-1)^2} \ln x \right], \quad (3.20)$$

$$I_2(x, \mu) = \frac{x}{8} \left[\ln \frac{\mu}{M_W} + \frac{7x-25}{4(x-1)} - \frac{x^2-14x+4}{2(x-1)^2} \ln x \right], \quad (3.21)$$

$$J(x) = \frac{x}{16} \left(1 - \frac{2 \ln x}{x-1} \right), \quad (3.22)$$

$$K(x, \mu) = \frac{x}{8} \left[\ln \frac{\mu}{M_W} + \frac{3(x+1)}{4(x-1)} - \frac{x(x+2)}{2(x-1)^2} \ln x \right], \quad (3.23)$$

$$S_0(x) = \frac{x}{4} \left[\frac{x^2-11x+4}{(x-1)^2} + \frac{6x^2}{(x-1)^3} \ln x \right]. \quad (3.24)$$

In the result, the Wilson coefficients in the left-handed side are in the low-scale basis, and those in the right-handed side are in the SMEFT. Both of them are evaluated at the weak scale, $\mu = \mu_W$. The other low-scale $\Delta F = 2$ operators do not receive one-loop corrections through the top quark decoupling.

The contributions from $\mathcal{O}_{qu}^{(1,8)}$ and $\mathcal{O}_{ud}^{(1,8)}$, in which the W and NG bosons that couple to virtual top quarks are exchanged, are shown in Fig. 3.1(a) and give a loop function $I_1(x, \mu)$. Those from $\mathcal{O}_{qq}^{(1,3)}$ and $\mathcal{O}_{qd}^{(1,8)}$ are shown in Fig. 3.1(b) and give $J(x)$. Those with the $K(x, \mu)$ function come from flavor-changing self-energy corrections to the down-type quarks in the effective operators [Fig. 3.1(c)], where the top quark is exchanged. The results for the quark–Higgs operators, $\mathcal{O}_{Hq}^{(1,3)}$ and \mathcal{O}_{Hd} [Fig. 3.1(d–f)], are consistent with those in Refs. [20, 21] and give loop functions $I_1(x, \mu)$, $I_2(x, \mu)$ and $S_0(x)$. The loop functions, $I_1(x, \mu)$, $I_2(x, \mu)$ and $K(x, \mu)$, depend on the matching scale μ explicitly, whereas $J(x)$ seems to be independent of it. The scale-dependent term associated with Fig. 3.1(b) is proportional to $\mathcal{O}(g^2)$ and neglected in our approximation.^{#2} We checked that this logarithmic dependence is consistent with the anomalous dimensions in Ref. [13–15]. As a result, the logarithmic dependence on μ_W cancels out by taking account of the RGEs in the leading-logarithmic limit.^{#3} This is expected because this dependence in the

^{#2} Such a divergence is canceled in the SM due to the GIM mechanism. In Fig. 3.1(b), the GIM mechanism does not work because $\mathcal{O}_{qq}^{(1,3)}$ and $\mathcal{O}_{qd}^{(1,8)}$ depend on the up-type quark flavor.

^{#3} Focusing on the top–Yukawa terms, we checked the following relations in the leading-logarithmic limit,

$$\frac{\partial (C_{1,4,5})_{ij}}{\partial \ln \mu_W} = \frac{\partial (C_{1,4,5})_{ij}^{\text{tree}}}{\partial \ln \mu_W} + \frac{\partial (C_{1,4,5})_{ij}^{1\text{-loop}}}{\partial \ln \mu_W} = 0. \quad (3.25)$$

matching conditions has the same origin as the beta functions in calculating loop diagrams (see Ref. [21]).^{#4 #5}

After matching onto the low-scale operators, they are evolved by the RGEs as usual. Then, the results are compared with the experimental data, i.e., the $K^0\text{--}\bar{K}^0$ and $B_q^0\text{--}\bar{B}_q^0$ ($q = d, s$) oscillations.

3.3 Formula for $\Delta F = 0$ process

In this section, we provide formulae for evaluating the EDMs induced by flavor-changing operators. At the EWSB scale, they are matched to the LEFT operators. We provide the one-loop matching formulae between the SMEFT $\Delta F = 1$ operators listed in Section 2.3 and the LEFT $\Delta F = 0$ CP -violating operators in Eq. (3.2).

The matching conditions are derived by integrating out SM heavy degrees of freedom, such as W, Z, H and t . At the tree level, we obtain the conditions,

$$(\tilde{C}_1^{ij})^{\text{tree}} = \frac{i}{4} \left[(C_{qd}^{(8)})_{j\bar{i}i} - (C_{qd}^{(8)})_{i\bar{j}j} \right], \quad (3.26)$$

$$(\tilde{C}_2^{ij})^{\text{tree}} = \frac{i}{4} \left[2 \left((C_{qd}^{(1)})_{j\bar{i}i} - (C_{qd}^{(1)})_{i\bar{j}j} \right) - \frac{1}{N_c} \left((C_{qd}^{(8)})_{j\bar{i}i} - (C_{qd}^{(8)})_{i\bar{j}j} \right) \right], \quad (3.27)$$

where the Wilson coefficients are evaluated at the EWSB scale, $\mu = \mu_W$. The other LEFT operators are not induced at the tree level.

In addition, the SMEFT $\Delta F = 1$ operators can generate $\Delta F = 0$ amplitudes through the one-loop matching conditions at the EWSB scale. We focus on the contributions from the loop diagrams with the top quark and the W boson. The conditions in the Feynman-'t Hooft gauge are obtained as

$$\begin{aligned} (\tilde{C}_1^{ij})^{1\text{-loop}} &= -\frac{\alpha}{2\pi s_W^2} \text{Im} \left[\lambda_t^{ji} (C_{ud}^{(8)})_{33ij} \right] I_1(x_t, \mu_W) - \frac{\alpha}{\pi s_W^2} \text{Im} \left[\lambda_t^{ji} (C_{qd}^{(8)})_{33ij} \right] J(x_t) \\ &\quad + \frac{\alpha}{4\pi s_W^2} \sum_{m=1}^3 \left\{ \text{Im} \left[\lambda_t^{jm} (C_{qd}^{(8)})_{m\bar{i}i} \right] + \text{Im} \left[\lambda_t^{mi} (C_{qd}^{(8)})_{j\bar{m}m} \right] \right\} K(x_t, \mu_W), \quad (3.28) \\ (\tilde{C}_2^{ij})^{1\text{-loop}} &= -\frac{\alpha}{\pi s_W^2} \text{Im} \left\{ \lambda_t^{ji} \left[(C_{ud}^{(1)})_{33ij} - \frac{1}{2N_c} (C_{ud}^{(8)})_{33ij} - (C_{Hd})_{ij} \right] \right\} I_1(x_t, \mu_W) \\ &\quad - \frac{2\alpha}{\pi s_W^2} \text{Im} \left\{ \lambda_t^{ji} \left[(C_{qd}^{(1)})_{33ij} - \frac{1}{2N_c} (C_{qd}^{(8)})_{33ij} \right] \right\} J(x_t) \\ &\quad + \frac{\alpha}{2\pi s_W^2} \sum_{m=1}^3 \left\{ \text{Im} \left[\lambda_t^{jm} \left[(C_{qd}^{(1)})_{m\bar{i}i} - \frac{1}{2N_c} (C_{qd}^{(8)})_{m\bar{i}i} \right] \right] \right. \\ &\quad \left. + \text{Im} \left[\lambda_t^{mi} \left[(C_{qd}^{(1)})_{j\bar{m}m} - \frac{1}{2N_c} (C_{qd}^{(8)})_{j\bar{m}m} \right] \right] \right\} K(x_t, \mu_W). \quad (3.29) \end{aligned}$$

^{#4} The logarithmic scale dependence in Eqs. (4.24)–(4.26) of Ref. [18] is inconsistent with that in the RGEs.

^{#5} In Appendix C, we also checked that double-penguin contributions to $\Delta F = 2$ operators vanish when the gauge bosons of the SM unbroken gauge symmetries are exchanged. This justifies our one-loop matching conditions.

All the Wilson coefficients are evaluated at the EWSB scale, $\mu = \mu_W$. The other LEFT operators for the EDMs do not receive one-loop corrections at this scale.

Similar to the LEFT $\Delta F = 2$ operators, below the EWSB scale, that of $\Delta F = 0$ are evolved by the RGEs in Appendix A. Then, the EDMs are evaluated around the hadron scale.

3.4 Discussions

In evaluations based on the SMEFT, the NP particles and the heavy SM particles such as the top-quark and the EW gauge boson are integrated out at different energy scales. The NP particles are decoupled at the NP scale, which are encoded into the SMEFT. Then, the heavy SM particles are decoupled at the EWSB scale, which are encoded into the LEFT. Since the NP effects in the conventional LEFT evaluations are at the one-loop level, the one-loop matching formulae at the EWSB scale are essential to reproduce the same order calculation of the conventional estimations. This is the qualitative reason why the one-loop matching formula is needed.

By the tree-level matching, terms including $\log M_{\text{NP}}/\mu_W$ appear and become dominant contributions if the NP scale is much larger than the EWSB scale. Then, finite terms coming from the one-loop matching formulae are $\mathcal{O}(10)\%$ compared with the tree-level contributions. Therefore, the one-loop matching formulae are essential to evaluate the low-scale observables with high precision.

3.5 Conclusion of matching formula

In this chapter, we provided tree and one-loop matching formulae for the SMEFT, which contribute to the $\Delta F = 2$ and 0 LEFT operators. In order to evaluate the low-scale observables, the operator matching needs to be performed at the one-loop level. This is because the NP contributions often appear together with the heavy SM particles at the one-loop level. By the one-loop matching formulae, the LEFT Wilson coefficients at the EWSB scale are changed by $\mathcal{O}(10)\%$ compared with the tree-level matching contributions. We conclude that the one-loop matching formulae are essential qualitatively and quantitatively.

In this chapter, we summarize low-scale observables such as $\Delta F = 0, 1$ and 2 observables which are discussed in this thesis. In Section 4.1, the indirect CP violation in $K^0 - \bar{K}^0$ oscillation are summarized, Section 4.2 the mass difference in B_d meson, Section 4.3 the nucleon EDMs. In Section 4.4, flavor changing observables relevant for Z mediated corrections discussed in Chapter 6 are summarized. In Section 4.4.1, the direct CP violation of the $K \rightarrow \pi\pi$ decays are summarized, Section 4.4.2 decay processes $K \rightarrow \pi\nu\bar{\nu}$ and Section 4.4.3 a decay rate of $K_L \rightarrow \mu^+\mu^-$.

4.1 ϵ_K

The indirect CP violation of the neutral kaon system, ϵ_K , includes the SM and NP contributions,

$$\epsilon_K = e^{i\phi_\epsilon} (\epsilon_K^{\text{SM}} + \epsilon_K^{\text{NP}}), \quad (4.1)$$

with $\phi_\epsilon = (43.51 \pm 0.05)^\circ$. The SM prediction is estimated as [27]

$$\epsilon_K^{\text{SM}} = (2.035 \pm 0.178) \times 10^{-3}, \quad (4.2)$$

where V_{cb} is determined by the inclusive semileptonic B decays. The NP contribution is represented as

$$\epsilon_K^{\text{NP}} = \frac{\tilde{\kappa}_\epsilon}{\sqrt{2}(\Delta M_K)_{\text{exp}}} [\text{Im}(M_{12}^K)^{\text{NP}}], \quad (4.3)$$

where $\tilde{\kappa}_\epsilon = 0.94$ [28, 29] and $(\Delta M_K)_{\text{exp}} = 3.483 \times 10^{-15}$ GeV [30] are used. Also, $M_{12}^K = \langle K^0 | \mathcal{H}_{\text{eff}}^{\Delta S=2} | \bar{K}^0 \rangle / 2M_K$ with $M_K = 0.4976$ GeV [30]. The Wilson coefficients are evaluated with the NLO-QCD RGEs [31], and hadron matrix elements in Ref. [32] are used. On the other hand, the experimental result is [30]

$$|\epsilon_K^{\text{exp}}| = (2.228 \pm 0.011) \times 10^{-3}. \quad (4.4)$$

From Eqs. (4.2) and (4.4), we obtain the bound on the NP contribution as

$$-0.16 \times 10^{-3} < \epsilon_K^{\text{NP}} < 0.55 \times 10^{-3}, \quad (4.5)$$

at the 2σ level.

4.2 ΔM_{B_d}

Both the SM and NP affect to the mass difference of the neutral B_d^0 meson, The SM and NP contributions are represented as

$$\Delta M_{B_d} = 2 \left| (M_{12}^{B_d})^{\text{SM}} + (M_{12}^{B_d})^{\text{NP}} \right| \equiv \Delta M_{B_d}^{\text{SM}} + \Delta M_{B_d}^{\text{NP}}, \quad (4.6)$$

where $M_{12}^{B_d} = \langle B^0 | \mathcal{H}_{\text{eff}}^{\Delta B=2} | \bar{B}^0 \rangle / 2M_{B_d}$ with $M_{B_d} = 5.27958$ GeV [30]. The first term in the right-hand side denotes the SM contribution, which is estimated as [33]

$$\Delta M_d^{\text{SM}} = (4.21 \pm 0.34) \times 10^{-13} \text{ GeV}. \quad (4.7)$$

The Wilson coefficients are evaluated with the NLO-QCD RGEs [31], and hadron matrix elements in Ref. [33] are used. On the other hand, the experimental result is obtained as [30]

$$\Delta M_d^{\text{exp}} = (3.3338 \pm 0.0125) \times 10^{-13} \text{ GeV}. \quad (4.8)$$

Thus, the NP contribution is required to satisfy,

$$0.20 \times 10^{-13} < \Delta M_d^{\text{NP}} < 1.56 \times 10^{-13}, \quad (4.9)$$

at the 2σ level.

4.3 Nucleon EDMs

Contributions of $\tilde{\mathcal{O}}_1^{ds}$ and $\tilde{\mathcal{O}}_1^{sd}$ are evaluated by the effective chiral Lagrangian technique [34]. Those operators generate CP -violating baryon-meson interactions through vacuum-expectation values (VEVs) of pseudoscalar mesons. Then, from baryon-meson loop diagrams, we obtain^{#1}

$$\frac{d_n}{e} \sim \left(-0.026 \tilde{C}_1^{ds} + 0.169 \tilde{C}_1^{sd} \right) \text{ GeV}^{-1}, \quad (4.10)$$

$$\frac{d_p}{e} \sim \left(0.023 \tilde{C}_1^{ds} - 0.149 \tilde{C}_1^{sd} \right) \text{ GeV}^{-1}, \quad (4.11)$$

where the Wilson coefficients are estimated at the hadron scale, $\mu = 1$ GeV. Here and hereafter, we set $\bar{\theta} = 0$ for simplicity^{#2}. The derivations of Eqs. (4.10) and (4.11) are given in Appendix F.

Four-quark operators, $\tilde{\mathcal{O}}^{db}$ and $\tilde{\mathcal{O}}^{bd}$, involve the bottom quark. In order to derive their contributions to the neutron EDM, we follow the strategy explored in Refs. [36–38]. The result becomes

$$\frac{d_n}{e} \sim 4.2 \times 10^{-4} \left(\tilde{C}^{bd} + 0.75 \tilde{C}^{db} \right) \text{ GeV}^{-1}, \quad (4.12)$$

^{#1} The nucleon EDMs are also induced by baryon-meson diagrams at the tree level [35]. However, we confirmed that they are sub-dominant.

^{#2} The Peccei-Quinn (PQ) mechanism is not assumed for realizing $\bar{\theta} = 0$. It is straightforward to extend the case for $\bar{\theta} \neq 0$. Then, the PQ mechanism is introduced to avoid the strong CP problem. The following conclusions do not change qualitatively.

$$\frac{d_p}{e} \sim 6.1 \times 10^{-4} \left(\tilde{C}^{bd} + 0.75 \tilde{C}^{db} \right) \text{GeV}^{-1}, \quad (4.13)$$

where the Wilson coefficients are estimated at the hadron scale, $\mu = 1 \text{ GeV}$. Here, the contribution to the proton EDM, Eq. (4.13), is derived by multiplying a ratio of the magnetic moments, μ_p/μ_n , to that of the neutron EDM, Eq. (4.12) (cf., Ref. [38]). On the other hand, \tilde{O}^{sb} and \tilde{O}^{bs} are much less constrained by the EDMs, because they do not depend on the down quark.

Let us summarize the current experimental limits and future prospects. The current bounds are obtained as [39, 40]

$$|d_n| < 3.0 \times 10^{-26} \text{ e cm}, \quad [90\% \text{ C.L.}] \quad (4.14)$$

$$|d_p| < 2.1 \times 10^{-25} \text{ e cm}. \quad (4.15)$$

In future, experiments are projected to achieve the sensitivities of $|d_n| \sim 10^{-28} \text{ e cm}$ [7] and $|d_p| \sim 10^{-29} \text{ e cm}$ [9].

4.4 Flavor changing observable in Z mediated correction

In this section, we summarize low-scale flavor changing observables relevant for Z mediated corrections, which are discussed in Chapter 6. As we will discuss in Chapter 6, the $\Delta F = 2$ observables are correlated with the various $\Delta F = 1$ ones through the Z boson. In this section, the $\Delta F = 1$ observables are summarized.

4.4.1 ϵ'/ϵ_K

The direct CP violation of the $K \rightarrow \pi\pi$ decays, includes the SM and NP mediated by Z -penguin contributions,

$$(\epsilon'/\epsilon_K) = (\epsilon'/\epsilon_K)^{\text{SM}} + (\epsilon'/\epsilon_K)^{\text{NP}}. \quad (4.16)$$

The latter contribution is approximated to be (cf., Ref. [41])

$$\begin{aligned} (\epsilon'/\epsilon_K)^{\text{NP}} = -B_8^{(3/2)}(m_c) \left[5.91 \times 10^7 \text{GeV}^2 \text{Im} \left((C^{(1)Hq})_{12} + (C^{(3)Hq})_{12} \right) \right. \\ \left. + 1.97 \times 10^8 \text{GeV}^2 \text{Im}(C_{Hd})_{12} \right], \quad (4.17) \end{aligned}$$

where the Wilson coefficients are estimated at the Z -boson mass scale, $\mu = m_Z$. By using lattice simulations [42–44], $B_8^{(3/2)}(m_c) = 0.76 \pm 0.05$ is obtained [45, 46]. Here, ϵ_K in the denominator is evaluated by the experimental value. The right-handed contribution is amplified by $c_W^2/s_W^2 \simeq 3.33$ compared to the left-handed one. Currently, the SM prediction deviates from the experimental result at the 2.8σ level. In this thesis, the discrepancy of ϵ'/ϵ_K is required to be explained within the 1σ range,

$$7.78 \times 10^{-4} < (\epsilon'/\epsilon_K)^{\text{NP}} < 14.4 \times 10^{-4}, \quad (4.18)$$

where Ref. [47] is used for the SM prediction at the NLO level.

4.4.2 $K \rightarrow \pi \nu \bar{\nu}$

The decay processes, $K^+ \rightarrow \pi^+ \nu \bar{\nu}$ and $K_L \rightarrow \pi^0 \nu \bar{\nu}$, are induced by NP mediated by the Z -penguin contributions, which are theoretical clean^{#3}. They are expressed as [41, 46]

$$\mathcal{B}(K^+ \rightarrow \pi^+ \nu \bar{\nu}) = \kappa_+ \left[\left(\frac{\text{Im}X_{\text{eff}}}{\lambda^5} \right)^2 + \left(\frac{\text{Re}\lambda_c}{\lambda} P_c(X) + \frac{\text{Re}X_{\text{eff}}}{\lambda^5} \right)^2 \right], \quad (4.19)$$

$$\mathcal{B}(K_L \rightarrow \pi^0 \nu \bar{\nu}) = \kappa_L \left[\frac{\text{Im}X_{\text{eff}}}{\lambda^5} \right]^2, \quad (4.20)$$

where $\lambda = |V_{us}|$, $\lambda_c = V_{cd}^* V_{cs}$, $\kappa_+ = (5.157 \pm 0.025) \times 10^{-11} (\lambda/0.225)^8$, $\kappa_L = (2.231 \pm 0.013) \times 10^{-10} (\lambda/0.225)^8$, and the charm contribution gives $P_c(X) = (9.39 \pm 0.31) \times 10^{-4} / \lambda^4 + (0.04 \pm 0.02)$. In terms of C_{Hq} and C_{Hd} , X_{eff} is approximated to be (cf., Ref. [21])

$$\text{Re}X_{\text{eff}} = -4.83 \times 10^{-4} - 5.62 \times 10^6 \text{GeV}^2 \text{Re}C_{H+}, \quad (4.21)$$

$$\text{Im}X_{\text{eff}} = 2.12 \times 10^{-4} + 5.62 \times 10^6 \text{GeV}^2 \text{Im}C_{H+}, \quad (4.22)$$

where the first terms in the right-hand sides are the SM contributions in each equation, and

$$C_{H+} = (C_{Hq}^{(1)})_{12} + (C_{Hq}^{(3)})_{12} + (C_{Hd})_{12}. \quad (4.23)$$

The Wilson coefficients are estimated at the Z -boson mass scale.

The SM predictions are known to be [21]

$$\mathcal{B}(K^+ \rightarrow \pi^+ \nu \bar{\nu})^{\text{SM}} = (8.4 \pm 1.0) \times 10^{-11}, \quad (4.24)$$

$$\mathcal{B}(K_L \rightarrow \pi^0 \nu \bar{\nu})^{\text{SM}} = (3.00 \pm 0.30) \times 10^{-11}, \quad (4.25)$$

while the experimental results^{#4} are [48, 50]

$$\mathcal{B}(K^+ \rightarrow \pi^+ \nu \bar{\nu})^{\text{exp}} < 1.85 \times 10^{-10} \text{ [90\% C.L.]}, \quad (4.26)$$

$$\mathcal{B}(K_L \rightarrow \pi^0 \nu \bar{\nu})^{\text{exp}} < 3.0 \times 10^{-9} \text{ [90\% C.L.]} \quad (4.27)$$

These experimental values will be improved in the near future. The NA62 experiment at CERN has already started the physics run and aims to measure $\mathcal{B}(K^+ \rightarrow \pi^+ \nu \bar{\nu})$ with a precision of 10% relative to the SM prediction [51]. The KOTO experiment at J-PARC aims to measure $\mathcal{B}(K_L \rightarrow \pi^0 \nu \bar{\nu})$ around the SM sensitivity by 2021 [52, 53].

^{#3}In particular, $K_L \rightarrow \pi^0 \nu \bar{\nu}$ is CP violating process, where the charm loop contribution is suppressed.

^{#4}The NA62 experiment has been running in 2016-2018, and the 2016-2017 dataset was analysed. In addition to 7 event candidates at the E787 and E949 experiments [48, 49], three candidate events were reported in the 2016-2017 dataset.

4.4.3 $K_L \rightarrow \mu^+ \mu^-$

The decay rate of $K_L \rightarrow \mu^+ \mu^-$, which is a CP -conserving process^{#5}, is sensitive to a real component of the flavor-changing Z couplings. There are large theoretical uncertainties from a long-distance (LD) contribution, because of huge long-distance contributions through $K_L \rightarrow \gamma^* \gamma^* \rightarrow \mu^+ \mu^-$ ^{#6}. In addition, an unknown sign of $\mathcal{A}(K_L \rightarrow \gamma\gamma)$ conceals a relative sign between the LD and a short-distance (SD) amplitudes. One can, therefore, estimate only the SD branching ratio, which is expressed as [41, 100, 101]

$$\mathcal{B}(K_L \rightarrow \mu^+ \mu^-)_{\text{SD}} = \kappa_\mu \left(\frac{\text{Re}\lambda_c}{\lambda} P_c(Y) + \frac{\text{Re}Y_{\text{eff}}}{\lambda^5} \right)^2, \quad (4.28)$$

where $\kappa_\mu = (2.01 \pm 0.02) \times 10^{-9} (\lambda/0.225)^8$, and the charm-quark contribution is $P_c(Y) = (0.115 \pm 0.018) \times (0.225/\lambda)^4$. Here, Y_{eff} is approximately given as (cf., Ref. [21])

$$\text{Re}Y_{\text{eff}} = -3.07 \times 10^{-4} - 5.62 \times 10^6 \text{GeV}^2 \text{Re}C_{H-}, \quad (4.29)$$

where the first term in the right-hand side is the SM contribution, and

$$C_{H-} = (C_{Hq}^{(1)})_{12} + (C_{Hq}^{(3)})_{12} - (C_{Hd})_{12}. \quad (4.30)$$

The Wilson coefficients are estimated at the Z -boson mass scale.

The SM value is obtained as [21]

$$\mathcal{B}(K_L \rightarrow \mu^+ \mu^-)_{\text{SD}}^{\text{SM}} = (0.83 \pm 0.10) \times 10^{-9}. \quad (4.31)$$

It is challenging to extract the SD contribution from the experimental value. An upper bound is estimated as [57]

$$\mathcal{B}(K_L \rightarrow \mu^+ \mu^-)_{\text{SD}}^{\text{exp}} < 2.5 \times 10^{-9}. \quad (4.32)$$

Since the constraint is much weaker than the SM uncertainties, we simply impose a bound,

$$-1.81 \times 10^{-10} (\text{GeV})^{-2} < \text{Re}C_{H-} < 4.85 \times 10^{-11} (\text{GeV})^{-2}. \quad (4.33)$$

Note that the electron mode $K_L \rightarrow e^+ e^-$ is suppressed by m_e^2/m_μ^2 , and the detector sensitivity to electrons in the LHCb is also weaker than the muon one.

^{#5} K_L is an almost CP -odd state, which decays to $\bar{l}\gamma_5 l$ through S-wave ($J=0, L=0, S=0$) processes.

^{#6}Note that there is no single photon exchange, because of $p_{K^0}^\mu (\bar{l}\gamma_\mu l) = (p+q)^\mu (\bar{u}(p)\gamma_\mu v(q)) = 0$. As the result, the SD contribution is comparable to the dominant LD contribution, and $K_L \rightarrow \mu^+ \mu^-$ becomes sensitive to physics at high energy scale.

4.4.4 $K_S \rightarrow \mu^+ \mu^-$

The decay, $K_S \rightarrow \mu^+ \mu^-$, proceeds via LD CP conserving P-wave and SD CP violating S-wave processes. Since the decay rate is dominated by the former, whose uncertainty is large, the sensitivity to the imaginary component of the flavor-changing Z couplings is diminished [54, 55, 57]. Interestingly, the SD contribution is enhanced through an interference between the K_L and K_S states in the neutral kaon beam^{#7} [56]. The effective branching ratio of $K_S \rightarrow \mu^+ \mu^-$ after including the interference is expressed as (cf., Ref. [56])

$$\mathcal{B}(K_S \rightarrow \mu^+ \mu^-)_{\text{eff}} = \mathcal{B}(K_S \rightarrow \mu^+ \mu^-) + D \cdot \mathcal{B}(K_S \rightarrow \mu^+ \mu^-)_{\text{int}}, \quad (4.35)$$

where a dilution factor D is an initial asymmetry between the numbers of K^0 and \bar{K}^0 ,

$$D = (N(K^0) - N(\bar{K}^0)) / (N(K^0) + N(\bar{K}^0)). \quad (4.36)$$

In the right-hand side, the branching ratio is approximated to be

$$\mathcal{B}(K_S \rightarrow \mu^+ \mu^-) = 4.99 \times 10^{-12} + 3.30 \times 10^8 \text{ GeV}^4 [2.39 \times 10^{-11} \text{ GeV}^{-2} + \text{Im} \mathcal{C}_{H-}]^2, \quad (4.37)$$

where the first and second terms in the right-hand side come from the LD and SD contributions, respectively. Here, the Wilson coefficients are estimated at the Z -boson mass scale. On the other hand, the interference contribution is given as^{#8}

$$\mathcal{B}(K_S \rightarrow \mu^+ \mu^-)_{\text{int}} = \begin{cases} -7.69 \times 10^7 \text{ GeV}^4 [2.39 \times 10^{-11} \text{ GeV}^{-2} + \text{Im} \mathcal{C}_{H-}] \\ \quad \times [1.73 \times 10^{-9} \text{ GeV}^{-2} - \text{Re} \mathcal{C}_{H-}], & (\eta_A = +) \\ 7.69 \times 10^7 \text{ GeV}^4 [2.39 \times 10^{-11} \text{ GeV}^{-2} + \text{Im} \mathcal{C}_{H-}] \\ \quad \times [1.86 \times 10^{-9} \text{ GeV}^{-2} + \text{Re} \mathcal{C}_{H-}]. & (\eta_A = -) \end{cases} \quad (4.39)$$

The Wilson coefficients are estimated at the Z -boson mass scale. The unknown relative sign between the LD and SD contributions in $K_L \rightarrow \mu^+ \mu^-$ gives two different predictions of $\mathcal{B}(K_S \rightarrow \mu^+ \mu^-)_{\text{int}}$,

^{#7}The decay intensity of the neutral kaon beam into f states is expressed as

$$\begin{aligned} I(t) &= (1 + D) \left| \langle f | \mathcal{H}_{\text{eff}}^{\Delta S=1} | K^0(t) \rangle \right|^2 / 2 + (1 - D) \left| \langle f | \mathcal{H}_{\text{eff}}^{\Delta S=1} | \bar{K}^0(t) \rangle \right|^2 / 2 \\ &= \frac{1}{2} |\mathcal{A}(K_S \rightarrow f)|^2 e^{-\Gamma_S t} + \frac{1}{2} |\mathcal{A}(K_L \rightarrow f)|^2 e^{-\Gamma_L t} + D \text{Re} \left[e^{-i\Delta M_K t} \mathcal{A}(K_S \rightarrow f)^* \mathcal{A}(K_L \rightarrow f) \right] e^{-(\Gamma_S + \Gamma_L)t/2}. \end{aligned} \quad (4.34)$$

Because of $\Gamma_S + \Gamma_L \simeq \Gamma_S$, an interference term proportional to D contributes to the $K_S \rightarrow \mu^+ \mu^-$ mode in the LHCb detector.

^{#8}Here, the interference effect is expressed as

$$\begin{aligned} &\sum_{\text{spin}} \mathcal{A}(K_L \rightarrow \mu^+ \mu^-)^* \mathcal{A}(K_S \rightarrow \mu^+ \mu^-) \\ &= \frac{16i G_F^4 M_W^4 F_K^2 M_K^2 m_\mu^2 \sin^2 \theta_W}{\pi^3} \text{Im}[\lambda_t] y'_{7A} \left\{ A_{L\gamma\gamma}^\mu - 2\pi \sin^2 \theta_W (\text{Re}[\lambda_t] y'_{7A} + \text{Re}[\lambda_c] y_c) \right\}, \end{aligned} \quad (4.38)$$

where $A_{L\gamma\gamma}^\mu$ is the dominant LD and a prefactor $\text{Im}[\lambda_t] y'_{7A}$ is the direct CP violating effect. Thus, the direct CP violating effect is enhanced by the dominant LD effects.

which are expressed by $\eta_{\mathcal{A}}$, (see Ref. [56, 58])

$$\eta_{\mathcal{A}} = \text{sgn} \left[A_{L\gamma\gamma}^{\mu} \right]. \quad (4.40)$$

The SM prediction depends on D and $\eta_{\mathcal{A}}$, which are determined by experiments. For $D = 0$, it is obtained as [54, 56, 57]

$$\mathcal{B}(K_S \rightarrow \mu^+ \mu^-)^{\text{SM}} = (5.18 \pm 1.50) \times 10^{-12}, \quad (4.41)$$

while for $D = 1$ and $\eta_{\mathcal{A}} = -1$, the SM prediction becomes [56]

$$\mathcal{B}(K_S \rightarrow \mu^+ \mu^-)_{\text{eff}}^{\text{SM}} = (8.59 \pm 1.50) \times 10^{-12}. \quad (4.42)$$

On the other hand, the current experimental bound based on the LHCb Run-1 result using the integrated luminosity 3 fb^{-1} is [59]

$$\mathcal{B}(K_S \rightarrow \mu^+ \mu^-)^{\text{exp}} < 0.8 \times 10^{-9}. \quad [90\% \text{ C.L.}] \quad (4.43)$$

The experimental sensitivity is expected to reach $\mathcal{B}(K_S \rightarrow \mu^+ \mu^-) = \mathcal{O}(10^{-11})$ by the end of the LHCb Run-2, and the Run-3 project is aiming to achieve the sensitivity as precise as the SM level [60].

SMEFT top-quark effects on $\Delta F = 2$ observables

This chapter is based on the work by the author [16]. We evaluate $\Delta F = 2$ observables with particular emphasis on a scale uncertainty coming from the large hierarchy between the NP scale and EWSB one. By using the matching formulae in Chapter 3, we calculate $\Delta F = 2$ Wilson coefficients of the LEFT at the EWSB scale, m_W , and study the matching scale uncertainty in the coefficients. In Section 5.1, we explain the matching scale uncertainty in conventional evaluations. In Section 5.2, we numerically analyze the scale uncertainty in a model independent way. In Section 5.3, we focus on the left-right symmetric model and investigate the effects of the scale uncertainty. We show that the magnitude of the scale uncertainty much depend on whether the tree-level contributions exist or not at the NP scale. The scale uncertainty can be $\mathcal{O}(1 - 100\%)$, which is reduced by the SMEFT.

5.1 Scale Uncertainty

In this section, we explain the matching scale uncertainty in conventional evaluations and provide our strategy for reducing the uncertainty. First of all, let us consider the conventional evaluations of the Wilson coefficients at the EWSB scale. The NP models are matched onto the low-scale operators by integrating out the heavy degrees of freedom, such as NP particles and heavy SM particles, W, Z, H and t , simultaneously. We call the matching scale as “EW matching scale”. The EW matching scale should be somewhere between the EWSB scale and the NP one. Since, however, absent discoveries of new particles at the LHC push the NP scale much higher than the EWSB one [4], an uncertainty of choosing the EW matching scale becomes large. The uncertainty of choosing the EW matching scale is the “matching scale uncertainty” in conventional evaluations. If the NP scale is not much far from the EWSB scale, the scale uncertainty does not become problem. Behind the conventional evaluations, it is assumed that the NP appear near the EWSB scale. However, experimental data may indicate much higher NP scale than the EWSB scale [4]. In the current perspective, it is important to investigate effects of the scale uncertainty.

The scale uncertainty mainly causes two problems. One is breaking down of the perturbation by the large, $\log M_{\text{NP}}/\mu_{\text{EW}}$. Because of this large log coming from the hierarchy between the NP scale, M_{NP} , and the EWSB one, μ_{EW} , one-loop calculations including the NP particles and

the SM ones become inappropriate, and higher order corrections of the perturbation cannot be negligible. Let us focus on the loop function $K(x_t, \mu_{\text{EW}})$ in Chapter 3, where μ_{EW} is the EW matching scale. The ratio of the loop function between the EWSB scale, $\mu_{\text{EW}} \simeq 80$ GeV, and the high energy scale, $M_{\text{NP}} = 10$ TeV, is estimated as $K(x_t, 10 \text{ TeV})/K(x_t, \mu_{\text{EW}}) \simeq 40$. This $\mathcal{O}(10)$ value mainly results from the large log in the loop function, $K(x_t, M_{\text{NP}})$. This large logarithm should be resummed by evolving the RGEs from M_{NP} to μ_{EW} .

Another problem is scale uncertainties in coupling constants such as the top Yukawa coupling and the QCD coupling. By the matching scale uncertainty, it is not clear in which energy scale the top mass and QCD coupling are evaluated. For example, the ratio of the top Yukawa coupling between the EWSB scale, $\mu_{\text{EW}} = 80$ GeV, and the high energy scale, $M_{\text{NP}} = 10$ TeV, is estimated as $y_t^2(80 \text{ GeV})/y_t^2(10 \text{ TeV}) \simeq 2$ in the $\overline{\text{MS}}$ scheme, which increases the scale uncertainty^{#1}.

Next, we move to our strategy for removing the scale uncertainty. In a word, our strategy is solving the renormalization group equations (RGEs) of the SMEFT [13–15] and using the one-loop matching formulae in Chapter 3. The above two problems coming from the EW matching scale uncertainty are resolved by the RGEs and the one-loop matching. Our strategy is divided into three processes. We describe the details for the each processes below.

1. *Matching at the NP scale.*— At the NP scale, the heavy NP particles are decoupled, and the NP models are matched onto the SMEFT. Without a hierarchy of mass scales between the NP particles, there does not exist uncertainty in the matching scale. Since, the hierarchy much depends on NP models, we do not discuss this effect in this thesis.
2. *Solving the RGEs in the SMEFT.*— The RGEs of the SMEFT are solved from the NP scale to the EWSB one. As results of the RGEs, the large log $M_{\text{NP}}/\mu_{\text{EW}}$ is resummed and the scale uncertainties in couplings disappear.
3. *Matching at the EWSB scale.*— At the EWSB scale, the heavy SM particles, such as W, Z, H and t , are decoupled, and the SMEFT are matched onto the LEFT summarized in Chapter 3. The EW matching scale dependences are also cancelled between the one-loop matching conditions and the SMEFT RGEs. Because of a small hierarchy of mass scales between the heavy SM particles, the uncertainty in this matching scale is small. See Chapter. 3 for the details.

Through these processes, the EW matching scale uncertainty is reduced, and two problems coming from the matching scale uncertainty are solved.

^{#1}This kind of uncertainty quite depends on the NP models. As discuss later, in the left-right symmetric model, this uncertainty of a leading contribution is accidentally cancelled by QCD RGEs in four-quark operators.

5.2 Scale Uncertainty in General Model

In this section, we investigate the EW matching scale uncertainty without specifying models. Based on the procedure in Sec. 5.1, we numerically analyze the EW matching scale uncertainty in the Wilson coefficients at the EWSB scale, m_W . Here, we emphasize that the EW matching scale uncertainty depends on the NP models. In general, Wilson coefficients at the NP scale depend on the top Yukawa and the QCD coupling, and the dependence is determined by specifying a NP model. Therefore, the scale uncertainty coming from evaluation scale of the coupling constants can not be included in this section. However, this model independent discussions are meaningful to understand effects of quantum corrections coming from the top Yukawa coupling above the EWSB scale.

Since, we are interested in estimations of $\Delta F = 2$ observables, we focus on the Wilson coefficients $(C_4)_{ij}(m_W)$. In this section, we numerically investigate the EW matching scale uncertainty in the Wilson coefficients $(C_4)_{ij}$ at the EWSB scale, m_W . As discussed in Chapter. 3, the NP contributions to $(C_4)_{ij}$ are expressed by the SMEFT coefficients, $(C_{qd}^{(8)})_{ijij}$, $(C_{ud}^{(8)})_{33ij}$, $(C_{qd}^{(8)})_{33ij}$, $(C_{qd}^{(8)})_{mjij}$ and $(C_{qd}^{(8)})_{imij}$, for $m = 1, 2, 3$. Here, it is noticed that at the EWSB scale, the SMEFT $\Delta F = 2$ coefficient, $(C_{qd}^{(8)})_{ijij}$, generates the low-scale one, $(C_4)_{ij}$, by the tree-level matching, and the others by the one-loop level one. Therefore, for a case that $(C_{qd}^{(8)})_{ijij}$ is generated at the NP scale, the top Yukawa corrections to $(C_4)_{ij}(m_W)$ are sub-leading contributions. On the other hand, for not the case, the top Yukawa corrections to $(C_4)_{ij}(m_W)$ are leading contributions, and the EW matching scale uncertainty becomes large. For simplicity, we consider a case where only one of the SMEFT coefficients takes a non-zero value at the NP scale, and the others are zero. In addition, we assume that the each SMEFT coefficient is set as $(C_{\text{SMEFT}}) = i/(M_{\text{NP}})^2$. We evaluate the Wilson coefficients $(C_4)_{ij}(m_W)$ by following three ways;

1. *SMEFT with RGEs.*— At the NP scale, M_{NP} , the SMEFT coefficient is set as $(C_{\text{SMEFT}}) = i/(M_{\text{NP}})^2$, and the RGEs are solved. At the W -boson mass scale m_W , the SMEFT coefficients are matched onto the Wilson coefficients $(C_4)_{ij}$.
2. *Conventional estimation 1.*— At the top quark mass scale m_t , the SMEFT coefficient is set as $(C_{\text{SMEFT}}) = i/(M_{\text{NP}})^2$, which is matched onto the Wilson coefficients $(C_4)_{ij}$ without the RGEs of the SMEFT. The QCD RGEs are solved from the top quark mass, m_t , to the W -boson one, m_W , and the Wilson coefficients $(C_4)_{ij}(m_W)$ is estimated.
3. *Conventional estimation 2.*— At the NP scale, M_{NP} , the SMEFT coefficient is set as $(C_{\text{SMEFT}}) = i/(M_{\text{NP}})^2$, which is matched onto the Wilson coefficient $(C_4)_{ij}$ without the RGEs of the SMEFT. The QCD RGEs are solved from the NP scale, M_{NP} to the W -boson one, m_W , and the Wilson coefficients $(C_4)_{ij}(m_W)$ is estimated.

Comparing these three estimations, we numerically analyze the EW matching scale uncertainty.

In Figs. 5.1-5.3, the Wilson coefficient, $(C_4)_{13}(m_W)$, is displayed as a function of the NP scale, M_{NP} , for each SMEFT coefficient. In the case for the Wilson coefficient $(C_{qd}^{(8)})_{1313}$, the top Yukawa corrections are sub-leading, and the scale uncertainty is also small. In order to investigate the differences of the *SMEFT with RGEs* from the *Conventional estimation 1,2* quantitatively, we define the difference as

$$\text{difference } (C_4) \equiv \frac{C_4(m_W)^{\text{SMEFT}} - C_4(m_W)^{\text{conventional}}}{C_4(m_W)^{\text{SMEFT}}}, \quad (5.1)$$

and the sub-leading top Yukawa corrections for $(C_{qd}^{(8)})_{1313}$ is displayed in the left panel of Figs. 5.2, which shows that the EW matching scale is $\mathcal{O}(1\%)$ for $(C_{qd}^{(8)})_{1313}$. The magnitude of the scale uncertainty roughly results from a form of the top Yukawa corrections, $y_t^2/(4\pi)^2 \log M_{\text{NP}}/m_W$.

In the other cases, the top Yukawa corrections are leading contributions to the $\Delta F = 2$ process, and the scale uncertainty is large. Fig. 5.2 and Fig. 5.3 show that the EW matching scale uncertainty is $\mathcal{O}(100\%)$. This is because $\Delta F = 1$ SMEFT operators contribute to the $\Delta F = 2$ processes only through the top Yukawa corrections. As the results, the magnitude of the scale uncertainty is roughly expressed as a form, $K(x_t, M_{\text{NP}})/K(x_t, m_W) \simeq 40$. Here, we emphasize that this large scale uncertainty represents the quantitative importance of the one-loop matching formulae. In the large NP scale than the EW one, the loop function coming from the matching formulae such as $K(x_t, \mu_W)$ is dominated by the large logarithm, which is also regarded as contributions from the tree-level matching. Therefore, the large scale uncertainty shows that the one-loop matching formulae quantitatively change evaluations based on the tree-level ones by $\mathcal{O}(10)\%$. Besides, some of plots show that $(C_4)_{13}$ for the *SMEFT with RGEs* can be zero because of an interference between the tree-level matching effects and the one-loop ones. We numerically confirmed that this behavior results from the RGEs effects.

5.3 Scale Uncertainty in the Left-Right Symmetric Models

In this section, as an application of our matching formulae, we investigate the EW matching scale uncertainty in the left-right symmetric models. In this model, at the tree-level, the SMEFT $\Delta F = 1$ flavor changing operators are generated, and the one-loop matching formulae in Chapter 3 are essential in the $\Delta F = 2$ processes at the EWSB scale.

5.3.1 Left-Right Symmetric Models

In this section, let us study left-right symmetric models to demonstrate the SMEFT corrections of the dynamical top quark as explored in Chapter. 3. In particular, we focus on the effects of the SMEFT $\Delta F = 1$ operators for the $\Delta F = 2$ transitions.

The left-right extension of the SM implements the parity violation in the weak interaction by spontaneously breaking the $\text{SU}(3)_C \times \text{SU}(2)_L \times \text{SU}(2)_R \times \text{U}(1)_{B-L}$ gauge symmetries [61–65].

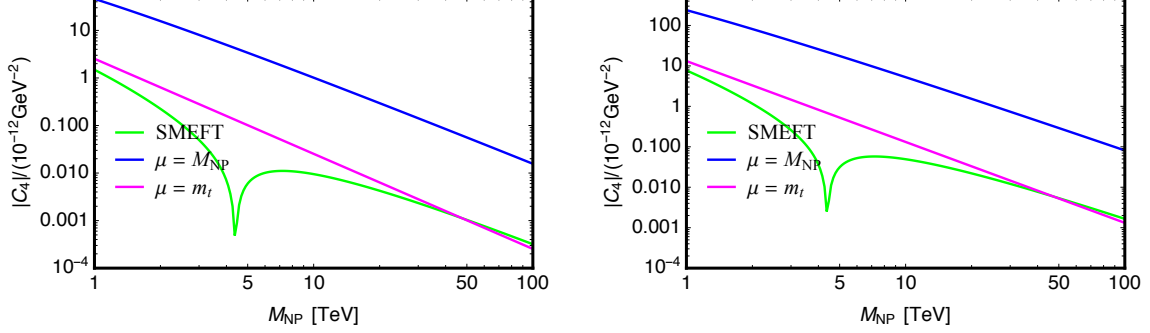


Figure 5.1: For the SMEFT coefficients, $(C_{qd}^{(8)})_{1113}$ (left) and $(C_{qd}^{(8)})_{1213}$ (right), the Wilson coefficient $(C_4)_{ij}(m_W)$ for ΔM_{B_d} are shown as a function of the NP scale, M_{NP} . Green, magenta and blue solid lines correspond to the three ways, *SMEFT with RGEs*, *Conventional estimation 1*, and *Conventional estimation 2*, respectively.

The new right-handed W boson generates FC charged currents in addition to the SM left-handed W boson. The quark interactions of the left- and right-handed W bosons are

$$\mathcal{L}_{\text{int}} = \frac{g_L}{\sqrt{2}}(V_L)_{ij}\bar{u}_i\gamma_\mu P_L d_j W_L^\mu + \frac{g_R}{\sqrt{2}}(V_R)_{ij}\bar{u}_i\gamma_\mu P_R d_j W_R^\mu + \text{h.c.}, \quad (5.2)$$

where the first term is for the SM W boson. The right-handed W boson, W_R , is obtained by replacing $L \leftrightarrow R$, in the second term. Here, the new coupling g_R and the mixing matrix V_R are introduced for W_R similarly to W_L .

The gauge symmetries are broken to $\text{SU}(3)_C \times \text{U}(1)_{em}$ by Higgs vacuum expectation values (VEVs). In the minimal setup, the VEV of the Higgs field, Δ_R , whose charges are $(\text{SU}(2)_L, \text{SU}(2)_R, \text{U}(1)_{B-L}) = (1, 3, -2)$, breaks the left-right symmetry, $\text{SU}(2)_L \times \text{SU}(2)_R \times \text{U}(1)_{B-L}$, to $\text{SU}(2)_L \times \text{U}(1)_Y$. The VEV of the Higgs bi-doublet, $\Phi \in (2, 2, 0)$, enables EWSB. On the other hand, the VEV of $\Delta_L \in (3, 1, 2)$ is assumed to be suppressed. The particle contents in the left-right symmetric model with charge symmetry are listed in Table 5.1

Their components are expressed as

$$\Delta_i = \begin{bmatrix} \Delta_i^+/\sqrt{2} & \Delta_i^{++} \\ \Delta_i^0 & -\Delta_i^+/\sqrt{2} \end{bmatrix} \quad (i = L, R), \quad \Phi = \begin{bmatrix} \phi_1^0 & \phi_2^+ \\ \phi_1^- & \phi_2^0 \end{bmatrix}. \quad (5.3)$$

The spontaneous symmetry breaking is achieved by the VEVs,

$$\langle \Delta_{L,R} \rangle = \frac{1}{\sqrt{2}} \begin{bmatrix} 0 & 0 \\ v_{L,R} & 0 \end{bmatrix}, \quad \langle \Phi \rangle = \frac{1}{\sqrt{2}} \begin{bmatrix} v \cos \beta & 0 \\ 0 & v \sin \beta e^{i\alpha} \end{bmatrix}. \quad (5.4)$$

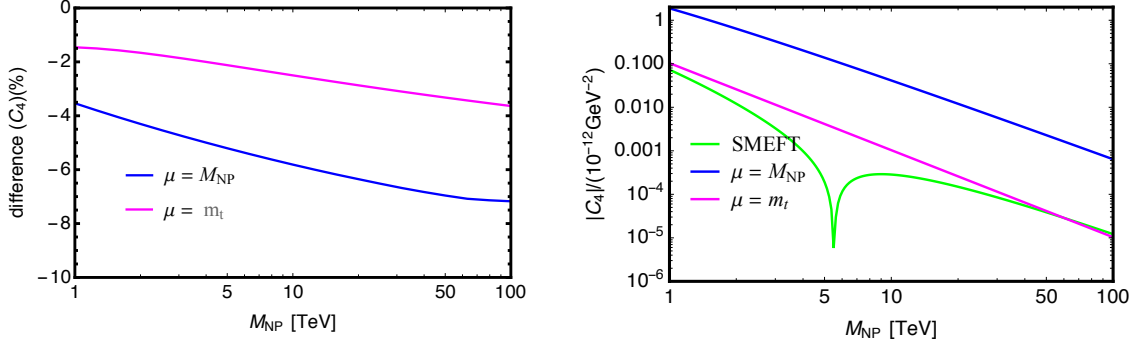


Figure 5.2: For the SMEFT coefficients, $(C_{qd}^{(8)})_{1313}$ (left) and $(C_{qd}^{(8)})_{2313}$ (right), the Wilson coefficient $(C_4)_{ij}(m_W)$ for ΔM_{B_d} are shown as a function of the NP scale, M_{NP} . Green, magenta and blue solid lines correspond to the three ways, *SMEFT with RGEs*, *Conventional estimation 1*, and *Conventional estimation 2*, respectively.

Table 5.1: Particle contents in the left-right symmetric model with charge symmetry.

Component fields	Gauge quantum numbers			
	$SU(3)_C$	$SU(2)_L$	$SU(2)_R$	$U(1)_{B-L}$
q_L^i	3	2	2	1/3
q_R^{ci}	$\bar{3}$	1	2	-1/3
l_L^i	1	2	1	-1
l_R^{ci}	1	1	2	1
Φ	1	2	2	0
Δ_L	1	3	1	2
Δ_R	1	1	3	-2

We impose a hierarchy among the Higgs VEVs, $v_R \gg v \cos \beta, v \sin \beta \gg v_L$, in order to be consistent with observed phenomena and to avoid fine-tunings in the scalar potential [66, 67]. An angle α is a spontaneous CP -violating phase. In addition to the QCD θ term, α induces the strong CP phase [68]^{#2}, which is severely constrained by the neutron electric dipole moment [39]. As we will see below, the following analysis is independent of α . The masses of the left and right-handed W bosons are approximately given by

$$M_{W_L}^2 \simeq \frac{g_L^2}{4} v^2, \quad M_{W_R}^2 \simeq \frac{g_R^2}{2} v_R^2, \quad (5.5)$$

for $v_R \gg v$ with $v \simeq 246$ GeV.

^{#2} See discussions in Refs. [69–71] for the strong CP problem with a generalized parity invariance \mathcal{P} .

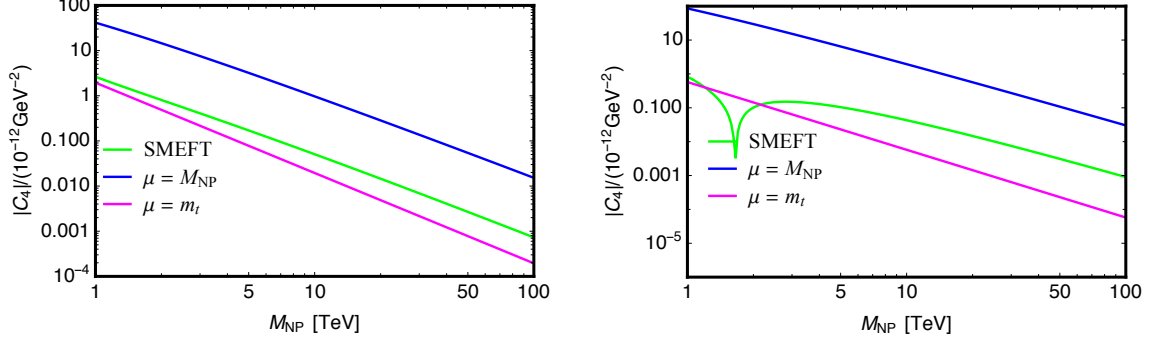


Figure 5.3: For the SMEFT coefficients, $(C_{qd}^{(8)})_{3313}$ (left) and $(C_{ud}^{(8)})_{3313}$ (right), the Wilson coefficient $(C_4)_{ij}(m_W)$ for ΔM_{B_d} are shown as a function of the NP scale, M_{NP} . Green, magenta and blue solid lines correspond to the three ways, *SMEFT with RGEs*, *Conventional estimation 1*, and *Conventional estimation 2*, respectively.

In addition to the W bosons, heavy Higgs bosons, H^0 and H^\pm , have FC couplings as

$$\begin{aligned}
 -\mathcal{L}_{\text{int}} \simeq & \frac{\sqrt{2}}{v \cos 2\beta} \left[\bar{d}(V_L^\dagger M_u V_R) P_R d H^0 + \bar{d}(V_R^\dagger M_u V_L) P_L d (H^0)^* \right. \\
 & \left. + \bar{u}(M_u V_R) P_R d H^+ + \bar{d}(V_R^\dagger M_u) P_L u H^- \right], \quad (5.6)
 \end{aligned}$$

with $H^0 = \cos \beta \phi_2^0 - \sin \beta e^{i\alpha} (\phi_1^0)^*$ and $H^+ = \cos \beta \phi_2^+ + \sin \beta e^{i\alpha} \phi_1^+$. Here, $v_R \gg v$ is assumed, and the up-type quark masses is $M_u = \text{diag}(m_u, m_c, m_t)$. The masses of the heavy Higgs bosons, $M_H \equiv \sqrt{\alpha_3} v_R / \sqrt{2 \cos 2\beta}$, are almost proportional to v_R . The parameter α_3 comes from the Higgs potential. The Higgs potential in the limit of $v_R \gg v$ is given in Appendix B.1.

The right-handed W boson and the heavy neutral Higgs boson, as well as the SM (left-handed) W boson, induce $\Delta F = 2$ transitions [72, 73]. They are severely constrained by the observed meson oscillations. First of all, let us briefly overview the conventional approach. In literature, the Wilson coefficients of the low-scale operators in Eq. (3.1) are set by integrating out W_R and H^0 as well as W_L and the up-type quarks [74, 75]:

$$(C_4)_{ij}^{H\text{-tree}} = -\frac{2\sqrt{2}G_F}{\cos^2 2\beta} \sum_{k,l} \frac{m_{u_k} m_{u_l}}{M_H^2} (\lambda^{LR})_k^{ij} (\lambda^{RL})_l^{ij}, \quad (5.7)$$

$$(C_4)_{ij}^{W_L-W_R} = \frac{g_L^2 g_R^2}{16\pi^2} \sum_{k,l} \frac{m_{u_k} m_{u_l}}{M_{W_L}^2 M_{W_R}^2} (\lambda^{LR})_k^{ij} (\lambda^{RL})_l^{ij} \mathcal{F}_A(x_k, x_l, \beta), \quad (5.8)$$

$$(C_4)_{ij}^{H\text{-s.e.}} = -\frac{g_L^2 g_R^2}{128\pi^2} \sum_{k,l} \frac{m_{u_k} m_{u_l}}{M_{W_L}^2 M_{W_R}^2} (\lambda^{LR})_k^{ij} (\lambda^{RL})_l^{ij} \mathcal{F}_B(\tau_L, \tau_R), \quad (5.9)$$

$$(C_4)_{ij}^{H\text{-vert.}} = -\frac{g_L^2 g_R^2}{16\pi^2} \sum_{k,l} \frac{m_{u_k} m_{u_l}}{M_{W_L}^2 M_{W_R}^2} (\lambda^{LR})_k^{ij} (\lambda^{RL})_l^{ij} \mathcal{F}_C(\tau_k, \tau_l, \tau_L, \tau_R), \quad (5.10)$$

where the parameters are defined as

$$\begin{aligned} (\lambda^{LR})_k^{ij} &\equiv (V_L^*)_{ki} (V_R)_{kj}, \quad x_k \equiv \frac{m_{u_k}^2}{M_{W_L}^2}, \\ \beta &\equiv \frac{M_{W_L}^2}{M_{W_R}^2}, \quad \tau_L \equiv \frac{M_{W_L}^2}{M_H^2}, \quad \tau_R \equiv \frac{M_{W_R}^2}{M_H^2}, \quad \tau_k \equiv \frac{m_{u_k}^2}{M_H^2}, \end{aligned} \quad (5.11)$$

and $(\lambda^{RL})_k^{ij}$ is given by replacing $L \leftrightarrow R$ in $(\lambda^{LR})_k^{ij}$. Here, the indices k, l are the up-type quark flavor, and the definitions of the loop functions $\mathcal{F}_A, \mathcal{F}_B$ and \mathcal{F}_C are summarized in Appendix B.2.^{#3}

Among the Wilson coefficients, the tree-level contribution, $(C_4)^{H\text{-tree}}$, is obtained by exchanging the heavy neutral Higgs boson. The one-loop contributions, $(C_4)^{H\text{-s.e.}}$ and $(C_4)^{H\text{-vert.}}$, are given by self-energy (s.e.) and vertex (vert.) corrections to the tree-level heavy neutral Higgs diagram, respectively. Here, the on-shell renormalization scheme is applied [74]. On the other hand, the one-loop contribution $(C_4)^{W_L\text{-}W_R}$ comes from a box diagram where both the left- and right-handed W bosons as well as the up-type quarks are exchanged.^{#4} It is important that $(C_4)^{W_L\text{-}W_R}$ itself depends on a choice of the gauge fixing. Here and hereafter, the Feynman-'t Hooft gauge is used. The gauge invariance of the transition amplitude is guaranteed by adding the one-loop neutral Higgs contributions, $(C_4)^{H\text{-s.e.}}$ and $(C_4)^{H\text{-vert.}}$ [74, 76–78].

In the conventional calculation (Ref. [75] as a representative case), after the above Wilson coefficients are set, the RGEs for the low-scale operators are solved [31]. However, it is noticed that the one-loop diagrams include the left-handed W boson and the up-type quarks, which are much lighter than the right-handed W and heavy Higgs bosons for, e.g., the LHC constraints [4, 79]. Hence, it is uncertain in which energy scale the Wilson coefficients should be input. Moreover, the heavy charged Higgs boson contributes to the $\Delta F = 2$ transitions through box diagrams with the SM W boson and the up-type quarks. Although the contribution is often neglected in the literature (see Ref. [78] for an early work), it may be comparable to $(C_4)^{H\text{-s.e.}}$ and $(C_4)^{H\text{-vert.}}$. Since the SM W boson and the up-type quarks are much lighter than the heavy charged Higgs boson, the scale uncertainty problem arises similarly to the above. In the next section, we study the $\Delta F = 2$ processes in left-right symmetric models by the procedure explored in Chapter. 3.

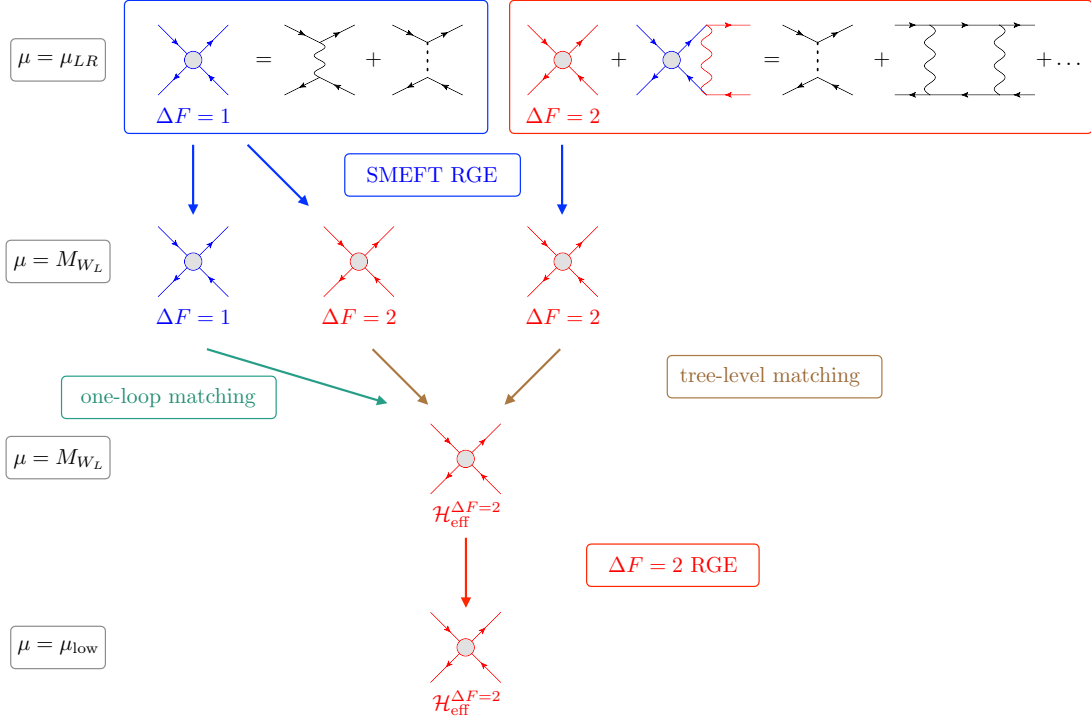


Figure 5.4: Schematic figure for the SMEFT framework in the left-right symmetric model.

5.3.2 Matching Scale Uncertainty

In this section, we focus on the top quark contribution coming from the one-loop matching conditions in Chapter 3. First of all, let us summarize the analysis procedure in Fig. 5.4. At the decoupling scale of the left-right symmetry (μ_{LR}), the Wilson coefficients in the SMEFT are evaluated. In addition to the $\Delta F = 2$ operators (the red colored diagrams in Fig. 5.4), there are $\Delta F = 1$ top-quark operators which eventually contribute to the $\Delta F = 2$ transitions (the blue colored diagrams). After solving the SMEFT RGEs, they are matched onto the low-scale operators at the EWSB scale, where we need to take account of the one-loop level matching condition. Below the EWSB scale, we follow the standard procedure for the $\Delta F = 2$ observables.

First, let us consider the matching condition of the SMEFT at $\mu = \mu_{LR}$ (the first line in the Fig. 5.4). At the tree level, one obtains the following $\Delta F = 1$ SMEFT operators at the dimension six after integrating out W_R ,

$$(C_{ud}^{(8)})_{33ij}^{\text{tree}} = -\frac{g_R^2}{M_{W_R}^2} (V_R^\dagger)_{i3} (V_R)_{3j}, \quad (5.12)$$

$$(C_{ud}^{(1)})_{33ij}^{\text{tree}} = \frac{1}{2N_c} (C_{ud}^{(8)})_{33ij}. \quad (5.13)$$

^{#3} Our results in Eqs. (5.9) and (5.10) are smaller than the result of Ref. [75] by a factor of 2.

^{#4} If W_R and H are sufficiently heavier than W_L , the W_R - W_R box contribution is much smaller than the W_L - W_R box one.

In addition, by exchanging the heavy neutral and charged Higgs bosons, we obtain the following $\Delta F = 1$ operators,

$$(C_{qd}^{(8)})_{33ij}^{\text{tree}} = -\frac{2\sqrt{2}G_F m_t^2}{\cos^2 2\beta M_H^2} (V_R^\dagger)_{i3} (V_R)_{3j}, \quad (5.14)$$

$$(C_{qd}^{(1)})_{33ij}^{\text{tree}} = \frac{1}{2N_c} (C_{qd}^{(8)})_{33ij}. \quad (5.15)$$

The details of the calculations are found in Appendix B.1. On the other hand, the $\Delta F = 2$ SMEFT operators are derived at the tree level from the exchange of the heavy neutral Higgs bosons as

$$(C_{qd}^{(8)})_{ijij}^{\text{tree}} = -\frac{2\sqrt{2}G_F m_t^2}{\cos^2 2\beta M_H^2} (\lambda^{LR})_t^{ij} (\lambda^{RL})_t^{ij}, \quad (5.16)$$

$$(C_{qd}^{(1)})_{ijij}^{\text{tree}} = \frac{1}{2N_c} (C_{qd}^{(8)})_{ijij}. \quad (5.17)$$

All the above tree-level Wilson coefficients are evaluated at $\mu = \mu_{LR}$.

As for the one-loop level matching, the self-energy and vertex corrections of the heavy neutral Higgs discussed above contribute to the $\Delta F = 2$ Wilson coefficients. Besides, in discussing the W_L - W_R box contributions, one needs to avoid double counting from the one-loop contribution with $(C_{ud}^{(8)})_{33ij}$, where the top-quark loop is enclosed by the SM W boson. The result is obtained as

$$(C_{qd}^{(8)})_{ijij}^{1\text{-loop}} = \frac{g_L^2 g_R^2 m_t^2}{16\pi^2 M_{W_L}^2 M_{W_R}^2} (\lambda^{LR})_t^{ij} (\lambda^{RL})_t^{ij} \left[\mathcal{F}_A(x_t, x_t, \beta) - \frac{1}{8} \mathcal{F}_B(\tau_L, \tau_R) - \mathcal{F}_C(\tau_t, \tau_t, \tau_L, \tau_R) \right] \\ + \frac{g_L^2 g_R^2}{4\pi^2 M_{W_R}^2} (\lambda^{LR})_t^{ij} (\lambda^{RL})_t^{ij} I_1(x_t, \mu_{LR}), \quad (5.18)$$

$$(C_{qd}^{(1)})_{ijij}^{1\text{-loop}} = \frac{1}{2N_c} (C_{qd}^{(8)})_{ijij}, \quad (5.19)$$

where the second term of $C_{qd}^{(8)}$ stands for the subtraction to avoid the double counting. We can see that the μ_{LR} dependence in $(C_{qd}^{(8)})_{ijij}^{1\text{-loop}}$ is dropped when the scale is set to be $\mu_{LR} = M_{W_R}$. In addition, the one-loop matching condition that comes from the H^\pm and W_L box diagrams is obtained as

$$(C_{qd}^{(8)})_{ijij}^{1\text{-loop}} = \frac{\sqrt{2}G_F}{\pi^2} \frac{g_L^2}{\cos^2 2\beta} \frac{m_t^2}{M_H^2} (\lambda^{LR})_t^{ij} (\lambda^{RL})_t^{ij} \left[\frac{1}{16} \mathcal{F}_D(x_t, x_t, \tau_L) + J(x_t) \right], \quad (5.20)$$

$$(C_{qd}^{(1)})_{ijij}^{1\text{-loop}} = \frac{1}{2N_c} (C_{qd}^{(8)})_{ijij}, \quad (5.21)$$

where the loop function \mathcal{F}_D defined in Appendix B.2 comes from H^\pm - W_L box diagrams, whose result is consistent with that in Ref. [78]. The contribution $J(x_t)$ is from the subtraction to avoid the double counting in similar to the W_R case. All the above Wilson coefficients for the one-loop level matching conditions are evaluated at $\mu = \mu_{LR}$.

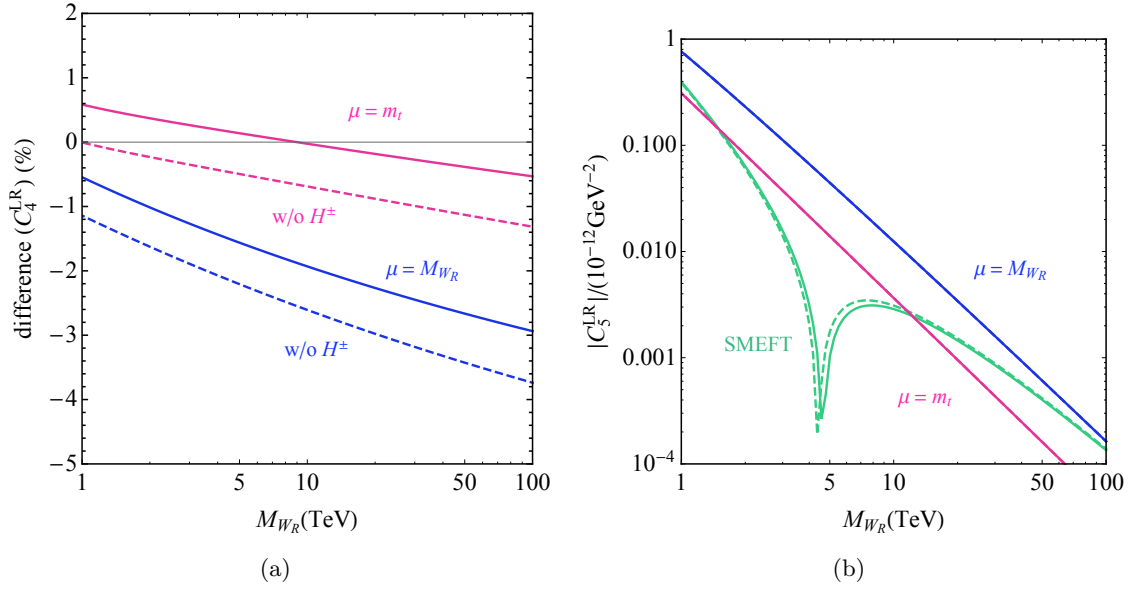


Figure 5.5: The low-scale Wilson coefficients $C_4(M_{W_L})$ (left) and $C_5(M_{W_L})$ (right) for ΔM_{B_s} in comparison with the conventional results. In the conventional approach, the Wilson coefficients, (5.7)–(5.10), are input at $\mu = M_{W_R}$ (blue) and m_t (magenta). The dashed lines do not include the contribution from the heavy charged Higgs boson.

After setting the Wilson coefficients for the dimension-six SMEFT operators at the scale $\mu = \mu_{LR}$, the SMEFT RGEs are solved to the EWSB scale, for which we choose $\mu = M_{W_L}$ (the second line in the Fig. 5.4). The one-loop level RGEs are summarized in Appendix A.1. At the EWSB scale, the SMEFT operators are matched onto the low-scale ones (the third line). The tree-level and one-loop level matching conditions are found in Eqs. (3.12)–(3.15) and Eqs. (3.16)–(3.18), respectively. After the EWSB matching, the calculations are performed as usual, i.e., in the same way as the conventional approach, which was defined in the previous section.

The differences of our analysis from the conventional one are the SMEFT top-quark effects and the heavy charged Higgs boson contributions. In order to investigate their effects quantitatively, we consider the $\Delta B = 2$ process, ΔM_{B_s} ^{#5}. Similar to the previous section, let us define the difference as

$$\text{difference}(X) \equiv \frac{X^{\text{SMEFT}} - X^{\text{conventional}}}{X^{\text{SMEFT}}} \quad \text{for } X = C_i(M_{W_L}), \Delta M_{B_s}, \quad (5.22)$$

where $C_i(M_{W_L})$ is the low-scale Wilson coefficients at the EWSB scale for ΔM_{B_s} , i.e., $i = 3$ and $j = 2$ in Eq. (3.1). X^{SMEFT} and $X^{\text{conventional}}$ represent the *SMEFT with RGEs* and the *Conventional estimation 1,2*, respectively. In the numerical analysis, we take $\tan \beta = m_b/m_t$,

^{#5}In the left-right symmetric models with the generalized charge symmetry \mathcal{C} , CP conserving mixing observables, such as ΔM_K and ΔM_{B_q} play important role. This is because, when additional phases θ_i for $i = u, c, t, d, s, b$ become zero, the coefficient C_4 takes real value, which escape from constraints from the CP violating observables, such as ϵ_K , $S_{\psi K_S}$ and $S_{\psi\phi}$.

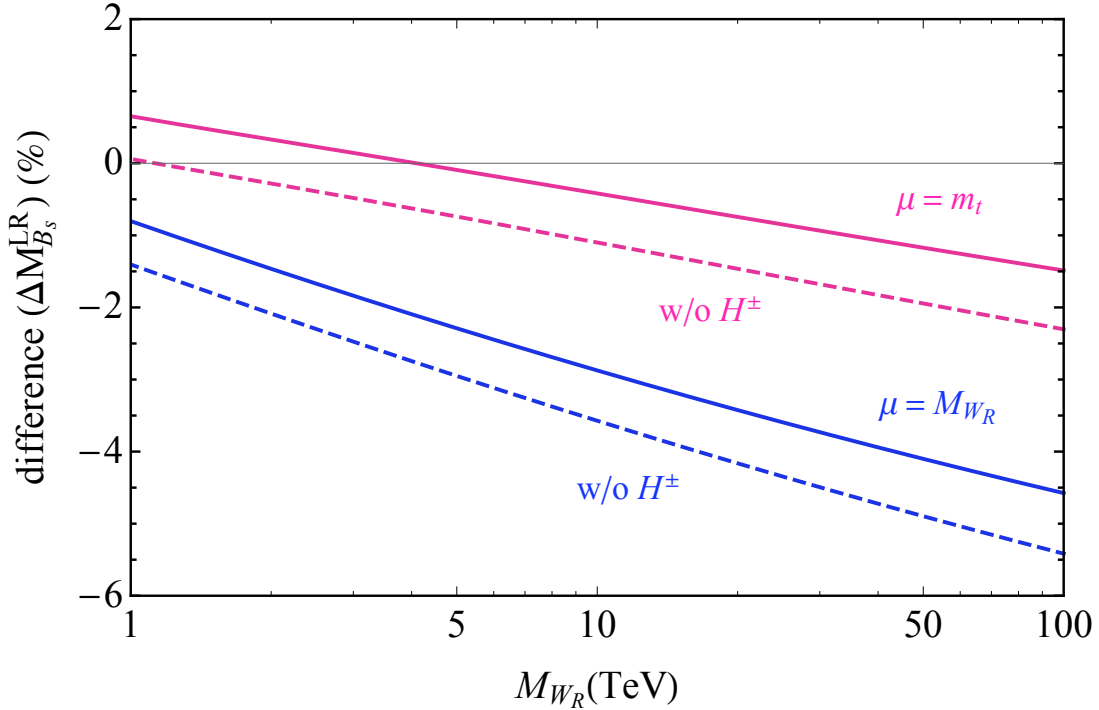


Figure 5.6: ΔM_{B_s} in comparison with the conventional results at $\mu = M_{W_R}$ (blue) and m_t (magenta). The dashed lines do not include the contribution from the heavy charged Higgs boson.

which naturally gives the fermion mass hierarchy $m_t \gg m_b$. The mass and scale are set as $M_H = 6M_{W_R}$ and $\mu_{LR} = M_{W_R}$, respectively. Also, we impose a generalized charge conjugation symmetry \mathcal{C} , which leads to $g_R = g_L$ and $V_R = K_u V_L^* K_d$ and $K_u = \text{diag}(e^{i\theta_u}, e^{i\theta_c}, e^{i\theta_t})$, $K_d = \text{diag}(e^{i\theta_d}, e^{i\theta_s}, e^{i\theta_b})$ [68, 75, 79]. In the evaluation of ΔM_{B_s} , the lattice results [33] are applied for B -parameters. We also use the RunDec program [80] for evaluating the running top quark masses.

In Fig. 5.5(a), the difference of $C_4(M_{W_L})$ is shown. The magenta and blue solid lines correspond to the *Conventional estimation 1* and *2*, respectively, where choices of the input scale of the Wilson coefficients are different. Since it is uncertain in which energy scale the Wilson coefficients should be input, we set Eqs. (5.7)–(5.10) at $\mu = M_{W_R}$ (blue) or at $\mu = m_t$ (magenta), and then, perform the low-scale RGEs to the lower scale. For instance, $\mu = m_t$ is chosen in Ref. [75]. It is found that the difference is less than three percents^{#6} below $\mu_{LR} = 100$ TeV. Although $\mu = m_t$ seems to be favored for the conventional result, the deviation is enhanced as μ_{LR} increases. Since the left-right symmetric model corresponds to the case where the tree-level

^{#6}In the left-right symmetric model, the coefficient, C_4 is proportional to a square of the top quark mass, and it seems that the scale uncertainty coming from the top Yukawa coupling becomes $\mathcal{O}(100\%)$. However, a cancellation between the QCD RGEs of C_4 and the top Yukawa QCD running occurs, and the scale uncertainty becomes small.

matching contributions at the NP scale, this numerical results are consistent with the previous ones.

Our analysis include both the top-quark effect and the heavy charged Higgs boson contribution. In order to investigate them individually, we show the results without introducing the latter contribution (dashed lines). Hence, in Fig. 5.5(a), the deviations of the dashed lines from zero are due to the SMEFT top-quark effects explored in Chapter. 3. It is found that the effects are less than four percents for $\mu_{LR} < 100$ TeV. Also, the difference between the solid and dashed lines comes from the the heavy charged Higgs contribution. We confirm that it is about one percent level and is comparable to the one-loop contributions, $(C_4)^{H\text{-s.e.}}$ and $(C_4)^{H\text{-vert.}}$, in the Feynman-'t Hooft gauge. The difference between the lines is insensitive to M_{W_R} , because the box contribution in Eq. (5.20), i.e., the \mathcal{F}_D term, dominates the total charged Higgs effects.

In Fig. 5.5(b), $C_5(M_{W_L})$ is displayed. The magenta and blue solid lines correspond to $\mu = M_{W_R}$ and $\mu = m_t$ for the conventional approach, respectively. In this case, C_5 is zero at the input scale and generated by C_4 through the RGEs down to $\mu = M_{W_L}$. The dependence of C_5 on M_{W_R} is thus from that of C_4 . The conventional analyses are compared with our SMEFT and H^\pm results (green). The difference between the solid and dashed lines comes from the heavy charged Higgs boson, which is shown to be sub-leading similarly to the above case of C_4 . We found that $C_5(M_{W_L})$ depends heavily on M_{W_R} and can be deviated from the conventional results by hundred percents. The result of the SMEFT deviates from the conventional cases by $\mathcal{O}(100\%)$ because of the RGEs evolution.^{#7}

In Fig. 5.6, the difference of ΔM_{B_s} is shown. Since it is dominated by C_4 at lower scales quantitatively, the result becomes similar to the one in Fig. 5.5(a). It is seen that the SMEFT and charged Higgs effects are less than five percents for $\mu_{LR} < 100$ TeV and are enhanced in larger μ_{LR} . We also checked that these results are unchanged by a choice of θ_q . Also, we can derive the same conclusions for ΔM_{B_d} as ΔM_{B_s} .

Before closing this section, let us comment on the charm-quark contribution. In the analysis, we focused on the top-quark contributions in the box diagrams and kept the charm-quark ones aside. This approximation is appropriate in the $B_{s,d}$ meson system. However, they are dominant in the K meson system, e.g., for ϵ_K in the left-right symmetric model [75]. Then, the SMEFT and charged Higgs corrections explored in this thesis become necessary, and long-distance effects should be taken into account. This topic will be studied in the future.

5.4 Conclusion of Matching Scale Uncertainty

Since the experimental constraints push the NP scale higher, the NP particle masses are likely to be much larger than the SM ones, i.e., the EWSB scale. Then, FCNC amplitudes should be investigated in the framework of the SMEFT rather than the LEFT. In a class of the NP

^{#7}We confirmed that this behavior of the curve does not occur within the leading-log approximation.

models, both of the NP and SM particles contribute to a loop diagram simultaneously. In order to reduce the uncertainty of the input scale of the Wilson coefficients particularly in such models, we studied the SMEFT corrections, paying attention to the top-quark effects. For the FCNC observables, the operator matching needs to be performed at the one-loop level, because the NP contributions are evaluated at the one-loop level. By using the complete one-loop matching formula for $\Delta F = 2$ transitions in Chapter 3, we discuss the matching scale uncertainty in the Wilson coefficients for $\Delta F = 2$ processes. We found that if the top Yukawa correction is a sub-leading contribution, the scale uncertainty is $\mathcal{O}(1)\%$, and otherwise, that is $\mathcal{O}(100)\%$. As mentioned in Section 5.2, these results represent that the one-loop matching formulae change the tree-level matching evaluations by $\mathcal{O}(10)\%$, which show quantitative importance of the one-loop matching formulae.

Besides, we investigated ΔM_{B_s} in the left-right symmetric models. The right-handed W boson generates the flavor transitions similarly to the left-handed one in the SM. The SMEFT corrections are studied and compared with the conventional results. We found that the Wilson coefficient C_4 is affected by $\mathcal{O}(1)\%$ and C_5 by $\mathcal{O}(100)\%$. Since the observable ΔM_{B_s} is dominated by the former quantitatively, the SMEFT effects for ΔM_{B_s} become comparable to the result in C_4 . In addition to the SMEFT effects, we discussed the contribution of the heavy charged Higgs boson. Although it can be comparable to the one-loop corrections to the heavy neutral Higgs boson contribution, which are necessary for the gauge invariance, the effect has often been neglected in the literature. It was found that the relative contribution is about one percent level and almost independent of M_{W_R} .

Although the difference between our and conventional results becomes smaller if $\mu = m_t$ is chosen for ΔM_{B_s} in the left-right symmetric models, the deviation becomes enhanced as μ_{LR} increases. In order to clarify in which energy scale the Wilson coefficients should be input, it is important to take account of the SMEFT RGEs and matching conditions for the NP models in high scales.

The results of this chapter show that the SMEFT evaluations based on the one-loop matching formulae provided in Chapter 3 are qualitatively and quantitatively essential in order to reduce the scale uncertainty.

Z mediated correction to flavor changing observable

This chapter is based on the work by the author [16, 81]. We evaluate the SMEFT corrections to flavor changing observables with particular emphasis on the Z mediated corrections. Through the Z boson, $\Delta F = 2$ observables are correlated with $\Delta F = 1$ ones. In Section 6.1, we explain the Z mediated SMEFT corrections. In Section 6.2, as an application of the scenario, we investigate the correlations between the $\Delta S = 2$ observables and the $\Delta S = 1$ ones in a model independent way. In Section 6.3, we focus on a specific scenario in the MSSM and investigate the effects of the Z mediated SMEFT corrections to the $\Delta S = 2$ observables. We show that the Z mediated SMEFT corrections by the right-handed NP effects generated by O_{Hd} can make experimental constraints coming from the $\Delta S = 2$ observables significantly severer.

6.1 Z mediated SMEFT correction

In this Chapter, we focus on the phenomenology of the SMEFT $\Delta F = 1$ operators, especially $\mathcal{O}_{Hq}^{(1,3)}$ and \mathcal{O}_{Hd} . These operators include the Z boson in the covariant derivative, and $\Delta F = 1$ and 2 observables are correlated each other by mediating the Z boson. Since, in particular, the $\Delta F = 2$ processes are generated at the one-loop level, it is important to carefully evaluate the gauge invariance in the processes. In fact, it was proved that the gauge invariance in the $\Delta F = 2$ processes are retained by including contributions from the Nambu-Goldstone boson of the SMEFT operators [20]. Therefore, in order to evaluate the NP effects in $\Delta F = 2$ processes mediated by the Z boson, it is qualitatively essential to follow the SMEFT framework. This Chapter is devoted to investigate quantitative importances of the Z mediated SMEFT corrections. In this section, we define the Z mediated SMEFT corrections, which are appropriately included in our matching formulae in Chapter 3.

Let us focus on the $\Delta F = 1$ SMEFT operators:

$$(\mathcal{O}_{Hq}^{(1)})_{ij} = (H^\dagger i \overleftrightarrow{D}_\mu H)(\bar{q}^i \gamma^\mu q^j), \quad (6.1)$$

$$(\mathcal{O}_{Hq}^{(3)})_{ij} = (H^\dagger i \overleftrightarrow{D}_\mu^I H)(\bar{q}^i \gamma^\mu \tau^I q^j), \quad (6.2)$$

$$(\mathcal{O}_{Hd})_{ij} = (H^\dagger i \overleftrightarrow{D}_\mu H)(\bar{d}^i \gamma^\mu d^j). \quad (6.3)$$

Above the EWSB scale, NP contributions are encoded to the following interactions:

$$\mathcal{L}_{\text{SMEFT}} \supset (C_{Hq}^{(1)})_{ij} (\mathcal{O}_{Hq}^{(1)})_{ij} + (C_{Hq}^{(3)})_{ij} (\mathcal{O}_{Hq}^{(3)})_{ij} + (C_{Hd})_{ij} (\mathcal{O}_{Hd})_{ij}. \quad (6.4)$$

After the EWSB, they generate the flavor-changing Z interactions of down-type quark:

$$\begin{aligned} \mathcal{L}_{\text{SMEFT}} \supset \Delta_{L,ij}^{\text{NP}} \left[Z_\mu + \frac{1}{m_Z} \partial_\mu G^0 - \frac{ig}{2m_W m_Z} G^- \overleftrightarrow{\partial}_\mu G^+ - \frac{g}{m_Z} (W_\mu^- G^+ + W_\mu^+ G^-) \right] (\bar{d}^i \gamma^\mu P_L d^j) \\ + (L \leftrightarrow R) + \text{h.c.} \end{aligned} \quad (6.5)$$

where $G^{0,\pm}$ is the Nambu-Goldstone boson, and the coefficients are defined as

$$\Delta_{L,ij}^{\text{NP}} = \frac{g_Z}{2} v^2 \left(C_{Hq}^{(1)} + C_{Hq}^{(3)} \right)_{ij}, \quad (6.6)$$

$$\Delta_{R,ij}^{\text{NP}} = \frac{g_Z}{2} v^2 (C_{Hd})_{ij}, \quad (6.7)$$

with $g_Z = \sqrt{g_2^2 + g_1^2}$. Thus, after the EWSB, the SMEFT operators, $(\mathcal{O}_{Hq}^{(1)})_{ij}$, $(\mathcal{O}_{Hq}^{(3)})_{ij}$ and $(\mathcal{O}_{Hd})_{ij}$, generate the Z mediated NP effects. In this thesis, we call their effects as “ Z mediated SMEFT corrections”.

As discussed in Chapter 3, by decoupling W , Z , H and t , the SMEFT $\Delta F = 1$ operators contribute to $\Delta F = 2$ processes as following

$$\begin{aligned} (C_1)_{ij}^{1\text{-loop}} &= \frac{\alpha \lambda_t^{ij}}{\pi s_W^2} (C_{Hq}^{(1)})_{ij} I_1(x_t, \mu_W) \\ &\quad - \frac{\alpha \lambda_t^{ij}}{\pi s_W^2} (C_{Hq}^{(3)})_{ij} I_2(x_t, \mu_W) + \frac{\alpha \lambda_t^{ij}}{4\pi s_W^2} \sum_{m=1}^3 \left[\lambda_t^{im} (C_{Hq}^{(3)})_{mj} + (C_{Hq}^{(3)})_{im} \lambda_t^{mj} \right] S_0(x_t), \end{aligned} \quad (6.8)$$

$$(C_5)_{ij}^{1\text{-loop}} = -\frac{2\alpha \lambda_t^{ij}}{\pi s_W^2} (C_{Hd})_{ij} I_1(x_t, \mu_W). \quad (6.9)$$

These matching formulae correspond to the Z mediated SMEFT corrections to $\Delta F = 2$ processes, which are consistent with [20, 21]. These effects were overlooked in the literature [41, 82–84]. Here, it is notice that the loop function, $I_1(x_t, \mu_W)$, includes the logarithm, $\ln \mu_W/m_W$. Therefore, by choosing the matching scale, μ as the NP scale, M_{NP} , we can include the leading SMEFT RGEs effects.

6.2 SMEFT correction in general Z model

In this section, we investigate the Z mediated SMEFT corrections to $\Delta F = 2$ observables without specifying a model. Based on the formulae in Sec. 6.1, we numerically estimate the $\Delta F = 2$ observables with particular emphasis on the kaon system. We also discuss correlations between the $\Delta S = 2$ observables and the $\Delta S = 1$ ones within the framework of the SMEFT.

For simplicity, we consider the following three scenarios,

1. $C_{Hq}^{(1)}$ scenario.— The coefficients, $C_{Hq}^{(3)}$ and C_{Hd} , are set as zero. At the NP scale, $M_{\text{NP}} = 1$ TeV, the coefficient $C_{Hq}^{(1)}$ is set as $C_{Hq}^{(1)} = C/(1 \text{ TeV})^2$, and the dimensionless complex parameter C is scanned. In this scenario, the Z mediated correction generates the $(C_1)_{ij}$ operator below the EWSB scale.

2. $C_{Hq}^{(3)}$ scenario.— The coefficients, $C_{Hq}^{(1)}$ and C_{Hd} are set as zero. At the NP scale, $M_{\text{NP}} = 1$ TeV, the coefficient $C_{Hq}^{(3)}$ is set as $C_{Hq}^{(3)} = C/(1 \text{ TeV})^2$, and the dimensionless complex parameter C is scanned. Similar to the $C_{Hq}^{(1)}$ scenario, the coefficient, $(C_1)_{ij}$ is generated below the EWSB scale.
3. C_{Hd} scenario.— The coefficients, $C_{Hq}^{(1)}$ and $C_{Hq}^{(3)}$ are set as zero. At the NP scale, $M_{\text{NP}} = 1$ TeV, the coefficient C_{Hd} is set as $C_{Hd} = C/(1 \text{ TeV})^2$, and the dimensionless complex parameter C is scanned. In this scenario, the Z mediated correction generate the $(C_5)_{ij}$ operator below the EWSB scale.

In this Chapter, by choosing μ_W as $M_{\text{NP}} = 1$ TeV, we consider the leading SMEFT RGEs effects.

For the each scenario, we study correlations between a $\Delta S = 2$ observable and $\Delta S = 1$ ones in the kaon system. As the $\Delta S = 2$ and $\Delta S = 1$ observables, we consider ϵ_K , ϵ'/ϵ_K , $\mathcal{B}(K_L \rightarrow \pi^0 \nu \bar{\nu})$, $\mathcal{B}(K^+ \rightarrow \pi^+ \nu \bar{\nu})$, $\mathcal{B}(K_L \rightarrow \mu^+ \mu^-)$ and $\mathcal{B}(K_S \rightarrow \mu^+ \mu^-)$. In Fig. 6.1 and Fig. 6.2, the correlations are shown. In Fig. 6.1, the observables are displayed by contour plots on $\text{Re } C - \text{Im } C$ plane, where the left and right panels correspond to the $C_{Hq}^{(1)}$ and $C_{Hq}^{(3)}$ scenario, respectively. Although both of the $C_{Hq}^{(3)}$ and $C_{Hq}^{(1)}$ scenarios generate only the $(C_1)_{12}$ operator, the coefficient $C_{Hq}^{(3)}$ is more severely constrained from ϵ_K than the $C_{Hq}^{(1)}$. This is because a ratio of the loop function $|I_2(x_t, \mu_W)/I_1(x_t, \mu_W)| \simeq 4$. In both of the above scenarios, the constraint from ϵ_K is smaller than the $\Delta S = 1$ observables. Similarly, in Fig. 6.2, the C_{Hd} scenario is displayed. The black and red dotted contours represent $\mathcal{B}(K_L \rightarrow \pi^0 \nu \bar{\nu})/\mathcal{B}(K_L \rightarrow \pi^0 \nu \bar{\nu})_{\text{SM}}$ and $\mathcal{B}(K^+ \rightarrow \pi^+ \nu \bar{\nu})/\mathcal{B}(K^+ \rightarrow \pi^+ \nu \bar{\nu})_{\text{SM}}$, respectively. In all scenarios, the constraints from $\mathcal{B}(K_S \rightarrow \mu^+ \mu^-)$ is weaker than the others, and the entire parameter regions in Fig. 6.1 and Fig. 6.2 are allowed. Besides, it becomes clear that the constraint from ϵ_K is not negligible in all scenarios. In particular, in the C_{Hd} scenario, the constraint is essential because of the chiral enhancement. Here, it is remarkable that the constraint from ϵ_K is appropriately taken into account by the one-loop matching conditions in Chapter 3, and the NP effects encoded in C_{Hd} are severely constrained. This is one of the result that the SMEFT effects is not negligible.

Although, in this section, we discussed the Z mediated corrections in the kaon system, those in the B meson systems were also discussed in [20].

6.3 Z mediated correction in the Minimal Supersymmetric Standard Model

In this section, as an application of the SMEFT corrections in the general Z models, we investigate the Z mediated corrections in the Minimal Supersymmetric Standard Model (MSSM). In order to understand the importance of the Z mediated corrections, we focus on a specific scenario in the MSSM, where the Z mediated corrections dominate the $\Delta F = 2$ observables.

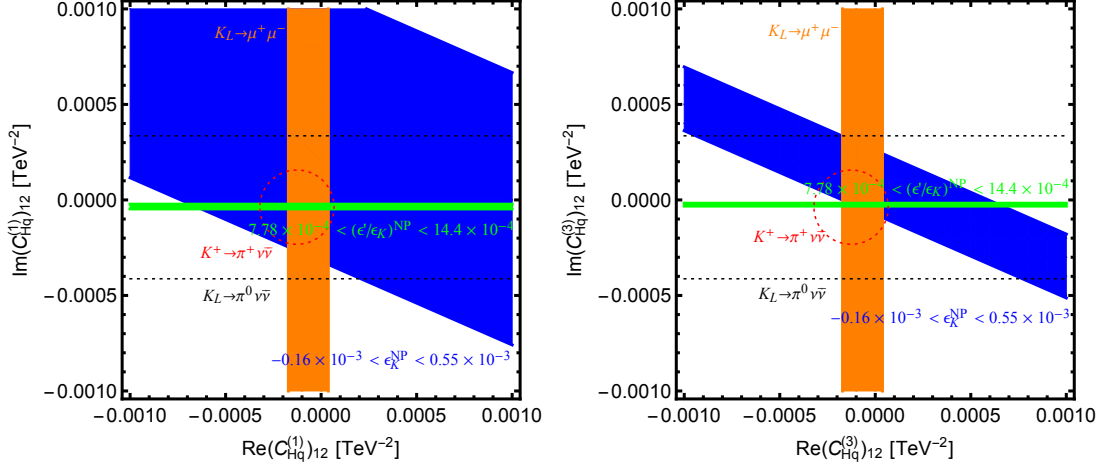


Figure 6.1: The correlations of observables through Z mediation in $(C_{Hq}^{(1)})_{12}$ (left panel) and $(C_{Hq}^{(3)})_{12}$ (right panel). The blue, green and orange regions are allowed by the experiments of ϵ_K , ϵ'/ϵ_K and $\mathcal{B}(K_L \rightarrow \mu^+ \mu^-)$, respectively. The black and red dotted contours represent $\mathcal{B}(K_L \rightarrow \pi^0 \nu \bar{\nu})/\mathcal{B}(K_L \rightarrow \pi^0 \nu \bar{\nu})_{\text{SM}}$ and $\mathcal{B}(K^+ \rightarrow \pi^+ \nu \bar{\nu})/\mathcal{B}(K^+ \rightarrow \pi^+ \nu \bar{\nu})_{\text{SM}}$, respectively.

6.3.1 MSSM

In this section, let us study the MSSM to demonstrate the SMEFT Z mediation corrections as explored in the previous section. The MSSM include many particles, which are the super-partner of the SM particles. The particle contents in the MSSM are listed in Table 6.3.1. In the MSSM, many CP violating parameters are included in following soft SUSY breaking terms [85, 86]:

$$\mathcal{L}_{\text{soft}} = -V_2 - V_3 + \mathcal{L}_G, \quad (6.10)$$

$$\begin{aligned} V_2 = & m_{H_1}^2 H_{1a}^* H_1^a + m_{H_2}^2 H_{2a}^* H_2^a - \left(m_3^2 \epsilon_{ab} H_1^a H_2^b + \text{h.c.} \right) \\ & + \tilde{Q}_{iLa}^* (m_{\tilde{Q}}^2)_{ij} \tilde{Q}_{jL}^a + \tilde{L}_{iLa}^* (m_{\tilde{L}}^2)_{ij} \tilde{L}_{jL}^a \\ & + \tilde{u}_{iR} (m_{\tilde{Q}}^2)_{ij} \tilde{u}_{jR}^* + \tilde{d}_{iR} (m_{\tilde{d}}^2)_{ij} \tilde{d}_{jR}^* + \tilde{e}_{iR} (m_{\tilde{e}}^2)_{ij} \tilde{e}_{jR}^*, \end{aligned} \quad (6.11)$$

$$V_3 = \epsilon_{ab} \left[(T_E)_{ij} H_1^a \tilde{L}_{iL}^b \tilde{e}_{jR}^* + (T_D)_{ij} H_1^a \tilde{Q}_{iL}^b \tilde{d}_{jR}^* + (T_U)_{ij} H_2^b \tilde{Q}_{iL}^a \tilde{u}_{jR}^* \right] + \text{h.c.}, \quad (6.12)$$

$$\mathcal{L}_G = \frac{1}{2} \left(M_1 \tilde{b} \tilde{b} + M_2 \tilde{w}^A \tilde{w}^A + M_3 \tilde{g}^X \tilde{g}^X \right) + \text{h.c.}, \quad (6.13)$$

where indices A runs 1, 2, 3, and $X = 1, \dots, 8$. Besides, the superpotential of the MSSM is obtained as

$$W = \epsilon_{ab} \left[(Y_E)_{ij} H_1^a L_i^b \bar{E}_j + (Y_D)_{ij} H_1^a Q_i^b \bar{D}_j + (Y_U)_{ij} H_2^b Q_i^a \bar{U}_j - \mu H_1^a H_2^b \right], \quad (6.14)$$

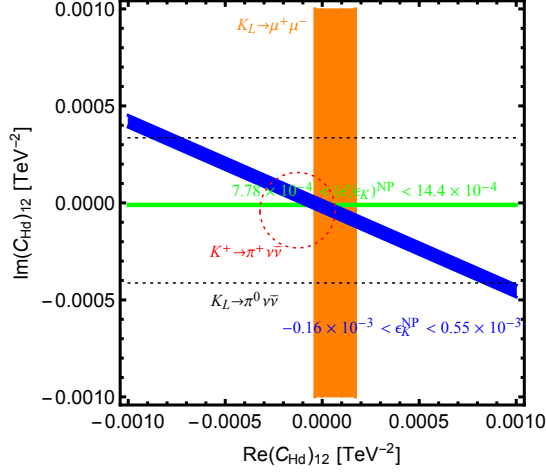


Figure 6.2: The correlations of observables through Z mediation in $(C_{Hd})_{12}$. The blue, green and orange regions are allowed by the experiments of ϵ_K , ϵ'/ϵ_K and $\mathcal{B}(K_L \rightarrow \mu^+ \mu^-)$, respectively. The black and red dotted contours represent $\mathcal{B}(K_L \rightarrow \pi^0 \nu \bar{\nu})/\mathcal{B}(K_L \rightarrow \pi^0 \nu \bar{\nu})_{\text{SM}}$ and $\mathcal{B}(K^+ \rightarrow \pi^+ \nu \bar{\nu})/\mathcal{B}(K^+ \rightarrow \pi^+ \nu \bar{\nu})_{\text{SM}}$, respectively.

where indexes a, b run 1, 2, and $i, j = 1, 2, 3$. After the EWSB, Higgs vacuum expectation values (VEVs) are obtained as

$$\langle H_i^0 \rangle = \frac{v_i}{\sqrt{2}}. \quad (6.15)$$

The Higgs VEVs satisfy the following relations:

$$v^2 = v_1^2 + v_2^2 = \frac{1}{\sqrt{2}G_F} \simeq (246 \text{ GeV})^2 \quad (6.16)$$

$$m_Z^2 = \frac{1}{4} (g_1^2 + g_2^2) v^2, \quad (6.17)$$

$$m_W^2 = \frac{1}{4} g_2^2 v^2. \quad (6.18)$$

After the EWSB, mass terms of the quarks are expressed as

$$\mathcal{L}_q^{\text{mass}} = -\frac{v_2}{\sqrt{2}} \bar{u}_R^c Y_U^T u_L - \frac{v_1}{\sqrt{2}} \bar{d}_R^c Y_D^T d_L + \text{h.c.} \quad (6.19)$$

The mass matrix of the quarks are diagonalized as $U_u^\dagger Y_U^T V_u = \sqrt{2} \text{diag}(m_u, m_c, m_t)/v_2$ and $U_d^\dagger Y_D^T V_d = \sqrt{2} \text{diag}(m_d, m_s, m_b)/v_1$. Besides, mass terms of the squarks are expressed as

$$\mathcal{L}_{\tilde{q}}^{\text{mass}} = -\Phi_u^\dagger \mathcal{M}_u^2 \Phi_u - \Phi_d^\dagger \mathcal{M}_d^2 \Phi_d, \quad (6.20)$$

Table 6.1: Superfields and particle contents.

Superfields	Component fiels		Gauge quantum numbers		
	Fermions	Bosons	$SU(3)_C$	$SU(2)_L$	$U(1)_Y$
$Q_i = \begin{pmatrix} U_i \\ D_i \end{pmatrix}$	$\begin{pmatrix} u_{iL} \\ d_{iL} \end{pmatrix}$	$\tilde{Q}_{iL} = \begin{pmatrix} \tilde{u}_{iL} \\ \tilde{d}_{iL} \end{pmatrix}$	3	2	1/6
\tilde{U}_i	$(u_{iR})^C = (u^C)_{iL}$	\tilde{u}_{iR}^*	$\bar{\mathbf{3}}$	1	-2/3
\tilde{D}_i	$(d_{iR})^C = (d^C)_{iL}$	\tilde{d}_{iR}^*	$\bar{\mathbf{3}}$	1	1/3
$L_i = \begin{pmatrix} N_i \\ E_i \end{pmatrix}$	$\begin{pmatrix} \nu_{iL} \\ e_{iL} \end{pmatrix}$	$\tilde{L}_{iL} = \begin{pmatrix} \tilde{\nu}_{iL} \\ \tilde{e}_{iL} \end{pmatrix}$	$\bar{\mathbf{1}}$	2	-1/2
\tilde{E}_i	$(e_{iR})^C = (e^C)_{iL}$	\tilde{e}_{iR}^*	$\bar{\mathbf{1}}$	1	1
G^X	\tilde{g}^X	g_μ^X	8	1	0
W^A	\tilde{w}^A	W_μ^A	1	3	0
B	\tilde{b}	B_μ	1	1	0
$H_1 = \begin{pmatrix} H_1^0 \\ H_1^- \end{pmatrix}$	$\tilde{h}_1 = \begin{pmatrix} \tilde{h}_1 \\ \tilde{h}_1^- \end{pmatrix}$	$H_1 = \begin{pmatrix} H_1^0 \\ H_1^- \end{pmatrix}$	1	2	-1/2
$H_2 = \begin{pmatrix} H_2^+ \\ H_2^0 \\ H_2^- \end{pmatrix}$	$\tilde{h}_1 = \begin{pmatrix} \tilde{h}_2^+ \\ \tilde{h}_2 \\ \tilde{h}_2^- \end{pmatrix}$	$H_2 = \begin{pmatrix} H_2^+ \\ H_2^0 \\ H_2^- \end{pmatrix}$	1	2	1/2

where $\Phi_u = (\tilde{u}_L, \tilde{c}_L, \tilde{t}_L, \tilde{u}_R, \tilde{c}_R, \tilde{t}_R)^T$ and $\Phi_d = (\tilde{d}_L, \tilde{s}_L, \tilde{b}_L, \tilde{d}_R, \tilde{s}_R, \tilde{b}_R)^T$. The squark mass matrices are obtained as

$$\mathcal{M}_u^2 = \begin{pmatrix} V_{\text{CKM}} \hat{m}_Q^2 V_{\text{CKM}}^\dagger + M_u^2 + \cos 2\beta M_Z^2 \left(\frac{1}{2} - \frac{2}{3} s_W^2 \right) \mathbf{1} & \frac{v_2 \hat{T}_U^\dagger - \mu M_u \cot \beta}{\sqrt{2}} \\ \frac{v_2 \hat{T}_U - \mu^* M_u \cot \beta}{\sqrt{2}} & \hat{m}_u^2 + M_u^2 + \cos 2\beta M_Z^2 \frac{2}{3} s_W^2 \mathbf{1} \end{pmatrix}, \quad (6.21)$$

$$\mathcal{M}_d^2 = \begin{pmatrix} \hat{m}_Q^2 + M_d^2 + \cos 2\beta M_Z^2 \left(-\frac{1}{2} + \frac{1}{3} s_W^2 \right) \mathbf{1} & \frac{v_1 \hat{T}_D^\dagger - \mu M_d \tan \beta}{\sqrt{2}} \\ \frac{v_1 \hat{T}_D - \mu^* M_d \tan \beta}{\sqrt{2}} & \hat{m}_d^2 + M_d^2 + \cos 2\beta M_Z^2 \frac{1}{3} s_W^2 \mathbf{1} \end{pmatrix}, \quad (6.22)$$

where $\hat{m}_Q^2 = V_d^\dagger m_Q^2 V_d$, $\hat{m}_u^2 = U_u^\dagger (m_u^2)^T U_u$, $\hat{m}_d^2 = U_d^\dagger (m_d^2)^T U_d$, $\hat{T}_U = U_u^\dagger T_U^T V_u$ and $\hat{T}_D = U_d^\dagger T_D^T V_d$, which are diagonalized as $R_u \mathcal{M}_u^2 R_u^\dagger = \text{diag} (m_{u_1}^2, m_{u_2}^2, m_{u_3}^2, m_{u_4}^2, m_{u_5}^2, m_{u_6}^2)$ and $R_d \mathcal{M}_d^2 R_d^\dagger = \text{diag} (m_{d_1}^2, m_{d_2}^2, m_{d_3}^2, m_{d_4}^2, m_{d_5}^2, m_{d_6}^2)$. Hereafter, the flavor violations are discussed in the basis where the Yukawa matrix of the quark is diagonalized.

In particular, the gaugino and matter interaction in the MSSM can contribute to the $\Delta F = 2$ observables through box type diagrams. As an example, we focus on the gluino contributions. The gluino-squark-quark interaction is obtained as

$$\mathcal{L}_{\text{int}} = -\sqrt{2} g_s \sum_{i=1}^3 \sum_{j=1}^6 \tilde{d}_j^* \tilde{g}^X (\lambda^X / 2) \left((\Gamma_L^d)_{ji} P_L + (\Gamma_R^d)_{ji} P_R \right) d_i + \text{h.c.} \quad (6.23)$$

The couplings $(\Gamma_{L,R}^d)_{ji}$ are defined as

$$(\Gamma_L^d)_{ji} = \sum_{k=1}^3 (R_d)_{jk} (V_d)_{ki}, \quad (6.24)$$

$$(\Gamma_R^d)_{ji} = - \sum_{k=1}^3 (R_d)_{j,k+3} (U_d)_{ki}. \quad (6.25)$$

The gluino and down-type squarks induce $\Delta F = 2$ transitions. They are severely constrained by the observed meson oscillations. First of all, let us consider the box diagram contributions. In literature [87], the Wilson coefficients of the LEFT in Eq. (3.1) are set by integrating out \tilde{g} and \tilde{d} :

$$(C_1)_{ij}^{\text{Box}} = \frac{\alpha_s^2}{m_{\tilde{g}}^2} (\Gamma_L^d)_{rj} (\Gamma_L^d)_{ri}^* (\Gamma_L^d)_{sj} (\Gamma_L^d)_{si}^* \left[\frac{1}{9} B_0(x_r, x_s) + \frac{11}{36} B_2(x_r, x_s) \right], \quad (6.26)$$

$$(C_1')_{ij}^{\text{Box}} = \frac{\alpha_s^2}{m_{\tilde{g}}^2} (\Gamma_R^d)_{rj} (\Gamma_R^d)_{ri}^* (\Gamma_R^d)_{sj} (\Gamma_R^d)_{si}^* \left[\frac{1}{9} B_0(x_r, x_s) + \frac{11}{36} B_2(x_r, x_s) \right], \quad (6.27)$$

$$(C_2)_{ij}^{\text{Box}} = \frac{\alpha_s^2}{m_{\tilde{g}}^2} (\Gamma_L^d)_{rj} (\Gamma_R^d)_{ri}^* (\Gamma_L^d)_{sj} (\Gamma_R^d)_{si}^* \left[\frac{17}{18} B_0(x_r, x_s) \right], \quad (6.28)$$

$$(C_2')_{ij}^{\text{Box}} = \frac{\alpha_s^2}{m_{\tilde{g}}^2} (\Gamma_R^d)_{rj} (\Gamma_L^d)_{ri}^* (\Gamma_R^d)_{sj} (\Gamma_L^d)_{si}^* \left[\frac{17}{18} B_0(x_r, x_s) \right], \quad (6.29)$$

$$(C_3)_{ij}^{\text{Box}} = \frac{\alpha_s^2}{m_{\tilde{g}}^2} (\Gamma_L^d)_{rj} (\Gamma_R^d)_{ri}^* (\Gamma_L^d)_{sj} (\Gamma_R^d)_{si}^* \left[-\frac{1}{6} B_0(x_r, x_s) \right], \quad (6.30)$$

$$(C_3')_{ij}^{\text{Box}} = \frac{\alpha_s^2}{m_{\tilde{g}}^2} (\Gamma_R^d)_{rj} (\Gamma_L^d)_{ri}^* (\Gamma_R^d)_{sj} (\Gamma_L^d)_{si}^* \left[-\frac{1}{6} B_0(x_r, x_s) \right], \quad (6.31)$$

$$(C_4)_{ij}^{\text{Box}} = \frac{\alpha_s^2}{m_{\tilde{g}}^2} \left\{ (\Gamma_L^d)_{rj} (\Gamma_L^d)_{ri}^* (\Gamma_R^d)_{sj} (\Gamma_R^d)_{si}^* \left[\frac{7}{3} B_0(x_r, x_s) - \frac{1}{3} B_2(x_r, x_s) \right] \right. \\ \left. + (\Gamma_L^d)_{rj} (\Gamma_R^d)_{ri}^* (\Gamma_R^d)_{sj} (\Gamma_L^d)_{si}^* \left[-\frac{11}{18} B_2(x_r, x_s) \right] \right\}, \quad (6.32)$$

$$(C_5)_{ij}^{\text{Box}} = \frac{\alpha_s^2}{m_{\tilde{g}}^2} \left\{ (\Gamma_L^d)_{rj} (\Gamma_L^d)_{ri}^* (\Gamma_R^d)_{sj} (\Gamma_R^d)_{si}^* \left[\frac{1}{9} B_0(x_r, x_s) + \frac{5}{9} B_2(x_r, x_s) \right] \right. \\ \left. + (\Gamma_L^d)_{rj} (\Gamma_R^d)_{ri}^* (\Gamma_R^d)_{sj} (\Gamma_L^d)_{si}^* \left[-\frac{5}{6} B_2(x_r, x_s) \right] \right\}, \quad (6.33)$$

where $x_{r,s} = m_{\tilde{d}_{r,s}}^2 / m_{\tilde{g}}^2$. The loop functions are defined as

$$B_0(x, y) = \frac{x \ln x}{(x-y)(x-1)^2} + \frac{y \ln y}{(y-x)(y-1)^2} + \frac{1}{(x-1)(y-1)}, \quad (6.34)$$

$$B_2(x, y) = \frac{x^2 \ln x}{(x-y)(x-1)^2} + \frac{y^2 \ln y}{(y-x)(y-1)^2} + \frac{1}{(x-1)(y-1)}. \quad (6.35)$$

From the SUSY scale μ_{SUSY} to the hadron scale, the QCD RGEs are solved and $\Delta F = 2$ observables are estimated. In the conventional calculation, the interference effects between the SM and SUSY contributions, O_{Hd} and $O_{Hq}^{(1,3)}$, are not included.

When the squark (quark) flavor is violated by scalar trilinear soft-breaking parameters, the above box diagrams are controlled by the squark mixing parameter, $(\delta_D)_{ij} = (T_D)_{ij} v \cos \beta / m_{\tilde{Q}}^2$.

For examples, the Wilson coefficient, C_1 , C'_1 and C_4 , are roughly expressed as

$$(C_1)_{12} \sim [(\delta_D)_{13}^*(\delta_D)_{23}]^2 / m_{\tilde{Q}}^2, \quad (6.36)$$

$$(C'_1)_{12} \sim [(\delta_D)_{31}(\delta_D)_{32}^*]^2 / m_{\tilde{Q}}^2, \quad (6.37)$$

$$(C_4)_{12} \sim (\delta_D)_{13}^*(\delta_D)_{23}(\delta_D)_{31}(\delta_D)_{32}^* / m_{\tilde{Q}}^2. \quad (6.38)$$

The contribution of $(C_4)_{12}$ dominates the $\Delta F = 2$ observable ϵ_K because of the chiral enhancement. In a specific case where $(\delta_D)_{13}^*(\delta_D)_{23} \sim 0$, the dominant contribution coming from $(C_4)_{12}$ vanishes, and the constraint from ϵ_K becomes weak. However, as explained in the next section, the Z mediated SUSY contribution drastically change this situation.

6.3.2 Z mediated SUSY corrections

Let us study the Z mediated correction in the MSSM. At the one-loop level, the SMEFT operators O_{Hd} and $O_{Hq}^{(1,3)}$ are generated by gluino loops in the MSSM. When the squark (quark) flavor is violated by scalar trilinear soft-breaking parameters, the dominant contributions are calculated from Fig. 6.3 as

$$(\mathcal{C}_{Hq}^{(1)})_{12} = -\frac{\alpha_s}{12\pi} \frac{\cos^2 \beta}{m_{\tilde{g}}^4} (T_D)_{13}^* (T_D)_{23} Z(x_{L1}, x_{L2}, x_{R3}), \quad (6.39)$$

$$(\mathcal{C}_{Hq}^{(3)})_{12} = -\frac{\alpha_s}{12\pi} \frac{\cos^2 \beta}{m_{\tilde{g}}^4} (T_D)_{13}^* (T_D)_{23} Z(x_{L1}, x_{L2}, x_{R3}), \quad (6.40)$$

$$(\mathcal{C}_{Hd})_{12} = \frac{\alpha_s}{6\pi} \frac{\cos^2 \beta}{m_{\tilde{g}}^4} (T_D)_{31} (T_D)_{32}^* Z(x_{R1}, x_{R2}, x_{L3}), \quad (6.41)$$

with $x_i = m_{\tilde{d}_i}^2 / m_{\tilde{g}}^2$. Here, $m_{\tilde{d}_{L(R)i}}$ is the left- (right-) handed squark soft mass for the i -th generation, $m_{\tilde{g}}$ is the gluino mass, and T_D is the scalar trilinear coupling of the down-type squarks. The Wilson coefficients are set at the SUSY scale.^{#1} The loop function is defined as

$$\begin{aligned} Z(x, y, z) = & -\frac{x^2 \ln x}{(x-1)(x-y)(x-z)^2} + \frac{y^2 \ln y}{(y-1)(x-y)(y-z)^2} \\ & -\frac{z}{(z-1)(x-z)(y-z)} + \frac{(2xy - yz - xz - xyz + z^3)z \ln z}{(z-1)^2(x-z)^2(y-z)^2}. \end{aligned} \quad (6.42)$$

In the limit of $y, z \rightarrow x$, it becomes

$$Z(x) = \frac{2 + 3x - 6x^2 + x^3 + 6x \ln x}{6x(x-1)^4}. \quad (6.43)$$

In addition, these LEFT $\Delta F = 2$ operators are generated by the $\Delta F = 1$ ones in the SMEFT through the one-loop matchings at the weak scale [18]. The conditions for \mathcal{C}_{Hq} and \mathcal{C}_{Hd} at the

^{#1} If the trilinear couplings $(T_D)_{13,23,31,32}$ are set in a scale higher than the SUSY scale, the flavor-violating squark soft masses $(m_{\tilde{d}_{L(R)}})_{12,21}$ are generated via RG corrections. They can be sizable and contribute to the kaon FCNCs when the input scale is much higher than the SUSY scale.

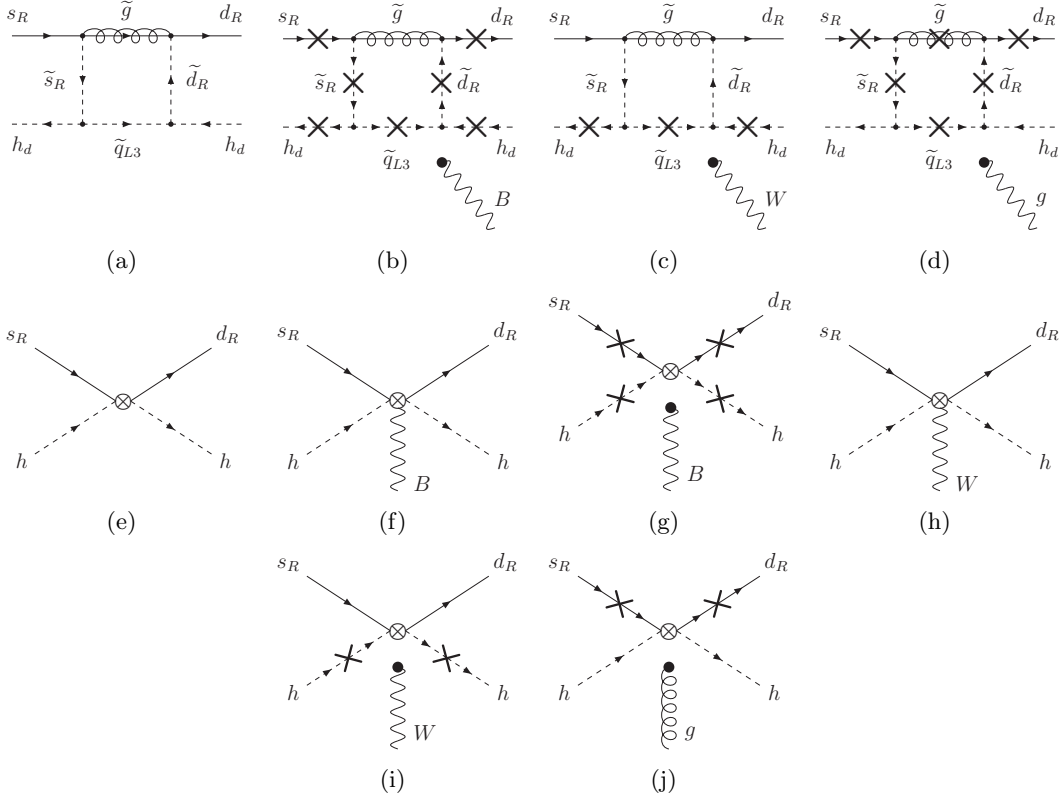


Figure 6.3: Feynman diagrams relevant for the matchings onto the operators $(O_{Hd})_{12}$, where the external gauge bosons are attached to each of the cross marks. Diagrams (a)–(d) are the one-loop gluino contributions, and (e)–(j) are the diagrams in the SMEFT. The diagrams contributing to $(O_{Hq}^{(1,3)})_{12}$ are similarly obtained.

scale μ_W are approximated as [20, 21]

$$(C_1)_{ij} = \frac{\alpha[\lambda_t]_{ij}}{\pi s_W^2} \left[(C_{Hq}^{(1)})_{ij} I_1(x_t, \mu_W) - (C_{Hq}^{(3)})_{ij} I_2(x_t, \mu_W) \right], \quad (6.44)$$

$$(C_5)_{ij}^{(1)} = -\frac{2\alpha[\lambda_t]_{ij}}{\pi s_W^2} (C_{Hd})_{ij} I_1(x_t, \mu_W), \quad (6.45)$$

with $x_t = m_t^2/m_W^2$. These results are gauge-independent.

By using the squark mixing parameter $(\delta_D)_{ij}$, the Wilson coefficients $(C_{Hq}^{(1,3)})_{ij}$ and $(C_{Hd})_{ij}$ are roughly expressed as

$$(C_1)_{ij} \sim (\lambda_t)_{ij} (\delta_D)_{i3}^* (\delta_D)_{j3} / m_Z^2, \quad (6.46)$$

$$(C_5)_{ij} \sim (\lambda_t)_{ij} (\delta_D)_{3i} (\delta_D)_{3j}^* / m_Z^2. \quad (6.47)$$

As explained in the previous section, the conventional contributions from the box diagrams are suppressed, if we focus on the specific scenario $(\delta_D)_{13}^* (\delta_D)_{23} \sim 0$. Even if this scenario, the coefficient $(C_5)_{ij}$ coming from the SMEFT Z mediated contribution is remained and becomes a

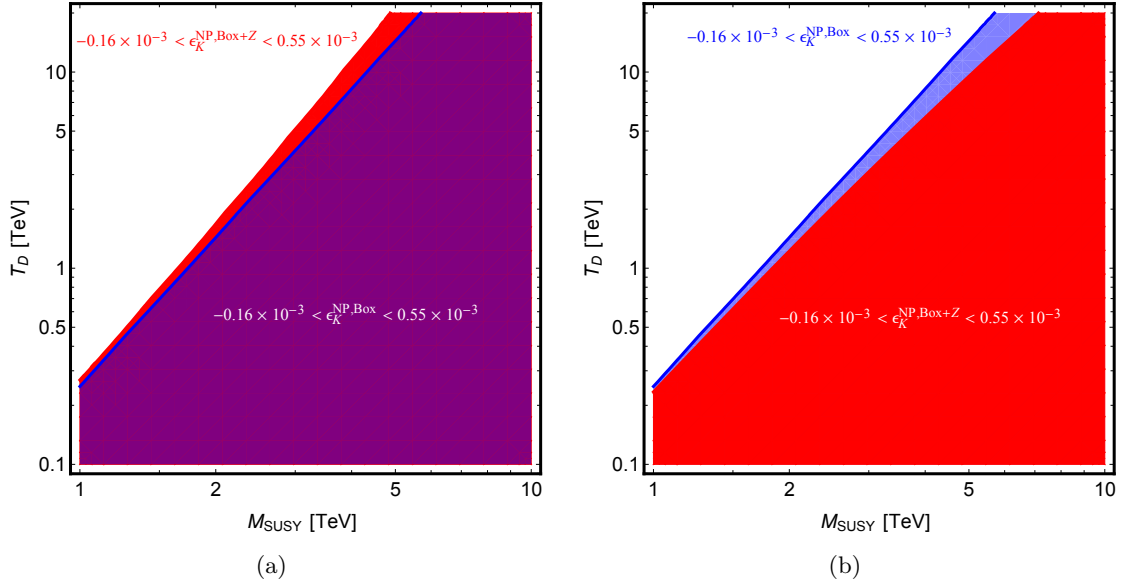


Figure 6.4: Contour plots of ϵ_K on the $M_{\text{SUSY}} - T_D$ plane in the case $[(+/-)T_D, iT_D, (+/-)T_D, T_D]$ (left/right). The experimental allowed regions of the conventional box contributions are shown in blue regions, and that of the SMEFT Z mediated contributions with box ones are shown in red regions.

dominant effect in ϵ_K , because of the chiral enhancement. In particular, this contribution is not suppressed by the SUSY mass scale if the squark mixing parameter is fixed, and the SMEFT Z mediated contribution becomes important in the high SUSY scale.

Next, we numerically analyze the SMEFT Z mediated contribution in ϵ_K and discuss some correlations between flavor changing observables. For simplicity, we focus on a simplified scenario, where the scalar trilinear coupling are parameterized as $[(T_D)_{13}, (T_D)_{23}, (T_D)_{31}, (T_D)_{32}] = [\pm T_D, iT_D, \pm T_D, T_D]$. In Fig. 6.4, contour plots of ϵ_K on the $M_{\text{SUSY}} - T_D$ plane are displayed. In the left and right plot, the cases $[+T_D, iT_D, +T_D, T_D]$ and $[-T_D, iT_D, -T_D, T_D]$ are shown, respectively. In the both plots, the experimentally allowed regions at the 2σ level of the conventional box contributions are shown in blue regions, and that of the SMEFT Z mediated contributions with box ones are shown in red regions. The allowed regions of the box contributions are not changed much. However, the relative sign of the SMEFT Z mediated contributions and the box one becomes opposite^{#2}. The plots show that the SMEFT Z mediated corrections may make the constraint for the SUSY scale be changed by $\mathcal{O}(100\%)$. Focusing on contour lines of ϵ_K , in large SUSY scale regions, the corrections becomes large. This is because, on the contour lines, the squark mixing parameter δ_D roughly takes fixed value, and the box contributions are suppressed by the SUSY scale as $m_{\tilde{Q}}^{-2}$.

^{#2}The contribution of the box diagrams is roughly expressed as $\sim i(T_D)^4 v^4 / m_{\tilde{Q}}^{10}$. On the other hand, the Z mediated contribution is expressed as $\sim \pm(\lambda_t)_{12}(T_D)^2 v^2 / m_Z^2 m_{\tilde{Q}}^4$

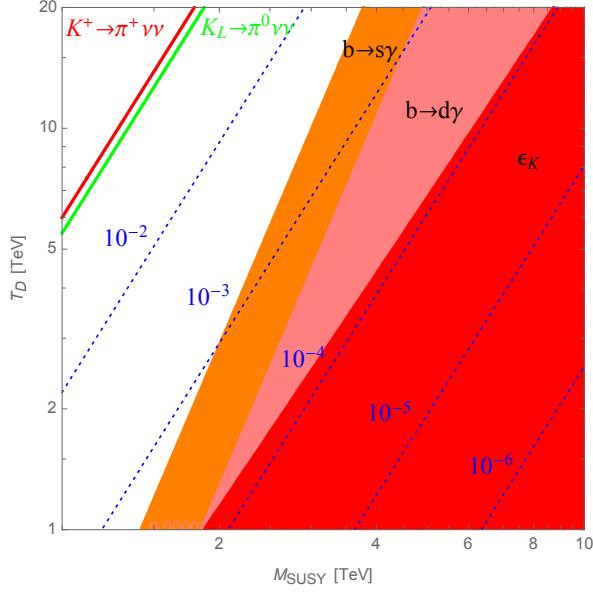


Figure 6.5: Correlations between ϵ_K , ϵ'/ϵ_K , $\mathcal{B}(K \rightarrow \pi\nu\bar{\nu})$ and $\mathcal{B}(\bar{B} \rightarrow X_{d,s}\gamma)$ on a $M_{\text{SUSY}} - T_D$ plane in the case $[0, 0, T_D, iT_D]$ (left/right). The right handed side of the red and green line are allowed by $\mathcal{B}(K^+ \rightarrow \pi^+\nu\bar{\nu})$ and $\mathcal{B}(K_L \rightarrow \pi^0\nu\bar{\nu})$, respectively with 90% confidence level. Similarly, the right handed side of the red, orange and pink regions are allowed by ϵ_K , $\mathcal{B}(\bar{B} \rightarrow X_s\gamma)$ and $\mathcal{B}(\bar{B} \rightarrow X_d\gamma)$, respectively at the 2σ level. The dotted lines are contour line of ϵ'/ϵ_K corresponding to 10^{-2} , 10^{-3} , 10^{-4} , 10^{-5} and 10^{-6} .

Through the SMEFT Z mediated contributions, there exist correlations between $\Delta F = 2$ and 1 observables. In the MSSM, additional observables such as $\mathcal{B}(\bar{B} \rightarrow X_{d,s}\gamma)$ also correlate with ϵ_K . For simplicity, we numerically show the correlations for the case $[0, 0, T_D, iT_D]$, where the conventional box diagram contributions from ϵ_K become negligible and the SMEFT Z mediated contributions become important. In Fig. 6.5, the correlations between ϵ_K , ϵ'/ϵ_K , $K \rightarrow \pi\nu\bar{\nu}$ and $\mathcal{B}(\bar{B} \rightarrow X_{d,s}\gamma)$ are displayed on the $M_{\text{SUSY}} - T_D$ plane. The experimentally allowed regions from $\mathcal{B}(K^+ \rightarrow \pi^+\nu\bar{\nu})$ and $\mathcal{B}(K_L \rightarrow \pi^0\nu\bar{\nu})$ are right handed sides of red and green colored lines, respectively. Besides, the right handed side of the red, orange and pink regions are allowed regions from ϵ_K , $\mathcal{B}(\bar{B} \rightarrow X_s\gamma)$ and $\mathcal{B}(\bar{B} \rightarrow X_d\gamma)$, respectively. The blue dotted lines are contours of ϵ'/ϵ_K . Since $\mathcal{B}(\bar{B} \rightarrow X_{d,s}\gamma)$ is roughly expressed as $(\delta_D)_{13,23}/m_{\tilde{Q}}$, the constraints from $\mathcal{B}(\bar{B} \rightarrow X_{d,s}\gamma)$ are severe in small SUSY scale regions. In this scenario $[0, 0, T_D, iT_D]$, the SMEFT Wilson coefficients take imaginary values, and the constraints from $\mathcal{B}(K_L \rightarrow \mu^+\mu^-)$ are negligible. Figure. 6.5 shows that the constraints from ϵ_K generated by the SMEFT Z mediated contributions can become much severe even though the conventional box contributions are negligible.

Finally, we mention that in the gluino mediated scenario, there also exist parameter regions of the scalar trilinear coupling where the experimental data of ϵ'/ϵ_K can be explained. For

simplicity, we restrict the parameter space such that two of $(T_D)_{13,23,31,32}$ are real. When $(T_D)_{23,32}$ are real, we checked that wide parameter regions to explain the discrepancy of ϵ'/ϵ_K are tightly excluded by $\mathcal{B}(\bar{B} \rightarrow X_{d,s}\gamma)$. Therefore, we consider the cases when $(T_D)_{13,31}$ are real. The scalar trilinear coupling are parameterized as

$$[(T_D)_{13}, (T_D)_{23}, (T_D)_{31}, (T_D)_{32}] = [\gamma_L, \alpha_L + i\beta_L, \gamma_R, \alpha_R + i\beta_R], \quad (6.48)$$

where α_i, β_i and γ_i are real parameters. Then, one obtains

$$\text{Im}[\mathcal{C}_{HQ}^{(1,3)}]_{12} \propto -\text{Im}[(T_D)_{13}^*(T_D)_{23}] = -\beta_L\gamma_L, \quad (6.49)$$

$$\text{Im}[\mathcal{C}_{HD}]_{12} \propto +\text{Im}[(T_D)_{31}(T_D)_{32}^*] = -\beta_R\gamma_R. \quad (6.50)$$

The L variables contribute to the left-handed Wilson coefficients, and the R variables to the right-handed ones. In order to evaluate the observables, we scan the whole parameter region of α_i, β_i , and γ_i where the vacuum stability conditions are satisfied.^{#3} The vacuum stability conditions are discussed in Appendix E.

When $\beta_L\gamma_L > 0$ and $\beta_R\gamma_R > 0$, the SUSY contribution to ϵ'/ϵ_K , is maximized, because the left-handed contribution, \mathcal{C}_{HQ} , constructively interferes with the right-handed one, \mathcal{C}_{HD} . In this case, $\mathcal{B}(K_L \rightarrow \pi^0\nu\bar{\nu})$ cannot exceed the SM prediction, because positive $\beta_L\gamma_L$ and $\beta_R\gamma_R$ tends to decrease the branching ratio, as can be seen from Eq. (4.22). In contrast, ϵ'/ϵ_K , cannot be accommodated with the result (4.18) for $\beta_L\gamma_L < 0$ and $\beta_R\gamma_R < 0$. When either $\beta_L\gamma_L$ or $\beta_R\gamma_R$ is negative, the discrepancy of ϵ'/ϵ_K , can also be explained. Because the right-handed contribution to ϵ'/ϵ_K , is larger than the left-handed one, $\beta_R\gamma_R > 0$ is favored to amplify ϵ'/ϵ_K .

Before proceeding to the analysis, let us summarize assumptions on model parameters. Since the vacuum stability condition is relaxed by large m_A , the heavy Higgs bosons are supposed to be decoupled. The squark masses are set to be degenerate, $m_{\tilde{Q}} \equiv m_{\tilde{Q},1} = m_{\tilde{Q},2} = m_{\tilde{Q},3} = m_{\tilde{D},1} = m_{\tilde{D},2} = m_{\tilde{D},3}$, for simplicity. The Higgsino mass parameter is also equal to $m_{\tilde{Q}}$, though dependences of the observables on it are weak. We take $\tan\beta = 5$, though the following results are insensitive to the choice, because the observables as well as the vacuum stability condition depend on it dominantly in a combination of $T_D \cos\beta$.

In Fig. 6.6, the maximal values of the SUSY contributions to ϵ'/ϵ_K are shown for $\beta_L\gamma_L > 0$ and $\beta_R\gamma_R > 0$ as a function of $m_{\tilde{Q}}$. There is a peak structure for each line. In smaller squark mass regions, the maximal value is determined by $\mathcal{B}(\bar{B} \rightarrow X_d\gamma)$. Defining the squark mixing parameter, $\delta_D = (T_D)_{ij}v \cos\beta/m_{\tilde{Q}}^2$, the SUSY contributions to ϵ'/ϵ_K , depend on it as $(\epsilon'/\epsilon_K)^{\text{SUSY}} \sim \delta_D^2$, whereas those to $\mathcal{B}(\bar{B} \rightarrow X_d\gamma)$ is $\sim \delta_D/m_{\tilde{Q}}$, where $m_{\tilde{g}} \sim m_{\tilde{Q}}$ is supposed. Thus, the maximal value of ϵ'/ϵ_K , increases as $m_{\tilde{Q}}$ becomes larger. In larger squark mass regions, the maximal value is determined by ϵ_K , $\mathcal{B}(\bar{B} \rightarrow X_s\gamma)$ and the vacuum stability condition as well as $\mathcal{B}(\bar{B} \rightarrow X_d\gamma)$. In particular, the gluino box contribution to ϵ_K depends on δ_D as $\sim \delta_D^4/m_{\tilde{Q}}^2$,

^{#3} We checked that the constraint from $\mathcal{B}(K_L \rightarrow \mu^+\mu^-)$ is weaker than the other constraints in the parameter region of our interest.

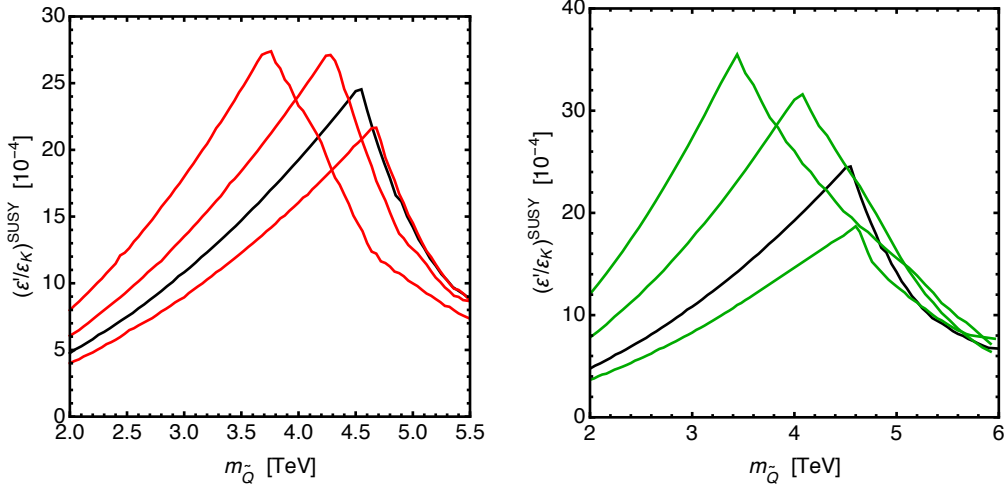


Figure 6.6: The maximal gluino contributions to ϵ'/ϵ_K , as a function of $m_{\tilde{Q}}$. The parameters are $\gamma_R/\beta_R = \gamma_L/\beta_L = 1$ and $m_{\tilde{g}}/m_{\tilde{Q}} = 1$ on the black line. In the left plot, $\gamma_R/\beta_R = \gamma_L/\beta_L = 0.6, 0.8, 1.2$ with $m_{\tilde{g}}/m_{\tilde{Q}} = 1$ from left to right of the red lines. In the right plot, $m_{\tilde{g}}/m_{\tilde{Q}} = 1.8, 1.4, 0.8$ with $\gamma_R/\beta_R = \gamma_L/\beta_L = 1$ from left to right of the green lines.

whereas the SUSY contributions via \mathcal{C}_{HQ} and \mathcal{C}_{HD} are not suppressed by $m_{\tilde{Q}}$, i.e., behaves as $\sim \lambda_t \delta_D^2 / m_Z^2$. When $m_{\tilde{Q}}$ is small, the latter contribution can be canceled enough by the former one. However, as $m_{\tilde{Q}}$ increases, the cancellation becomes weaker in the parameter region allowed by the other constraints. Hence, the bounds on the trilinear couplings become severer to satisfy the constraint of ϵ_K . Consequently, the maximal value of ϵ'/ϵ_K decreases.

In the figures, γ_i/β_i or $m_{\tilde{g}}/m_{\tilde{Q}}$ is also varied. On the black line, $\gamma_R/\beta_R = \gamma_L/\beta_L = 1$ and $m_{\tilde{g}}/m_{\tilde{Q}} = 1$ are chosen. In the left plot, $\gamma_R/\beta_R = \gamma_L/\beta_L = 0.6, 0.8, 1.2$ with $m_{\tilde{g}}/m_{\tilde{Q}} = 1$ from left to right of the red lines. On the other hand, $m_{\tilde{g}}/m_{\tilde{Q}} = 1.8, 1.4, 0.8$ with $\gamma_R/\beta_R = \gamma_L/\beta_L = 1$ from left to right of the green lines in the right plot. The maximum value increases when γ_i/β_i is small and $m_{\tilde{g}}/m_{\tilde{Q}}$ is large. Also, it is found that the current discrepancy of ϵ'/ϵ_K can be explained if the squark mass is smaller than 5.6 TeV.

6.4 Conclusion of Z mediated correction to $\Delta F = 2$ observable

The SMEFT framework is qualitatively essential to retain the gauge invariance in the NP effects of $\Delta F = 2$ processes mediated by the Z boson. The one-loop matching formulae in Chapter 3 appropriately include the Z mediated correction to $\Delta F = 2$. In this chapter, we investigated the quantitative importance of the Z mediated SMEFT corrections. In the general Z model, we showed that the right-handed NP effects coming from $(C_{Hd})_{12}$ are enhanced by hadron matrix elements, and the constraints from ϵ_K are severe. Besides, the SMEFT corrections provide various correlations between $\Delta F = 1$ and 2 observables by the dynamical Z boson. Compared with the $\Delta S = 1$ observables such as ϵ'/ϵ_K , $\mathcal{B}(K_L \rightarrow \mu^+ \mu^-)$, it was shown that ϵ_K provides an

complementary information on the $\Delta S = 1$. In addition, we also discussed the SUSY effects in the Z mediated SMEFT corrections. In the MSSM, we showed that there exists the case where the Z mediated corrections dominate ϵ_K , and constraints of the SUSY scale can be changed by $\mathcal{O}(100\%)$. In the MSSM, we also discussed correlations between ϵ_K and $\Delta F = 1$ observables such as ϵ'/ϵ_K , $K \rightarrow \pi\nu\nu$ and $\mathcal{B}(\bar{B} \rightarrow X_{d,s}\gamma)$. We found that there exist parameter regions where the constraints from the $\Delta F = 2$ and 1 observables are satisfied even if the squark mass is smaller than 5.6 TeV. As these results, we conclude that the SMEFT corrections are quantitatively essential to discuss the correlations between flavor changing observables.

Nucleon EDM from SMEFT flavor-changing operator

This chapter is based on the work by the author [17]. We investigate flavor changing operators effects on nucleon electric dipole moments (EDM) within the framework of the SMEFT. We focus on contributions of dimension-six $\Delta F = 1$ operators of the down-type quarks to nucleon EDMs with particular emphasis on the top quark effects. It is found that some of the SMEFT operators are already excluded for the NP scale $M_{\text{NP}} \lesssim 100$ GeV by the neutron EDM, and future experiments may be able to probe those in $M_{\text{NP}} \lesssim 2-10$ TeV. In addition, we show that the EDMs and $\Delta F = 2$ observables will reveal allowed parameter regions of the SMEFT operators complementarily.

7.1 Flavor conserving process by flavor changing operators

Electric dipole moments (EDMs), which are CP -violating observables, are one of the most sensitive observables. Currently, the experimental bound of the neutron is [39]

$$|d_n| < 3.0 \times 10^{-26} e \text{ cm}, \quad (7.1)$$

at the 90% confidence level. On the other hand, the indirect limit on the proton EDM is derived from ^{199}Hg [88, 89] as [40]

$$|d_p| < 2.1 \times 10^{-25} e \text{ cm}. \quad (7.2)$$

In future, several experiments aim to improve the sensitivity by two orders of magnitudes for the neutron EDM [7, 8]. Also, a storage ring experiment is projected to measure the proton EDM at the level of $10^{-29} e \text{ cm}$ [9].

As we have mentioned in Chapter 3, although the EDMs are flavor-conserving observables, flavor-violating interactions can contribute to them. In the SM, the W -boson interactions change quark flavors. Thus, a class of NP can induce EDMs through quark flavor-changing interactions by exchanging the W boson. Such contributions are represented by the SMEFT [10–12]. Here, all the SM particles including the W, Z, H and the t are retained. Above the EWSB, NP contributions to flavor and CP violations are encoded in higher dimensional operators in the SMEFT. At the EWSB scale, they are matched onto the effective operators in the LEFT by integrating out W, Z, H and t . Low-scale observables such as the EDMs are evaluated by using the LEFT.

In this Chapter, we study the nucleon EDMs from SMEFT flavor-changing operators. They are induced by $\Delta F = 1$ operators through radiative corrections of the W boson. In particular, we will focus on top-quark loop contributions, because they tend to be large due to the large top quark mass (cf. Chapter 5). The radiative corrections are taken into account by solving the renormalization group equations (RGEs) in the SMEFT [13–15], which are listed in Appendix F. In addition, the SMEFT operators are matched onto those in the LEFT at the EWSB scale. The one-loop matching conditions are necessary, because the contributions of the $\Delta F = 1$ operators to EDMs are induced by radiative corrections. The one-loop formulae were already provided in Chapter 3. These operators also contribute to $\Delta F = 2$ observables such as ϵ_K and ΔM_d through the W -boson loops. Since these observables are sensitive to NP contributions, we will discuss correlation between the contributions to the EDMs and the $\Delta F = 2$ observables.

7.2 Numerical analysis of EDM

In this section, we study contributions of the SMEFT $\Delta F = 1$ operators to the nucleon EDMs and $\Delta F = 2$ observables, ϵ_K and ΔM_{B_d} . In Fig. 7.1, the neutron and proton EDMs are estimated. On each line, one of the Wilson coefficients is set to be $C_i = i/M_{\text{NP}}^2$ at the NP scale, M_{NP} . The other coefficients are zero. The effective operators missing in the list do not contribute to the EDMs as well as the $\Delta F = 2$ observables.^{#1} Once the operator is set, the RGEs are solved, and the matching conditions are taken into account. In the top panels, the four-quark operators mix the first two generations of the down-type quark. On the other hand, the operators in the bottom panels include the bottom quark. In low M_{NP} regions, it is found that the nucleon EDMs are suppressed, where the loop functions defined in Chapter 3, I_1 and K , vanish.

In the plots, the horizontal red and blue dotted lines correspond to the current experimental bound and the future sensitivity, respectively. For the latter, we quote $|d_n| = 10^{-28} e \text{ cm}$ and $|d_p| = 10^{-29} e \text{ cm}$. Currently, the EDM constraints are weak. The NP contributions are excluded only for $M_{\text{NP}} \lesssim 100 \text{ GeV}$ of $(C_{ud}^{(1,8)})_{3312}$ and $(C_{qd}^{(1)})_{3312}$. The sensitivities are expected to be improved greatly. The neutron and proton EDMs can probe the NP scale up to 2–10 TeV. On the other hand, the contributions to the EDMs are suppressed for the operators including the bottom quark. This is because the hadron matrix elements of such operators are small (see Eq. (4.12)). Currently, the constraint is weaker than $M_{\text{NP}} \lesssim 100 \text{ GeV}$ according to the bottom panel of the figure, and the sensitivity may reach at most 3 TeV in future.

Let us study correlations between the EDMs and the $\Delta F = 2$ observables. The results depend on the SMEFT operators. The $\Delta S = 1$ operators of $(C_{qd}^{(1,8)})_{3312}$, $(C_{ud}^{(1,8)})_{3312}$ and $(C_{Hd})_{12}$ contribute to the EDMs and ϵ_K via radiative corrections. Similarly, the $\Delta B = 1$ operators of

^{#1} There are operators which can contribute to the EDMs through self-energy corrections. The matching conditions are provided in Section ??, and it is straightforward to analyze them.

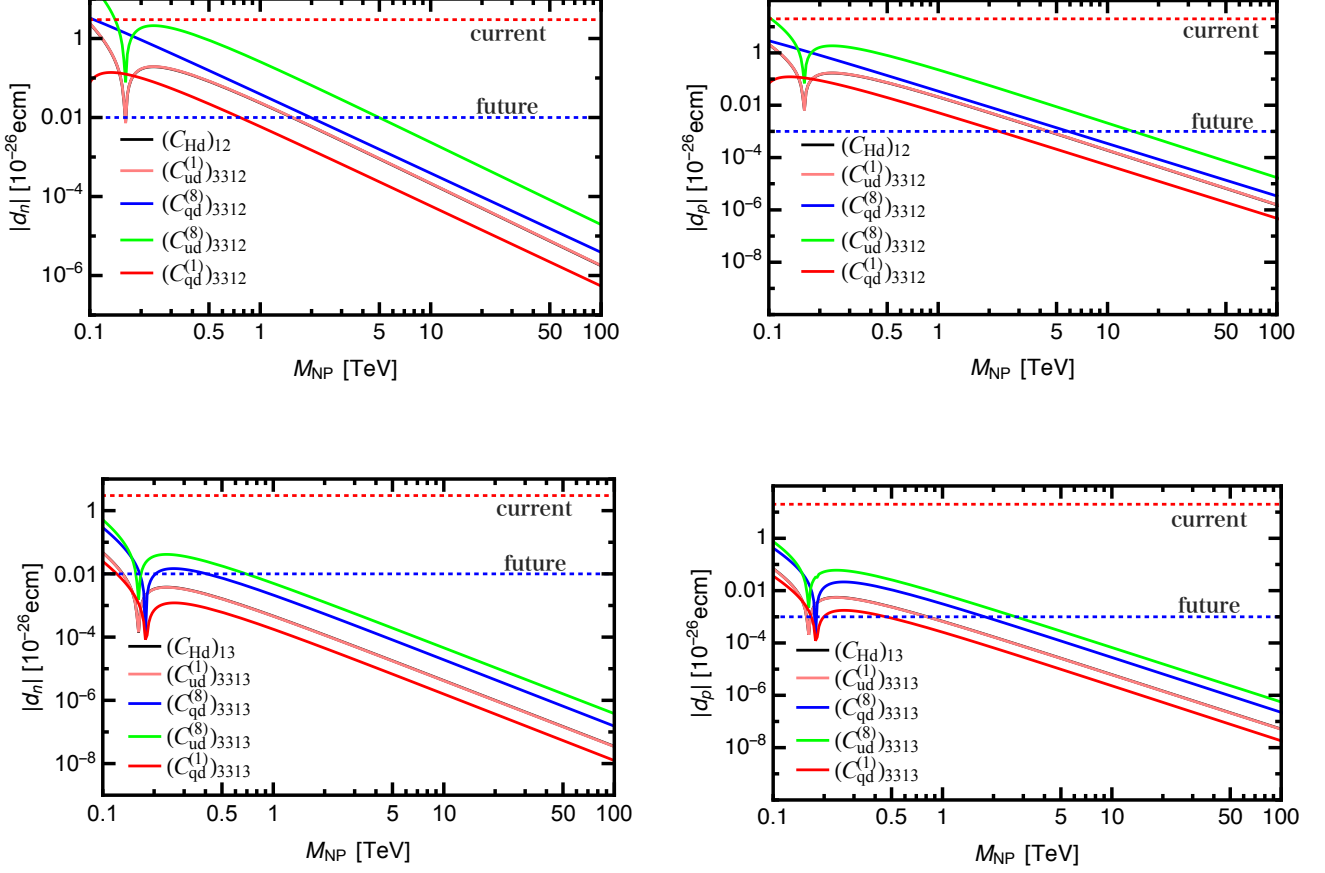


Figure 7.1: The neutron and proton EDMs are estimated for the SMEFT $\Delta F = 1$ operators of the down and strange quarks with the top quarks in the top panels. Those for the down and bottom quarks are shown in the bottom panels. The Wilson coefficients are i/M_{NP}^2 at the NP scale M_{NP} . The red and blue dotted lines are the current experimental limit and the future sensitivity.

$(C_{qd}^{(1,8)})_{3313}$, $(C_{ud}^{(1,8)})_{3313}$ and $(C_{Hd})_{13}$ affect ΔM_{B_d} as well as the EDMs. In Figs. 7.2–7.6, the EDMs and the $\Delta F = 2$ observables are estimated for each operator. Here, the real and imaginary parts of each Wilson coefficient are varied at the NP scale of 1 TeV, while the other coefficients are set to be zero at this scale. In the plots, the current limits from ϵ_K and ΔM_{B_d} are drawn by the blue band, where the region inside the band is allowed at the 2σ level. On the other hand, contours of the neutron and proton EDM are shown by the bands with different colors.

Currently, all the parameter regions are allowed by the EDMs (see also Fig. 7.1). In future, the EDMs can be sizable for the $\Delta S = 1$ operators. It is noticed that, since the parameter dependence of the EDMs is different from that of ϵ_K , they provide an independent information on the effective operators. For some of the $\Delta B = 1$ operators especially $(C_{qd}^{(8)})_{3313}$ and $(C_{ud}^{(8)})_{3313}$, future measurements of the proton EDMs will also be able to compete with the constraint from

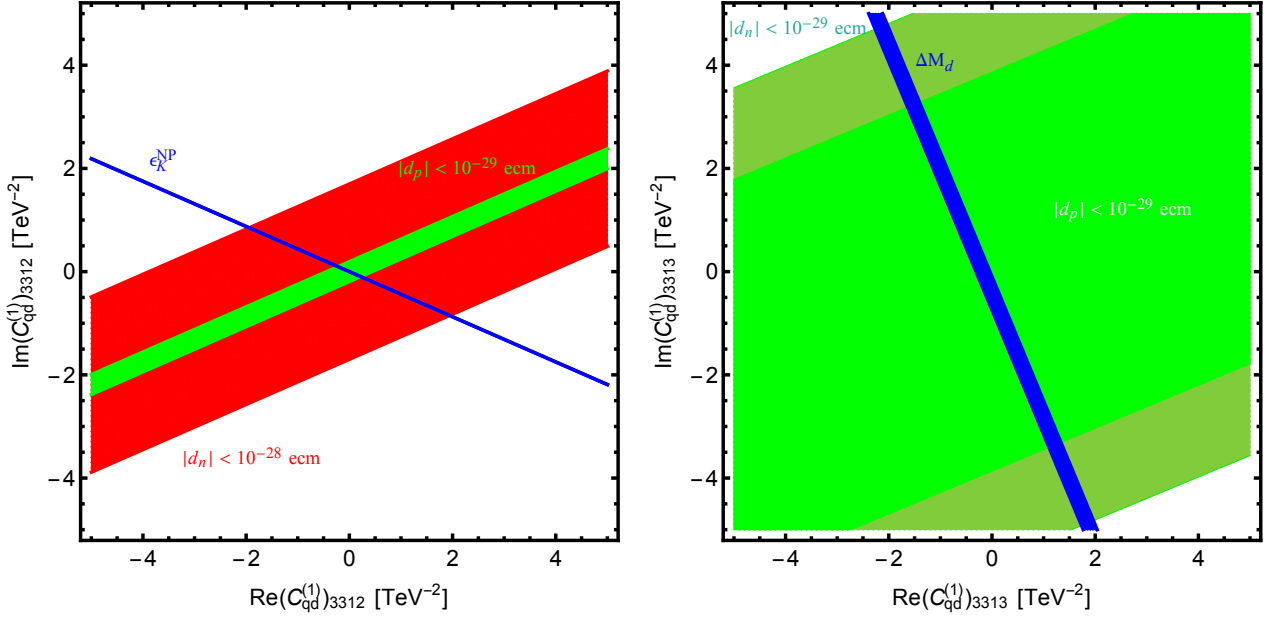


Figure 7.2: Contours of the EDMs and ϵ_K (left) and ΔM_{B_d} (right). Outside regions of the red and light green bands are probed by the future experiment in the left panel. On the other hand, the deep green region in the right panel corresponds to $|d_n| < 10^{-30}$ e cm, which is below the future sensitivity. In the left panel, the blue region is allowed by ϵ_K at the 2σ level, and the region in the right panel is allowed by ΔM_{B_d} at the 2σ level.

ΔM_{B_d} .

Next, let us consider $C_{qq}^{(1,3)}$, $C_{qu}^{(1,8)}$, and $(C_{Hq}^{(1)})_{12,13}$. We found that they do not contribute to the EDMs because of the Lorentz structures of these operators. In fact, they generate only the vector-type operators of the four quarks below the EWSB scale, which do not violate the CP symmetry.

Similarly, the operators of $(C_{Hq}^{(3)})_{12,13}$ do not contribute to the EDMs through the four-quark operators. Let us consider another contribution. It is noticed that these operators include W boson interactions by taking the Higgs VEV as

$$\begin{aligned}
 (H^\dagger i \overleftrightarrow{D}_\mu^I H)(\bar{q}^i \gamma^\mu \tau^I q^j) &= iv^2 \left[(\bar{u}^i \gamma^\mu P_L d^j) \left(\frac{\sqrt{2}}{v} \partial_\mu G^+ - i \frac{g_2}{\sqrt{2}} W_\mu^+ \right) \right. \\
 &\quad \left. + (\bar{d}^i \gamma^\mu P_L u^j) \left(-\frac{\sqrt{2}}{v} \partial_\mu G^- - i \frac{g_2}{\sqrt{2}} W_\mu^- \right) \right] + \dots \quad (7.3)
 \end{aligned}$$

in the Feynman-'t Hooft gauge, where G^\pm is the NG bosons. Here, all the quark fields are left-handed in these interactions. Then, they seem to generate the electric and chromoelectric dipole moments through penguin diagrams of the W boson loops. However, it can be checked that such contributions vanish by paying attention to the chirality structure of the quark. Hence, the operators of $(C_{Hq}^{(3)})_{12,13}$ do not contribute to the nucleon EDMs.

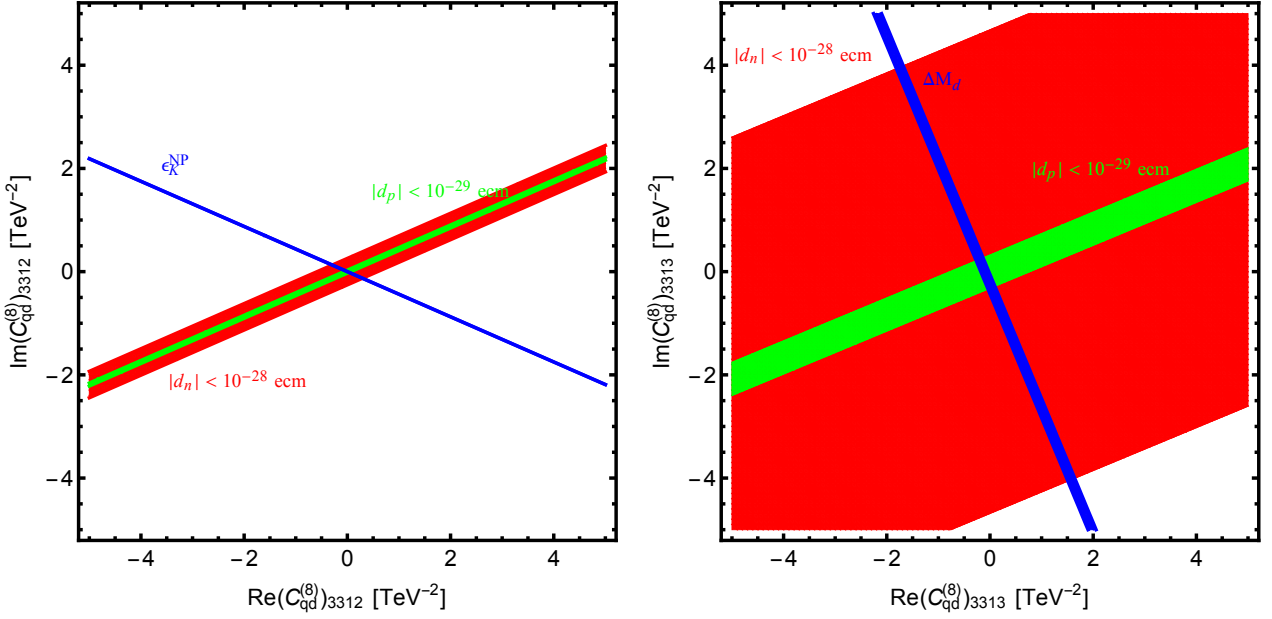


Figure 7.3: Same as Fig. 7.2, but the green region in the right panel corresponds to $|d_n| < 10^{-29} e \text{ cm}$, which is one order of magnitude weaker than the future sensitivity.

Finally, let us comment on C_{dd} . This operator can also contribute to the EDMs through the RGEs and matching conditions. However, these contributions are found to be very small, and we do not discuss them anymore.

7.3 Conclusion of nucleon EDM from SMEFT flavor-changing operator

We studied the nucleon EDMs induced by the SMEFT $\Delta F = 1$ operators and their correlations with the $\Delta F = 2$ observables. In the conventional LEFT evaluations, the correlations are not clear, because the heavy SM particles such as W and t are not dynamical. On the other hand, the SMEFT operators generate the correlations through the W boson loops because of the dynamical heavy SM particles. Therefore, the SMEFT effects on the nucleon EDMs are qualitatively important when we consider the correlations between the nucleon EDMs and flavor changing observables.

It was found that some of the operators are already excluded for $M_{\text{NP}} \lesssim 100 \text{ GeV}$ by the neutron EDM, and future experiments may be able to probe those in $M_{\text{NP}} \lesssim 2\text{--}10 \text{ TeV}$. Compared with ϵ_K , it was shown that the nucleon EDMs can provide a complementary information on the $\Delta S = 1$ effective operators in future, though the EDMs from the $\Delta B = 1$ operators are tiny and cannot compete with the constraints from ΔM_{B_d} .

In addition, similar to the evaluations of $\Delta F = 2$ observables discussed in Chapter 5, the

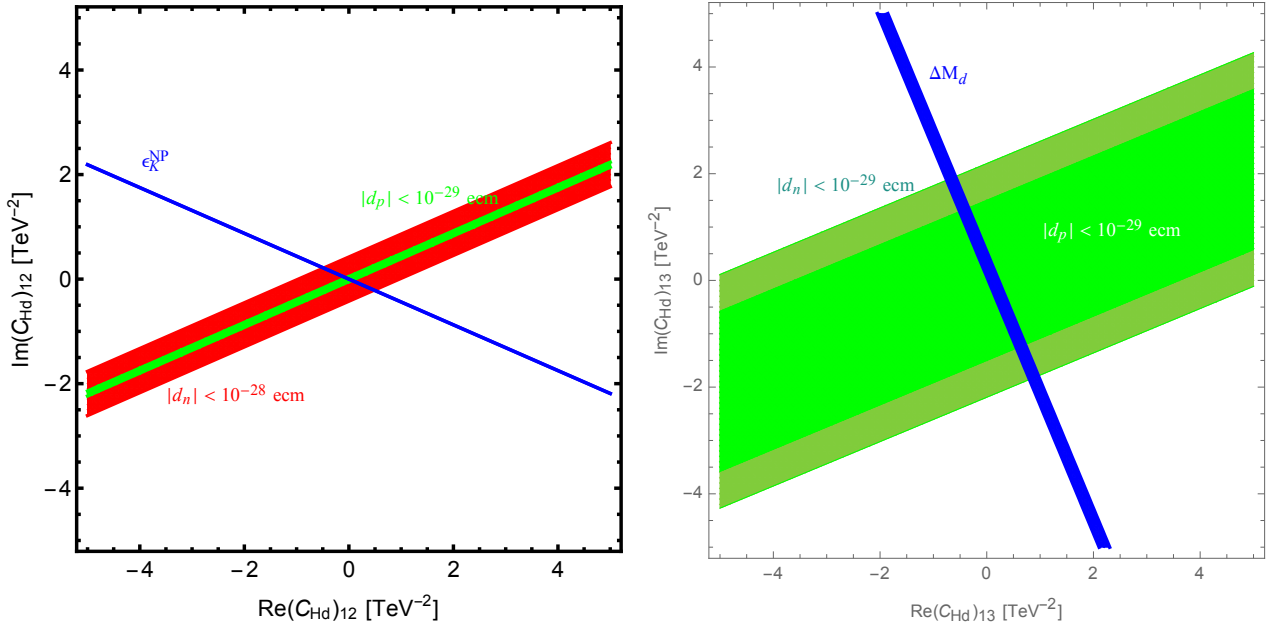


Figure 7.4: Same as Fig. 7.2, but the pink region in the left panel corresponds to $|d_n| < 10^{-29} \text{ e cm}$, which is one order of magnitude weaker than the future sensitivity. Besides, the deep green region in the right panel is $|d_n| < 10^{-31} \text{ e cm}$, which is much smaller than the future sensitivity.

SMEFT framework can reduce the scale uncertainty in the nucleon EDMs. As a result, we conclude that the SMEFT are quantitatively and qualitatively essential to investigate the NP effects on the nucleon EDMs.

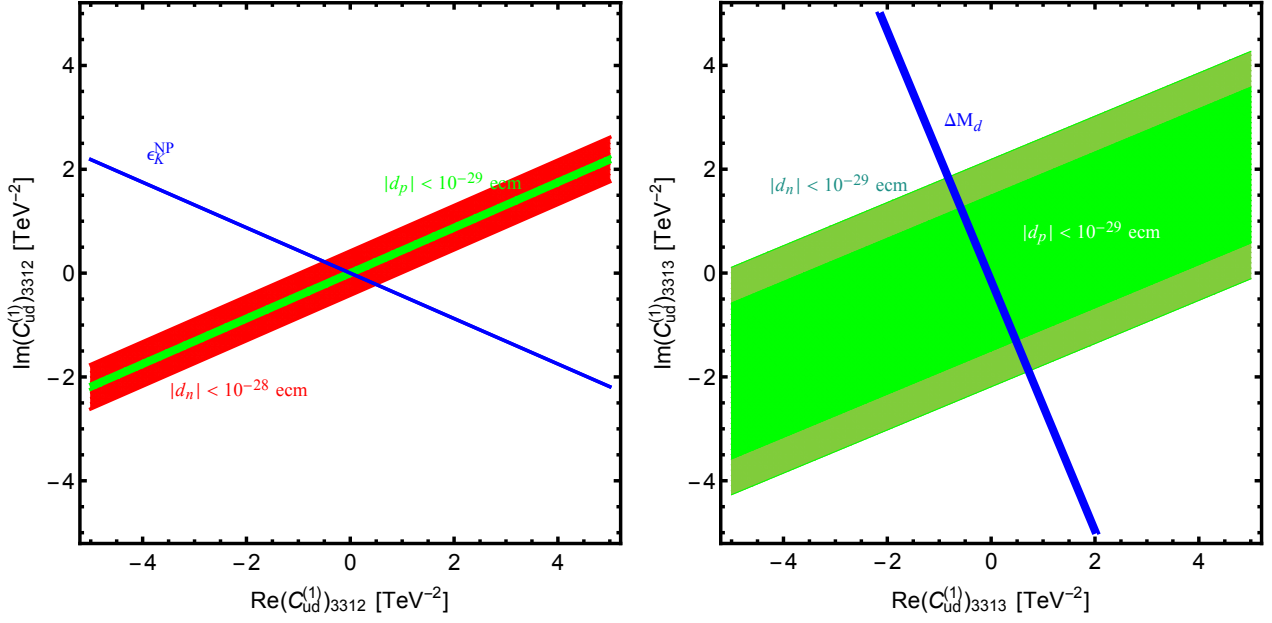


Figure 7.5: Same as Fig. 7.2, but the purple and green regions in the left panel correspond to $< 10^{-30}$ e cm, which are weaker than the future sensitivities. Also, the deep green region in the right panel is $|d_n| < 10^{-31}$ e cm.

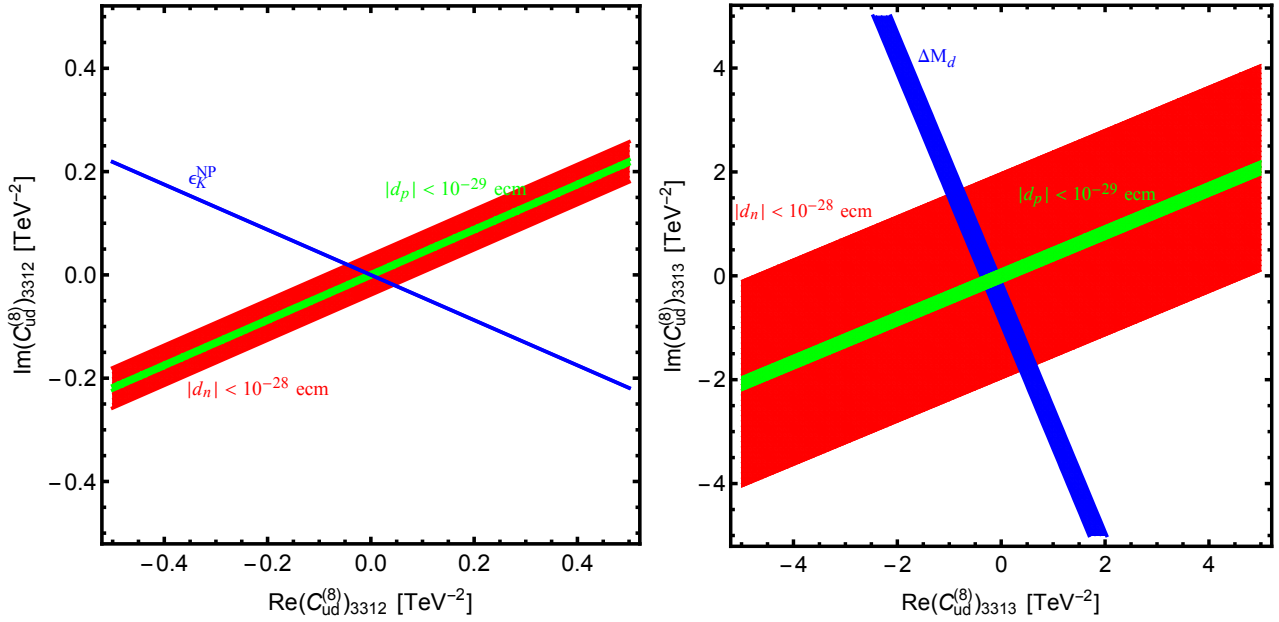


Figure 7.6: Same as Fig. 7.2, but the deep green region in the right panel is $|d_n| < 10^{-31}$ e cm.

Chapter

8

Conclusion

The standard model of the particle physics describes nature very well. Nevertheless, there are some unsolved problems within the SM. Although, the unsolved problems in the SM make the NP scale near the EWSB one be fascinating, we face the possibility that the NP scale is much higher than the EWSB scale because of still no evidence for the new particle production at the end of run 2 of the LHC experiment. At the current stage, indirect searches of the NP with flavor and CP violating observables become more important.

In the flavor-changing processes, many observables have been precisely determined in both of theoretical calculations and experimental data. In future, the precisions in the flavor experiments will be further improved, and theoretical precise calculations become more important. Besides, in the flavor-conserving CP violating processes, several experiments are proposed to measure nucleon EDMs, whose sensitivities would be improved by 2–3 orders of magnitudes in near future. Although the EDMs are flavor-conserving processes, they have a sensitivity to flavor violations through the W -boson interactions. Thus, NP effects on quark flavor-changing neutral currents can contribute to quark EDMs simultaneously by exchanging the W boson. Since the EDMs are very sensitive to NP, they can also probe flavor-changing contributions to the NP.

In conventional evaluations of the low-scale observables related to the flavor and/or CP violation, heavy degrees of freedom, such as NP particles and heavy SM particles are simultaneously decoupled, and the NP model is matched onto the LEFT. Because of a hierarchy between the NP scale and the EWSB one, the conventional approach is broken down, and some problems occur. For example, the matching scale uncertainty at the EWSB scale appears in the conventional LEFT approach. Besides, in the NP effects of $\Delta F = 2$ processes mediated by the Z boson, the gauge invariance is not retained, because the NP contributions are encoded in the LEFT without quantum corrections from the NG boson. In addition, flavor-changing operators in the LEFT can not correlate to the EDMs without specifying a NP model because of no W boson. In order to resolve these problems, an effective field theory in which the heavy SM degrees of freedom are retained is needed. The SMEFT is one of the promising effective field theories above the EWSB scale: this effective field theory includes all the SM particles as dynamical degrees of freedom. In the SMEFT approach, the NP effects are encoded in the

SMEFT at the NP scale. After evaluating the SMEFT RGEs, the SMEFT are matched onto the LEFT at the EWSB scale, and the low-scale observables are calculated by using the LEFT. By this approach, the matching scale uncertainty can be eliminated. Besides, thanks to the dynamical heavy SM particles in the SMEFT, the gauge invariance in the NP effects of $\Delta F = 2$ processes mediated by the Z boson, and the correlations between the nucleon EDMs and flavor changing observables are restored. Although the important points of the SMEFT approach are the SMEFT RGEs and matching at the EWSB scale, the one-loop matching at the EWSB scale had not been calculated. Since the NP effects in the conventional LEFT evaluations are at the one-loop level, the one-loop matching formulae at the EWSB scale are also essential in order to realize the high precision calculations in the SMEFT.

In this thesis, we established a systematic way to estimate flavor and/or CP violating observables within the SMEFT by providing the one-loop matching formulae. By the established SMEFT approach, we investigated the scale uncertainty in $\Delta F = 2$ processes, Z mediated SMEFT correction in the $\Delta F = 2$ processes, and the SMEFT $\Delta F = 1$ operators effects on the nucleon EDMs.

In Chapter 3, we have studied the one-loop matching conditions related to the SMEFT $\Delta F = 1$ operators. We found that the SMEFT $\Delta F = 1$ operators contribute to both of $\Delta F = 2$ and 0 processes by decoupling W , Z , H and the top quark t . Besides, it was found that by the one-loop matching formulae, the LEFT Wilson coefficients at the EWSB scale are changed by $\mathcal{O}(10)\%$ compared with the tree-level matching contributions.

In Chapter 5, we have studied the scale uncertainty in $\Delta F = 2$ processes with the one-loop matching formulae. By a model independent approach, we found that the magnitude of the scale uncertainty in the LEFT Wilson coefficient is $\mathcal{O}(1-100)\%$. As an application of this approach, we also investigated ΔM_{B_s} in the left-right symmetric model and confirmed that the scale uncertainty is $\mathcal{O}(1)\%$. These scale uncertainty in $\Delta F = 2$ processes are removed by adopting the SMEFT approach. Therefore, the SMEFT approach enables us to evaluate the NP contributions to the low-scale observables relevant for the flavor and/or CP violation with high precision by eliminating the matching scale uncertainty.

In Chapter 6, we have investigated the Z mediated SMEFT corrections to $\Delta F = 2$ observables in the kaon system. Although they were overlooked so far, we showed that the SMEFT corrections make experimental constraints coming from ϵ_K drastically change. By a model independent approach, we found that the right-handed NP effects encoded in $(C_{Hd})_{12}$ are enhanced, and the constraint from ϵ_K becomes severer. Besides, the SMEFT corrections provide various correlations between $\Delta F = 1$ and 2 observables by the dynamical Z boson. Compared with the $\Delta S = 1$ observables such as ϵ'/ϵ_K , $\mathcal{B}(K_L \rightarrow \mu^+\mu^-)$, it was shown that ϵ_K provides an complementary information on the $\Delta S = 1$. As an application of this approach, we also considered Z mediated gluino contributions. In a simplified scenario, it was found that the

Z mediated SMEFT corrections may make the constraint for the SUSY scale be changed by $\mathcal{O}(100\%)$ compared with the conventional box diagram contributions. Besides, we found that the gluino mediated contributions are consistent with the experimental data such as ϵ_K , ϵ'/ϵ_K and $\mathcal{B}(\bar{B} \rightarrow X_{d,s}\gamma)$, if the squark mass is smaller than 5.6 TeV. Therefore, the SMEFT approach enables us to take into account the various correlations between flavor changing observables, especially the severe constraints from ϵ_K in C_{Hd} .

In Chapter 7, we have also studied the SMEFT $\Delta F = 1$ operators contributions to the nucleon EDMs. We studied flavor changing operators effects on the nucleon EDMs within the framework of the SMEFT. In particular, we focused on the SMEFT $\Delta F = 1$ operators, and discussed the contributions of those operators to $\Delta F = 0$ and 2 observables through the top quark decoupling. It was found that NP scale is larger than 100 GeV by the current EDMs experiments, and the future experiments may achieve a sensitivity of 2–10 TeV. Therefore, the SMEFT approach enables us to investigate the correlations between the nucleon EDMs and the $\Delta F = 2$ observables without specifying the NP model.

As a result, we conclude that the SMEFT approach is quantitatively and qualitatively essential to evaluate the NP effects on the low-scale observables when the NP scale is much higher than the EWSB one.

A.1 Renormalization group equations of SMEFT

In this appendix, we summarize the SMEFT RGEs which are relevant for the $\Delta F = 2$ observables at the one-loop level. We focus on the anomalous dimensions which depend on the top-Yukawa or QCD couplings. In the following expressions, we define

$$\dot{C}_a \equiv (4\pi)^2 \frac{dC_a}{d \ln \mu}, \quad X_t \equiv \frac{\pi\alpha}{s_W^2} x_t. \quad (\text{A.1})$$

The anomalous dimensions at $\mathcal{O}(y_t^2)$ and $\mathcal{O}(g_s^2)$ are obtained as (see Refs. [13–15] for the complete one-loop formula of the SMEFT RGEs):

$$\begin{aligned} (\dot{C}_{Hq}^{(1)})_{pr} = X_t & \left[\lambda_t^{pr} (C_{H\Box} + C_{HD}) - 2\lambda_t^{pr} (C_{Hu})_{33} + 3\lambda_t^{pt} (C_{Hq}^{(1)})_{tr} + 3\lambda_t^{tr} (C_{Hq}^{(1)})_{pt} \right. \\ & - 9\lambda_t^{pt} (C_{Hq}^{(3)})_{tr} - 9\lambda_t^{tr} (C_{Hq}^{(3)})_{pt} \\ & + 2\lambda_t^{ts} \left(6(C_{qq}^{(1)})_{prst} + 6(C_{qq}^{(1)})_{stpr} + (C_{qq}^{(1)})_{ptsr} + (C_{qq}^{(1)})_{srpt} + 3(C_{qq}^{(3)})_{ptsr} + 3(C_{qq}^{(3)})_{srpt} \right) \\ & \left. - 12\lambda_t^{kk} (C_{qu}^{(1)})_{pr33} + 12\lambda_t^{kk} (C_{Hq}^{(1)})_{pr} + \lambda_t^{pt} (C_{Hq}^{(1)})_{tr} + \lambda_t^{tr} (C_{Hq}^{(1)})_{pt} \right], \quad (\text{A.2}) \end{aligned}$$

$$\begin{aligned} (\dot{C}_{Hq}^{(3)})_{pr} = X_t & \left[-\lambda_t^{pr} C_{H\Box} - 3\lambda_t^{pt} (C_{Hq}^{(1)})_{tr} - 3\lambda_t^{tr} (C_{Hq}^{(1)})_{pt} + \lambda_t^{pt} (C_{Hq}^{(3)})_{tr} + \lambda_t^{tr} (C_{Hq}^{(3)})_{pt} \right. \\ & - 2\lambda_t^{ts} \left(6(C_{qq}^{(3)})_{prst} + 6(C_{qq}^{(3)})_{stpr} + (C_{qq}^{(1)})_{ptsr} + (C_{qq}^{(1)})_{srpt} - (C_{qq}^{(3)})_{ptsr} - (C_{qq}^{(3)})_{srpt} \right) \\ & \left. + 12\lambda_t^{kk} (C_{Hq}^{(3)})_{pr} + \lambda_t^{pt} (C_{Hq}^{(3)})_{tr} + \lambda_t^{tr} (C_{Hq}^{(3)})_{pt} \right], \quad (\text{A.3}) \end{aligned}$$

$$(\dot{C}_{Hd})_{pr} = X_t \left[-12\lambda_t^{kk} (C_{ud}^{(1)})_{33pr} + 12\lambda_t^{ts} (C_{qd}^{(1)})_{stpr} + 12\lambda_t^{kk} (C_{Hd})_{pr} \right], \quad (\text{A.4})$$

$$\begin{aligned} (\dot{C}_{Hu})_{pr} = X_t & \left[-2\lambda_t^{kk} \delta_{p3} \delta_{3r} (C_{H\Box} + C_{HD}) - 4\lambda_t^{ts} \delta_{p3} \delta_{3r} (C_{Hq}^{(1)})_{st} + 6\lambda_t^{kk} \delta_{p3} (C_{Hu})_{3r} + 6\lambda_t^{kk} \delta_{3r} (C_{Hu})_{p3} \right. \\ & - 4\lambda_t^{kk} \left(3(C_{uu})_{pr33} + 3(C_{uu})_{33pr} + (C_{uu})_{p33r} + (C_{uu})_{3rp3} \right) \\ & \left. + 12\lambda_t^{ts} (C_{qu}^{(1)})_{stpr} + 12\lambda_t^{kk} (C_{Hu})_{pr} + 2\lambda_t^{kk} \delta_{p3} (C_{Hu})_{3r} + 2\lambda_t^{kk} \delta_{r3} (C_{Hu})_{p3} \right], \quad (\text{A.5}) \end{aligned}$$

$$\dot{C}_{H\Box} = X_t \left[-2 \left(-6\lambda_t^{sr} (C_{Hq}^{(1)})_{rs} + 18\lambda_t^{sr} (C_{Hq}^3)_{rs} + 6\lambda_t^{kk} (C_{Hu})_{33} \right) + 24\lambda_t^{kk} C_{H\Box} \right], \quad (\text{A.6})$$

$$\dot{C}_{HD} = X_t \left[-2 \left(-24\lambda_t^{sr} (C_{Hq}^{(1)})_{rs} + 24\lambda_t^{kk} (C_{Hu})_{33} \right) + 24\lambda_t^{kk} C_{HD} \right], \quad (\text{A.7})$$

$$\begin{aligned} (\dot{C}_{uu})_{prst} = X_t & \left[-2\lambda_t^{kk} \delta_{p3} \delta_{3r} (C_{Hu})_{st} - 2\lambda_t^{kk} \delta_{s3} \delta_{3t} (C_{Hu})_{pr} \right. \\ & - 2\lambda_t^{wv} \delta_{r3} \delta_{p3} (C_{qu}^{(1)})_{vwst} - 2\lambda_t^{wv} \delta_{t3} \delta_{s3} (C_{qu}^{(1)})_{vwpr} \\ & + \frac{1}{3} \lambda_t^{wv} \delta_{p3} \delta_{r3} (C_{qu}^{(8)})_{vwst} + \frac{1}{3} \lambda_t^{wv} \delta_{s3} \delta_{t3} (C_{qu}^{(8)})_{vwpr} \\ & - \lambda_t^{wv} \delta_{s3} \delta_{3r} (C_{qu}^{(8)})_{vwpt} - \lambda_t^{wv} \delta_{t3} \delta_{p3} (C_{qu}^{(8)})_{vwsr} \\ & \left. + 2\lambda_t^{kk} \delta_{p3} (C_{uu})_{3rst} + 2\lambda_t^{kk} \delta_{s3} (C_{uu})_{pr3t} + 2\lambda_t^{kk} \delta_{r3} (C_{uu})_{p3st} + 2\lambda_t^{kk} \delta_{t3} (C_{uu})_{prs3} \right] \\ & + 4\pi\alpha_s \left[\frac{1}{3} (C_{qu}^{(8)})_{wvpt} \delta_{rs} + \frac{1}{3} (C_{qu}^{(8)})_{wvsr} \delta_{pt} - \frac{1}{3N_c} (C_{qu}^{(8)})_{wvst} \delta_{pr} - \frac{1}{3N_c} (C_{qu}^{(8)})_{wvpr} \delta_{st} \right. \\ & + \frac{1}{3} (C_{uu})_{pwut} \delta_{rs} + \frac{1}{3} (C_{uu})_{swwr} \delta_{pt} + \frac{1}{3} (C_{uu})_{wtpw} \delta_{rs} + \frac{1}{3} (C_{uu})_{wrs w} \delta_{pt} \\ & - \frac{1}{3N_c} (C_{uu})_{pwvr} \delta_{st} - \frac{1}{3N_c} (C_{uu})_{swwt} \delta_{pr} - \frac{1}{3N_c} (C_{uu})_{wrpw} \delta_{st} \\ & - \frac{1}{3N_c} (C_{uu})_{wtsw} \delta_{pr} + \frac{1}{6} (C_{ud}^{(8)})_{ptw} \delta_{rs} + \frac{1}{6} (C_{ud}^{(8)})_{srw} \delta_{pt} - \frac{1}{6N_c} (C_{ud}^{(8)})_{prw} \delta_{st} \\ & \left. - \frac{1}{6N_c} (C_{ud}^{(8)})_{stw} \delta_{pr} + 6(C_{uu})_{ptsr} - \frac{6}{N_c} (C_{uu})_{prst} \right], \quad (\text{A.8}) \end{aligned}$$

$$\begin{aligned} (\dot{C}_{ud}^{(1)})_{prst} = X_t & \left[-4\lambda_t^{kk} \delta_{p3} \delta_{3r} (C_{Hd})_{st} - 4\lambda_t^{wv} \delta_{p3} \delta_{r3} (C_{qd}^{(1)})_{vwst} + 2\lambda_t^{kk} \delta_{p3} (C_{ud}^{(1)})_{3rst} + 2\lambda_t^{kk} \delta_{r3} (C_{ud}^{(1)})_{p3st} \right] \\ & + 3 \left(\frac{N_c^2 - 1}{N_c^2} \right) 4\pi\alpha_s (C_{ud}^{(8)})_{prst}, \quad (\text{A.9}) \end{aligned}$$

$$\begin{aligned} (\dot{C}_{ud}^{(8)})_{prst} = X_t & \left[-4\lambda_t^{wv} \delta_{r3} \delta_{p3} (C_{qd}^{(8)})_{vwst} + 2\lambda_t^{kk} \delta_{p3} (C_{ud}^{(8)})_{3rst} + 2\lambda_t^{kk} \delta_{r3} (C_{ud}^{(8)})_{p3st} \right] \\ & + 4\pi\alpha_s \left[\frac{4}{3} (C_{uu})_{pwvr} \delta_{st} + \frac{4}{3} (C_{uu})_{wrpw} \delta_{st} + \frac{4}{3} (C_{dd})_{swwt} \delta_{pr} + \frac{4}{3} (C_{dd})_{wtsw} \delta_{pr} \right. \\ & + \frac{4}{3} (C_{qu}^{(8)})_{wvpr} \delta_{st} + \frac{4}{3} (C_{qd}^{(8)})_{wvst} \delta_{pr} \\ & \left. + \frac{2}{3} (C_{ud}^{(8)})_{prw} \delta_{st} + \frac{2}{3} (C_{ud}^{(8)})_{wvst} \delta_{pr} - 12 \frac{1}{N_c} (C_{ud}^{(8)})_{prst} + 12 (C_{ud}^{(1)})_{prst} \right], \quad (\text{A.10}) \end{aligned}$$

$$\begin{aligned} (\dot{C}_{qu}^{(1)})_{prst} = X_t & \left[\frac{4}{3} \lambda_t^{wr} \delta_{s3} \left((C_{qu}^{(1)})_{pw3t} + \frac{4}{3} (C_{qu}^{(8)})_{pw3t} \right) + \frac{4}{3} \lambda_t^{pv} \delta_{t3} \left((C_{qu}^{(1)})_{rv3s} + \frac{4}{3} (C_{qu}^{(8)})_{rv3s} \right) \right. \\ & + 2\lambda_t^{pr} (C_{Hu})_{st} - 4\lambda_t^{kk} \delta_{s3} \delta_{3t} (C_{Hq}^{(1)})_{pr} + \frac{1}{3} \left(2\lambda_t^{pv} \delta_{s3} (C_{qu}^{(1)})_{vr3t} + 2\lambda_t^{vr} \delta_{3t} (C_{qu}^{(1)})_{pvs3} \right) \\ & - \frac{1}{9} \left(\lambda_t^{pv} \delta_{s3} (C_{qu}^{(8)})_{vr3t} + \lambda_t^{vr} \delta_{3t} (C_{qu}^{(8)})_{pvs3} \right) \\ & - \frac{2}{3} \left(\lambda_t^{vw} \delta_{s3} \delta_{3t} (C_{qq}^{(1)})_{pvwr} + \lambda_t^{wv} \delta_{s3} \delta_{3t} (C_{qq}^{(1)})_{pwwr} + \lambda_t^{pr} (C_{uu})_{3ts3} + \lambda_t^{pr} (C_{uu})_{3ts3} \right) \\ & \left. - 2 \left(\lambda_t^{vw} \delta_{s3} \delta_{3t} (C_{qq}^{(3)})_{pvwr} + \lambda_t^{wv} \delta_{s3} \delta_{3t} (C_{qq}^{(3)})_{pwwr} \right) \right] \end{aligned}$$

$$\begin{aligned}
 & + \left(\lambda_t^{pv} \delta_{s3} (C_{qu}^{(8)})_{vr3t} + \lambda_t^{vr} \delta_{3t} (C_{qu}^{(8)})_{pvs3} \right) - 8\lambda_t^{wv} \delta_{s3} \delta_{3t} (C_{qq}^{(1)})_{prvw} - 4\lambda_t^{pr} (C_{uu})_{33st} \\
 & + \lambda_t^{pv} (C_{qu}^{(1)})_{vrst} + 2\lambda_t^{kk} \delta_{s3} (C_{qu}^{(1)})_{pr3t} + \lambda_t^{vr} (C_{qu}^{(1)})_{pvst} + 2\lambda_t^{kk} \delta_{t3} (C_{qu}^{(1)})_{prs3} \Big] \\
 & - 3 \left(\frac{N_c^2 - 1}{N_c^2} \right) 4\pi\alpha_s (C_{qu}^{(8)})_{prst}, \tag{A.11}
 \end{aligned}$$

$$\begin{aligned}
 (\dot{C}_{qu}^{(8)})_{prst} = & X_t \left[8\lambda_t^{wr} \delta_{s3} \left((C_{qu}^{(1)})_{pw3t} + \frac{4}{3} (C_{qu}^{(8)})_{pw3t} \right) + 8\lambda_t^{pv} \delta_{t3} \left((C_{qu}^{(1)})_{rv3s} + \frac{4}{3} (C_{qu}^{(8)})_{rv3s} \right) \right. \\
 & - \frac{2}{3} \left(\lambda_t^{pv} \delta_{s3} (C_{qu}^{(8)})_{vr3t} + \lambda_t^{vr} \delta_{3t} (C_{qu}^{(8)})_{pvs3} \right) \\
 & - 4 \left(\lambda_t^{vw} \delta_{s3} \delta_{3t} (C_{qq}^{(1)})_{pvwr} + \lambda_t^{wv} \delta_{s3} \delta_{3t} (C_{qq}^{(1)})_{pwwr} - \lambda_t^{pv} \delta_{s3} (C_{qu}^{(1)})_{vr3t} - \lambda_t^{vr} \delta_{3t} (C_{qu}^{(1)})_{pvs3} \right) \\
 & - 4 \left(\lambda_t^{pr} (C_{uu})_{3ts3} + \lambda_t^{pr} (C_{uu})_{3ts3} \right) - 12 \left(\lambda_t^{vw} \delta_{s3} \delta_{3t} (C_{qq}^{(3)})_{pvwr} + \lambda_t^{wr} \delta_{s3} \delta_{3t} (C_{qq}^{(3)})_{pwwr} \right) \\
 & \left. + \lambda_t^{pv} (C_{qu}^{(8)})_{vrst} + 2\lambda_t^{kk} \delta_{s3} (C_{qu}^{(8)})_{pr3t} + \lambda_t^{vr} (C_{qu}^{(8)})_{pvst} + 2\lambda_t^{kk} \delta_{t3} (C_{qu}^{(8)})_{prs3} \right] \\
 & + 4\pi\alpha_s \left[\frac{4}{3} (C_{qq}^{(1)})_{pwwr} \delta_{st} + \frac{4}{3} (C_{qq}^{(1)})_{wrpw} \delta_{st} + 4(C_{qq}^{(3)})_{pwwr} \delta_{st} + 4(C_{qq}^{(3)})_{wrpw} \delta_{st} \right. \\
 & + \frac{2}{3} (C_{qu}^{(8)})_{prww} \delta_{st} + \frac{2}{3} (C_{qu}^{(8)})_{prww} \delta_{st} + \frac{4}{3} (C_{qu}^{(8)})_{wvst} \delta_{pr} \\
 & + \frac{2}{3} (C_{ud}^{(8)})_{stww} \delta_{pr} + \frac{4}{3} (C_{uu})_{swwt} \delta_{pr} + \frac{4}{3} (C_{uu})_{wtsw} \delta_{pr} \\
 & \left. - 6 \left(N_c - \frac{2}{N_c} \right) (C_{qu}^{(8)})_{prst} - 12(C_{qu}^{(1)})_{prst} \right], \tag{A.12}
 \end{aligned}$$

$$\begin{aligned}
 (\dot{C}_{qq}^{(1)})_{prst} = & X_t \left[\lambda_t^{pr} (C_{Hq}^{(1)})_{st} + \lambda_t^{st} (C_{Hq}^{(1)})_{pr} \right. \\
 & + \frac{1}{6} \left(\lambda_t^{pr} (C_{qu}^{(8)})_{st33} + \lambda_t^{st} (C_{qu}^{(8)})_{pr33} \right) - \frac{1}{4} \left(\lambda_t^{pt} (C_{qu}^{(8)})_{sr33} + \lambda_t^{sr} (C_{qu}^{(8)})_{pt33} \right) \\
 & - \lambda_t^{pr} (C_{qu}^{(1)})_{st33} - \lambda_t^{st} (C_{qu}^{(1)})_{pr33} \\
 & \left. + \lambda_t^{pv} (C_{qq}^{(1)})_{vrst} + \lambda_t^{sv} (C_{qq}^{(1)})_{prvt} + \lambda_t^{vr} (C_{qq}^{(1)})_{pvst} + \lambda_t^{vt} (C_{qq}^{(1)})_{prsv} \right] \\
 & + 4\pi\alpha_s \left[3(C_{qq}^{(1)})_{ptsr} + 9(C_{qq}^{(3)})_{ptsr} - \frac{6}{N_c} (C_{qq}^{(1)})_{prst} \right. \\
 & + \frac{1}{6} (C_{qq}^{(1)})_{swwr} \delta_{pt} + \frac{1}{6} (C_{qq}^{(1)})_{pwwt} \delta_{rs} + \frac{1}{6} (C_{qq}^{(1)})_{wrs w} \delta_{pt} + \frac{1}{6} (C_{qq}^{(1)})_{wtpw} \delta_{rs} \\
 & - \frac{1}{3N_c} (C_{qq}^{(1)})_{pwwr} \delta_{st} - \frac{1}{3N_c} (C_{qq}^{(1)})_{swwt} \delta_{pr} - \frac{1}{3N_c} (C_{qq}^{(1)})_{wrpw} \delta_{st} - \frac{1}{3N_c} (C_{qq}^{(1)})_{wts w} \delta_{pr} \\
 & + \frac{1}{2} (C_{qq}^{(3)})_{swwr} \delta_{pt} + \frac{1}{2} (C_{qq}^{(3)})_{pwwt} \delta_{rs} + \frac{1}{2} (C_{qq}^{(3)})_{wrs w} \delta_{pt} + \frac{1}{2} (C_{qq}^{(3)})_{wtpw} \delta_{rs} \\
 & - \frac{1}{N_c} (C_{qq}^{(3)})_{pwwr} \delta_{st} - \frac{1}{N_c} (C_{qq}^{(3)})_{swwt} \delta_{pr} - \frac{1}{N_c} (C_{qq}^{(3)})_{wrpw} \delta_{st} - \frac{1}{N_c} (C_{qq}^{(3)})_{wts w} \delta_{pr} \\
 & + \frac{1}{12} (C_{qu}^{(8)})_{srww} \delta_{pt} + \frac{1}{12} (C_{qu}^{(8)})_{ptww} \delta_{rs} - \frac{1}{6N_c} (C_{qu}^{(8)})_{prww} \delta_{st} - \frac{1}{6N_c} (C_{qu}^{(8)})_{stww} \delta_{pr} \\
 & \left. + \frac{1}{12} (C_{qd}^{(8)})_{srww} \delta_{pt} + \frac{1}{12} (C_{qd}^{(8)})_{ptww} \delta_{rs} - \frac{1}{6N_c} (C_{qd}^{(8)})_{prww} \delta_{st} - \frac{1}{6N_c} (C_{qd}^{(8)})_{stww} \delta_{pr} \right], \tag{A.13}
 \end{aligned}$$

$$\begin{aligned}
 (\dot{C}_{qq}^{(3)})_{prst} = & X_t \left[-\lambda_t^{pr}(C_{Hq}^{(3)})_{st} - \lambda_t^{st}(C_{Hq}^{(3)})_{pr} - \frac{1}{4} \left(\lambda_t^{pt}(C_{qu}^{(8)})_{sr33} + \lambda_t^{sr}(C_{qu}^{(8)})_{pt33} \right) \right. \\
 & \left. + \lambda_t^{pv}(C_{qq}^{(3)})_{vrst} + \lambda_t^{sv}(C_{qq}^{(3)})_{prvt} + \lambda_t^{vr}(C_{qq}^{(3)})_{pvst} + \lambda_t^{vt}(C_{qq}^{(3)})_{prsv} \right] \\
 & + 4\pi\alpha_s \left[-3(C_{qq}^{(3)})_{ptsr} - \frac{6}{N_c}(C_{qq}^{(3)})_{prst} + 3(C_{qq}^{(1)})_{ptsr} \right. \\
 & + \frac{1}{6}(C_{qq}^{(1)})_{pwwt}\delta_{rs} + \frac{1}{6}(C_{qq}^{(1)})_{swwr}\delta_{pt} + \frac{1}{6}(C_{qq}^{(1)})_{wtpw}\delta_{rs} + \frac{1}{6}(C_{qq}^{(1)})_{wrsu}\delta_{pt} \\
 & + \frac{1}{2}(C_{qq}^{(3)})_{pwwt}\delta_{sr} + \frac{1}{2}(C_{qq}^{(3)})_{swwr}\delta_{pt} + \frac{1}{2}(C_{qq}^{(3)})_{wtpw}\delta_{rs} + \frac{1}{2}(C_{qq}^{(3)})_{wrsu}\delta_{pt} \\
 & \left. + \frac{1}{12}(C_{qu}^{(8)})_{ptww}\delta_{rs} + \frac{1}{12}(C_{qu}^{(8)})_{srww}\delta_{pt} + \frac{1}{12}(C_{qd}^{(8)})_{ptww}\delta_{rs} + \frac{1}{12}(C_{qd}^{(8)})_{srww}\delta_{pt} \right], \tag{A.14}
 \end{aligned}$$

$$\begin{aligned}
 (\dot{C}_{dd})_{prst} = & 4\pi\alpha_s \left[6(C_{dd})_{ptsr} - \frac{6}{N_c}(C_{dd})_{prst} \right. \\
 & + \frac{1}{3}(C_{dd})_{pwwt}\delta_{rs} + \frac{1}{3}(C_{dd})_{wtpw}\delta_{rs} + \frac{1}{3}(C_{dd})_{wrsu}\delta_{pt} - \frac{1}{3N_c}(C_{dd})_{pwwr}\delta_{st} \\
 & - \frac{1}{3N_c}(C_{dd})_{swut}\delta_{pr} - \frac{1}{3N_c}(C_{dd})_{wtsu}\delta_{pr} - \frac{1}{3N_c}(C_{dd})_{wrpu}\delta_{st} \\
 & + \frac{1}{3}(C_{qd}^{(8)})_{wvsr}\delta_{pt} + \frac{1}{3}(C_{qd}^{(8)})_{wvpt}\delta_{rs} - \frac{1}{3N_c}(C_{qd}^{(8)})_{wvpr}\delta_{st} - \frac{1}{3N_c}(C_{qd}^{(8)})_{wvst}\delta_{pr} \\
 & \left. + \frac{1}{6}(C_{ud}^{(8)})_{wvpt}\delta_{rs} + \frac{1}{6}(C_{ud}^{(8)})_{wvsr}\delta_{pt} - \frac{1}{6N_c}(C_{ud}^{(8)})_{wvpr}\delta_{st} - \frac{1}{6N_c}(C_{ud}^{(8)})_{wvst}\delta_{pr} \right], \tag{A.15}
 \end{aligned}$$

$$\begin{aligned}
 (\dot{C}_{qd}^{(1)})_{prst} = & X_t \left[2\lambda_t^{pr}(C_{Hd})_{st} - 2\lambda_t^{pr}(C_{ud}^{(1)})_{33st} + \lambda_t^{pv}(C_{qd}^{(1)})_{vrst} + \lambda_t^{vr}(C_{qd}^{(1)})_{pvst} \right] \\
 & - 3 \left(\frac{N_c^2 - 1}{N_c^2} \right) 4\pi\alpha_s (C_{qd}^{(8)})_{prst}, \tag{A.16}
 \end{aligned}$$

$$\begin{aligned}
 (\dot{C}_{qd}^{(8)})_{prst} = & X_t \left[-2\lambda_t^{pr}(C_{ud}^{(8)})_{33st} + \lambda_t^{pv}(C_{qd}^{(8)})_{vrst} + \lambda_t^{vr}(C_{qd}^{(8)})_{pvst} \right] \\
 & + 4\pi\alpha_s \left[\frac{4}{3}(C_{qq}^{(1)})_{pwwr}\delta_{st} + \frac{4}{3}(C_{qq}^{(1)})_{wrpu}\delta_{st} + 4(C_{qq}^{(3)})_{pwwr}\delta_{st} + 4(C_{qq}^{(3)})_{wrpu}\delta_{st} \right. \\
 & + \frac{2}{3}(C_{qu}^{(8)})_{prww}\delta_{st} + \frac{2}{3}(C_{qd}^{(8)})_{prww}\delta_{st} + \frac{4}{3}(C_{qd}^{(8)})_{wvst}\delta_{pr} + \frac{2}{3}(C_{ud}^{(8)})_{wvst}\delta_{pr} \\
 & \left. + \frac{4}{3}(C_{dd})_{swut}\delta_{pr} + \frac{4}{3}(C_{dd})_{wtsu}\delta_{pr} - 6 \left(N_c - \frac{2}{N_c} \right) (C_{qd}^{(8)})_{prst} - 12(C_{qd}^{(1)})_{prst} \right]. \tag{A.17}
 \end{aligned}$$

A.2 QCD RGEs for EDMs

In this section, we summarize the RGEs of flavor-conserving effective operators for the CP violation in QCD [105]. The RGEs for the Wilson coefficients of these operators are given as

$$\mu \frac{\partial \mathbf{C}}{\partial \mu} = \mathbf{C}\mathbf{\Gamma}, \tag{A.18}$$

where the Wilson coefficients are written in a column vector as

$$\mathbf{C} = \left(C_1^q, C_2^q, C_3, C_4^q, C_5^q, \tilde{C}_1^{q'q}, \tilde{C}_2^{q'q}, \tilde{C}_1^{qq'}, \tilde{C}_2^{qq'}, \tilde{C}_3^{q'q}, \tilde{C}_4^{q'q} \right). \quad (\text{A.19})$$

The anomalous matrix is calculated at one-loop level as

$$\mathbf{\Gamma} = \begin{pmatrix} \frac{\alpha_s}{4\pi} \gamma_s & \mathbf{0} & \mathbf{0} \\ \frac{1}{(4\pi)^2} \gamma_{sf} & \frac{\alpha_s}{4\pi} \gamma_f & \mathbf{0} \\ \frac{1}{(4\pi)^2} \gamma'_{sf} & \mathbf{0} & \frac{\alpha_s}{4\pi} \gamma'_f \end{pmatrix} \quad (\text{A.20})$$

where

$$\gamma_s = \begin{pmatrix} +8C_F & 0 & 0 \\ +8C_F & +16C_F - 4N & 0 \\ 0 & +2N & N + 2n_f + \beta_0 \end{pmatrix}, \quad (\text{A.21})$$

$$\gamma_f = \begin{pmatrix} -12C_F + 6 & +\frac{1}{N} - \frac{1}{2} \\ +\frac{48}{N} + 24 & +4C_F + 6 \end{pmatrix}, \quad (\text{A.22})$$

$$\gamma'_f = \begin{pmatrix} -12C_F & 0 & 0 & 0 & +\frac{1}{N} & -1 \\ -6 & +\frac{6}{N} & 0 & 0 & -\frac{1}{2} & -C_F + \frac{1}{2N} \\ 0 & 0 & -12C_F & 0 & +\frac{1}{N} & -1 \\ 0 & 0 & -6 & +\frac{6}{N} & -\frac{1}{2} & -C_F + \frac{1}{2N} \\ +\frac{24}{N} & -24 & +\frac{24}{N} & -24 & +4C_F & 0 \\ -12 & -24C_F + \frac{12}{N} & -12 & -24C_F + \frac{12}{N} & +6 & -8C_F - \frac{6}{N} \end{pmatrix}, \quad (\text{A.23})$$

$$\gamma_{sf} = \begin{pmatrix} +4 & +4 & 0 \\ -32N - 16 & -16 & 0 \end{pmatrix}, \quad (\text{A.24})$$

and

$$\gamma'_{sf} = \begin{pmatrix} 0 & 0 & 0 \\ 0 & 0 & 0 \\ 0 & 0 & 0 \\ 0 & 0 & 0 \\ -16N \frac{m_{q'}}{m_q} \frac{Q_{q'}}{Q_q} & 0 & 0 \\ -16 \frac{m_{q'}}{m_q} \frac{Q_{q'}}{Q_q} & -16 \frac{m_{q'}}{m_q} & 0 \end{pmatrix}, \quad (\text{A.25})$$

where $C_F = (N^2 - 1)/(2N)$ is the Casimir constant of the fundamental representation, $N(= 3)$ is the number of the color, n_f is the number of light flavor quarks, and $\beta_0 = 11/3 \times N - 2/3 \times n_f$ is the leading-order beta function of strong coupling constant.

Left-right symmetric models

B.1 Higgs sector in left-right symmetric models

In this section, we briefly review the Higgs sector in the left-right symmetric models. After the left-right symmetry is broken, the scalar potential with $v_L = 0$ [67] is

$$\begin{aligned}
V = & -\mu_1^2 \text{Tr}(\Phi^\dagger \Phi) - \mu_2^2 \left[\text{Tr}(\tilde{\Phi} \Phi^\dagger) + \text{Tr}(\tilde{\Phi}^\dagger \Phi) \right] \\
& + \lambda_1 \left[\text{Tr}(\Phi^\dagger \Phi) \right]^2 + \lambda_2 \left\{ \left[\text{Tr}(\tilde{\Phi} \Phi^\dagger) \right]^2 + \left[\text{Tr}(\tilde{\Phi}^\dagger \Phi) \right]^2 \right\} \\
& + \lambda_3 \text{Tr}(\tilde{\Phi} \Phi^\dagger) \text{Tr}(\tilde{\Phi}^\dagger \Phi) + \lambda_4 \text{Tr}(\Phi^\dagger \Phi) \left[\text{Tr}(\tilde{\Phi} \Phi^\dagger) + \text{Tr}(\tilde{\Phi}^\dagger \Phi) \right] \\
& + \alpha_1 \text{Tr}(\Phi^\dagger \Phi) \text{Tr}(\langle \Delta_R^\dagger \rangle \langle \Delta_R \rangle) + \alpha_2 \left[e^{i\delta} \text{Tr}(\tilde{\Phi}^\dagger \Phi) + e^{-i\delta} \text{Tr}(\tilde{\Phi} \Phi^\dagger) \right] \\
& + \alpha_3 \text{Tr}(\Phi^\dagger \Phi \langle \Delta_R \rangle \langle \Delta_R^\dagger \rangle), \tag{B.1}
\end{aligned}$$

where $\tilde{\Phi} = \sigma_2 \Phi^* \sigma_2$. Under this scalar potential, the Higgs bi-doublet Φ obtains complex VEVs as Eq. (5.4) and the spontaneous CP -violating phase α emerges at the EWSB vacuum.

In the limit of $v_R \gg v$, the following linear combinations diagonalize the neutral and charged Higgs mass matrices,

$$H^0 = \cos \beta \phi_2^0 - \sin \beta e^{i\alpha} \phi_1^{0*}, \tag{B.2}$$

$$h^0 = \sin \beta e^{-i\alpha} \phi_2^0 + \cos \beta \phi_1^{0*}, \tag{B.3}$$

$$H^+ = \cos \beta \phi_2^+ + \sin \beta e^{i\alpha} \phi_1^+, \tag{B.4}$$

$$G^+ = \sin \beta \phi_2^+ - \cos \beta e^{i\alpha} \phi_1^+, \tag{B.5}$$

where H^0 (H^+) is the heavy neutral (charged) Higgs, G^+ the NG boson, and h^0 includes SM Higgs and NG boson components. The heavy Higgs masses are obtained as

$$M_{H^0}^2 = M_{H^\pm}^2 = \frac{\alpha_3 v_R^2}{2 \cos 2\beta} \equiv M_H^2. \tag{B.6}$$

The Yukawa interactions in the gauge eigenstate basis are

$$-\mathcal{L}_Y = \bar{Q}_L \left(Y \Phi + \tilde{Y} \tilde{\Phi} \right) Q_R + \text{h.c.}$$

$$\begin{aligned}
 &\supset \bar{U}_L S_L^u M_U S_R^{u\dagger} U_R + \bar{D}_L S_L^d M_D S_R^{d\dagger} D_R + \text{h.c.} \\
 &\equiv \bar{u}_L M_U u_R + \bar{d}_L M_D d_R + \text{h.c.},
 \end{aligned} \tag{B.7}$$

with the mass matrices,

$$S_L^u M_U S_R^{u\dagger} = \frac{v}{\sqrt{2}} \left(Y \cos \beta + \tilde{Y} \sin \beta e^{-i\alpha} \right), \tag{B.8}$$

$$S_L^d M_D S_R^{d\dagger} = \frac{v}{\sqrt{2}} \left(Y \sin \beta e^{i\alpha} + \tilde{Y} \cos \beta \right). \tag{B.9}$$

Here, $u_{L,R}$ and $d_{L,R}$ represent the quark mass eigenstates with $M_U = \text{diag}(m_u, m_c, m_t)$ and $M_D = \text{diag}(m_d, m_s, m_b)$. The unitary matrices $S_{L,R}^{u,d}$ satisfy

$$V_L = S_L^{u\dagger} S_L^d, \quad V_R = S_R^{u\dagger} S_R^d. \tag{B.10}$$

From Eq. (B.8) and (B.9), Y and \tilde{Y} are written as

$$\begin{aligned}
 Y &= \frac{\sqrt{2}}{v \cos 2\beta} \left(\cos \beta S_L^u M_U S_R^{u\dagger} - \sin \beta e^{-i\alpha} S_L^d M_D S_R^{d\dagger} \right), \\
 \tilde{Y} &= \frac{\sqrt{2}}{v \cos 2\beta} \left(-\sin \beta e^{i\alpha} S_L^u M_U S_R^{u\dagger} + \cos \beta S_L^d M_D S_R^{d\dagger} \right).
 \end{aligned} \tag{B.11}$$

Then, the Yukawa interactions are represented in the mass eigenstate basis as

$$\begin{aligned}
 -\mathcal{L}_Y &= \bar{Q}_L \left(Y \Phi + \tilde{Y} \tilde{\Phi} \right) Q_R + \text{h.c.} \\
 &= \bar{u}_L S_L^{u\dagger} \left(Y \phi_1^0 + \tilde{Y} \phi_2^{0*} \right) S_R^u u_R + \bar{d}_L S_L^{d\dagger} \left(Y \phi_2^0 + \tilde{Y} \phi_1^{0*} \right) S_R^d d_R \\
 &\quad + \bar{u}_L S_L^{u\dagger} \left(Y \phi_2^+ - \tilde{Y} \phi_1^+ \right) S_R^d d_R + \bar{d}_L S_L^{d\dagger} \left(Y \phi_1^- - \tilde{Y} \phi_2^- \right) S_R^u u_R + \text{h.c.} \\
 &= \frac{\sqrt{2}}{v} \bar{u}_L S_L^{u\dagger} \left[S_L^u M_U S_R^{u\dagger} h^* + \frac{1}{\cos 2\beta} \left(S_L^d M_D S_R^{d\dagger} - \sin 2\beta e^{i\alpha} S_L^u M_U S_R^{u\dagger} \right) H^{0*} \right] S_R^u u_R \\
 &\quad + \frac{\sqrt{2}}{v} \bar{d}_L S_L^{d\dagger} \left[S_L^d M_D S_R^{d\dagger} h + \frac{1}{\cos 2\beta} \left(S_L^u M_U S_R^{u\dagger} - \sin 2\beta e^{-i\alpha} S_L^d M_D S_R^{d\dagger} \right) H^0 \right] S_R^d d_R \\
 &\quad + \frac{\sqrt{2}}{v} \bar{u}_L S_L^{u\dagger} \left[e^{-i\alpha} S_L^d M_D S_R^{d\dagger} G^+ + \frac{1}{\cos 2\beta} \left(S_L^u M_U S_R^{u\dagger} - \sin 2\beta e^{-i\alpha} S_L^d M_D S_R^{d\dagger} \right) H^+ \right] S_R^d d_R \\
 &\quad + \frac{\sqrt{2}}{v} \bar{d}_L S_L^{d\dagger} \left[-e^{i\alpha} S_L^u M_U S_R^{u\dagger} G^- - \frac{1}{\cos 2\beta} \left(S_L^d M_D S_R^{d\dagger} - \sin 2\beta e^{i\alpha} S_L^u M_U S_R^{u\dagger} \right) H^- \right] S_R^u u_R + \text{h.c.} \\
 &= \frac{\sqrt{2}}{v} \bar{u}_L \left[M_U h^* + \frac{1}{\cos 2\beta} \left(V_L M_D V_R^\dagger - \sin 2\beta e^{i\alpha} M_U \right) H^{0*} \right] u_R \\
 &\quad + \frac{\sqrt{2}}{v} \bar{d}_L \left[M_D h + \frac{1}{\cos 2\beta} \left(V_L^\dagger M_U V_R - \sin 2\beta e^{-i\alpha} M_D \right) H^0 \right] d_R \\
 &\quad + \frac{\sqrt{2}}{v} \bar{u}_L \left[e^{-i\alpha} V_L M_D G^+ + \frac{1}{\cos 2\beta} \left(M_U V_R - \sin 2\beta e^{-i\alpha} V_L M_D \right) H^+ \right] d_R \\
 &\quad + \frac{\sqrt{2}}{v} \bar{d}_L \left[-e^{i\alpha} V_L^\dagger M_U G^- - \frac{1}{\cos 2\beta} \left(M_D V_R^\dagger - \sin 2\beta e^{i\alpha} V_L^\dagger M_U \right) H^- \right] u_R + \text{h.c.} \tag{B.12}
 \end{aligned}$$

Therefore, the heavy Higgs interactions with quarks become

$$\begin{aligned}
 -\mathcal{L}_Y \simeq & \frac{\sqrt{2}m_{u_k}}{v \cos 2\beta} \bar{d}_i (V_L^\dagger)_{ik} (V_R)_{kj} P_R d_j H^0 + \frac{\sqrt{2}m_{u_k}}{v \cos 2\beta} \bar{d}_i (V_R^\dagger)_{ik} (V_L)_{kj} P_L d_j H^{0*} \\
 & + \frac{\sqrt{2}m_{u_k}}{v \cos 2\beta} \bar{u}_k (V_R)_{ki} P_R d_i H^+ + \frac{\sqrt{2}m_{u_k}}{v \cos 2\beta} \bar{d}_i (V_R^\dagger)_{ik} P_L u_k H^-,
 \end{aligned} \tag{B.13}$$

where the terms proportional to $\tan 2\beta$ are dismissed, because $\tan 2\beta = \mathcal{O}(m_b/m_t)$.

After integrating out the heavy charged Higgs boson, one obtains the effective operator,

$$\begin{aligned}
 \mathcal{L}_{\text{eff}} \simeq & \frac{2\sqrt{2}G_F}{\cos^2 2\beta} \frac{m_t^2}{M_{H^\pm}^2} (V_R^\dagger)_{i3} (V_R)_{3j} (\bar{d}_i P_L t) (\bar{t} P_R d_j) \\
 = & -\frac{\sqrt{2}G_F}{\cos^2 2\beta} \frac{m_t^2}{M_{H^\pm}^2} (V_R^\dagger)_{i3} (V_R)_{3j} (\bar{t}_\alpha \gamma^\mu P_L t_\beta) (\bar{d}_{i,\beta} \gamma_\mu P_R d_{j,\alpha}),
 \end{aligned} \tag{B.14}$$

where α, β denote color indices. By rearranging the colors, the Wilson coefficients become

$$(C_{qd}^{(8)})_{33ij}^{\text{tree}}|_{q=u} = -\frac{2\sqrt{2}G_F}{\cos^2 2\beta} \frac{m_t^2}{M_{H^\pm}^2} (V_R^\dagger)_{i3} (V_R)_{3j}, \tag{B.15}$$

$$(C_{qd}^{(1)})_{33ij}^{\text{tree}}|_{q=u} = \frac{1}{2N_c} (C_{qd}^{(8)})_{33ij}|_{q=u}. \tag{B.16}$$

for $q = u$. The Wilson coefficients for $q = d$ is generated by the heavy neutral Higgs exchange.

After integrating out the heavy neutral Higgs boson, one obtains

$$\begin{aligned}
 \mathcal{L}_{\text{eff}} \simeq & \frac{2\sqrt{2}G_F}{\cos^2 2\beta} \frac{m_t^2}{M_{H^0}^2} (V_R^\dagger)_{i3} (V_L)_{3k} (V_L^\dagger)_{l3} (V_R)_{3j} (\bar{d}_i P_L d_k) (\bar{d}_l P_R d_j) \\
 = & -\frac{\sqrt{2}G_F}{\cos^2 2\beta} \frac{m_t^2}{M_{H^0}^2} (V_R^\dagger)_{i3} (V_L)_{3k} (V_L^\dagger)_{l3} (V_R)_{3j} (\bar{d}_{l,\alpha} \gamma^\mu P_L d_{k,\beta}) (\bar{d}_{i,\beta} \gamma_\mu P_R d_{j,\alpha}).
 \end{aligned} \tag{B.17}$$

In the mass eigenstate basis, the $SU(2)_L$ quark double is shown as $q = (u_L, V_L d_L)^T$. Thus, the Wilson coefficients for $q = d$ become

$$(C_{qd}^{(8)})_{33ij}^{\text{tree}}|_{q=d} = -\frac{2\sqrt{2}G_F}{\cos^2 2\beta} \frac{m_t^2}{M_H^2} (V_R^\dagger)_{i3} (V_R)_{3j}, \tag{B.18}$$

$$(C_{qd}^{(1)})_{33ij}^{\text{tree}}|_{q=d} = \frac{1}{2N_c} (C_{qd}^{(8)})_{33ij}|_{q=d}. \tag{B.19}$$

Consequently, Eqs. (5.14) and (5.15) are obtained.

B.2 Loop functions

The loop functions which are necessary for the $\Delta F = 2$ transition amplitudes in the left-right model are summarized. They are defined as

$$\mathcal{F}_A(x_i, x_j, \beta) = \left(1 + \frac{x_i x_j \beta}{4}\right) \mathcal{I}_1(x_i, x_j, \beta) - \frac{1 + \beta}{4} \mathcal{I}_2(x_i, x_j, \beta), \tag{B.20}$$

$$\begin{aligned} \mathcal{F}_B(\tau_L, \tau_R) &= (\tau_L^2 + \tau_R^2 + 10\tau_L\tau_R + 1) \mathcal{I}_3(\tau_L, \tau_R) \\ &\quad + (\tau_L^2 + \tau_R^2 + 10\tau_L\tau_R - 2\tau_L - 2\tau_R + 1) \mathcal{I}_4(\tau_L, \tau_R), \end{aligned} \quad (\text{B.21})$$

$$\mathcal{F}_C(\tau_i, \tau_j, \tau_L, \tau_R) = 2(\tau_L + \tau_R) \mathcal{I}_3(\tau_L, \tau_R) - \left[\frac{\tau_i \sqrt{\tau_L \tau_R}}{\tau_i - 4\sqrt{\tau_L \tau_R}} \mathcal{I}_5(\tau_i, \tau_L, \tau_R) + (i \rightarrow j) \right], \quad (\text{B.22})$$

$$\mathcal{F}_D(x_i, x_j, \tau_L) = x_i x_j \mathcal{I}_1(x_i, x_j, \tau_L) - \mathcal{I}_2(x_i, x_j, \tau_L). \quad (\text{B.23})$$

The functions, \mathcal{I}_1 – \mathcal{I}_5 , are denoted by the Passarino-Veltman functions as [102]

$$\mathcal{I}_1(x_i, x_j, \beta) = -M_{W_L}^2 M_{W_R}^2 D_0(0, 0, 0, 0; 0, 0; m_{u_i}, m_{u_j}, M_{W_L}, M_{W_R}), \quad (\text{B.24})$$

$$\mathcal{I}_2(x_i, x_j, \beta) = -4M_{W_R}^2 D_{00}(0, 0, 0, 0; 0, 0; m_{u_i}, m_{u_j}, M_{W_L}, M_{W_R}), \quad (\text{B.25})$$

$$\mathcal{I}_3(\tau_L, \tau_R) = B_0(0; M_{W_L}, M_{W_R}) - \text{Re}[B_0(M_H^2; M_{W_L}, M_{W_R})], \quad (\text{B.26})$$

$$\mathcal{I}_4(\tau_L, \tau_R) = M_H^2 \sum_{n=0}^2 \text{Re} [C_n(M_H^2, 0, M_H^2; M_{W_L}, M_{W_R}, M_{W_R})], \quad (\text{B.27})$$

$$\begin{aligned} \mathcal{I}_5(\tau_i, \tau_L, \tau_R) &= M_H^2 \left\{ C_0(0, 0, 0; M_{W_L}, m_{u_i}, M_{W_R}) \right. \\ &\quad \left. - \text{Re} \left[C_0 \left(\frac{M_H^2}{4}, \frac{M_H^2}{4}, M_H^2; M_{W_L}, m_{u_i}, M_{W_R} \right) \right] \right\}, \end{aligned} \quad (\text{B.28})$$

where we follow the notation of Refs. [103, 104]. The absorptive parts in the loop functions are discarded [75]. We also obtain the following analytical formulae:

$$\mathcal{I}_1(x_i, x_j, \beta) = \frac{x_i \ln x_i}{(1-x_i)(1-x_i\beta)(x_i-x_j)} + (i \leftrightarrow j) - \frac{\beta \ln \beta}{(1-\beta)(1-x_i\beta)(1-x_j\beta)}, \quad (\text{B.29})$$

$$\mathcal{I}_2(x_i, x_j, \beta) = \frac{x_i^2 \ln x_i}{(1-x_i)(1-x_i\beta)(x_i-x_j)} + (i \leftrightarrow j) - \frac{\ln \beta}{(1-\beta)(1-x_i\beta)(1-x_j\beta)}, \quad (\text{B.30})$$

$$\begin{aligned} \mathcal{I}_3(\tau_L, \tau_R) &= -1 + \frac{1}{2} \left[\tau_L - \tau_R - \frac{\tau_L + \tau_R}{\tau_L - \tau_R} \right] \ln \frac{\tau_L}{\tau_R} \\ &\quad - \frac{\sqrt{(1-\tau_L-\tau_R)^2 - 4\tau_L\tau_R}}{2} \ln \frac{1-\tau_L-\tau_R - \sqrt{(1-\tau_L-\tau_R)^2 - 4\tau_L\tau_R}}{1-\tau_L-\tau_R + \sqrt{(1-\tau_L-\tau_R)^2 - 4\tau_L\tau_R}}, \end{aligned} \quad (\text{B.31})$$

$$\begin{aligned} \mathcal{I}_4(\tau_L, \tau_R) &= 1 - \frac{\tau_L - \tau_R}{2} \ln \frac{\tau_L}{\tau_R} \\ &\quad + \frac{(\tau_L - \tau_R)^2 - (\tau_L + \tau_R)}{2\sqrt{(1-\tau_L-\tau_R)^2 - 4\tau_L\tau_R}} \ln \frac{1-\tau_L-\tau_R - \sqrt{(1-\tau_L-\tau_R)^2 - 4\tau_L\tau_R}}{1-\tau_L-\tau_R + \sqrt{(1-\tau_L-\tau_R)^2 - 4\tau_L\tau_R}}, \end{aligned} \quad (\text{B.32})$$

$$\begin{aligned} \mathcal{I}_5(\tau_i, \tau_L, \tau_R) &= \frac{\tau_i(\tau_R - \tau_L) \ln \tau_i + \tau_L(\tau_i - \tau_R) \ln \tau_L + \tau_R(\tau_L - \tau_i) \ln \tau_R}{(\tau_R - \tau_L)(\tau_L - \tau_i)(\tau_i - \tau_R)} \\ &\quad - \text{Re} \left\{ \ln \frac{\tau_L \tau_R}{\tau_i^2} + \frac{1}{4\tau_i - 2\tau_L - 2\tau_R + 1} \right. \\ &\quad \times \left[8\kappa \left(\frac{1}{4}, \tau_i, \tau_L \right) \ln \frac{\kappa \left(\frac{1}{4}, \tau_i, \tau_L \right) + \tau_i + \tau_L - \frac{1}{4}}{2\sqrt{\tau_i \tau_L}} + (L \rightarrow R) \right. \\ &\quad \left. \left. - 4\kappa(1, \tau_L, \tau_R) \ln \frac{\kappa(1, \tau_L, \tau_R) + \tau_L + \tau_R - 1}{2\sqrt{\tau_L \tau_R}} \right] \right\}, \end{aligned} \quad (\text{B.33})$$

with

$$\kappa(x, y, z) = \sqrt{x^2 + y^2 + z^2 - 2(xy + yz + zx)}. \quad (\text{B.34})$$

When the relation, $m_{u_i}^2, M_{W_L}^2 \ll M_{W_R}^2 \ll M_H^2$, are satisfied, one can use the following approximations:

$$\mathcal{I}_3(\tau_L, \tau_R) \simeq -1 + (1 - \tau_R) \ln \left(\frac{1}{\tau_R} - 1 \right) \approx -1 - \ln \tau_R, \quad (\text{B.35})$$

$$\mathcal{I}_4(\tau_L, \tau_R) \simeq 1 + \tau_R \ln \left(\frac{1}{\tau_R} - 1 \right) \approx 1, \quad (\text{B.36})$$

$$\mathcal{I}_5(\tau_i, \tau_L, \tau_R) \simeq \frac{\tau_i \ln(\tau_i/\tau_R) - \tau_L \ln(\tau_L/\tau_R)}{\tau_R(\tau_i - \tau_L)}, \quad (\text{B.37})$$

which are consistent with Ref. [75]. Numerically, the second term of \mathcal{I}_5 in Eq. (B.33), $\text{Re}\{\dots\}$, is much smaller than the first term for $M_H \gg M_{W_R}$.

Double penguin contributions

In this section, we apply the one-loop matching conditions in Sec. ?? to double-penguin diagrams, where $\Delta F = 2$ processes are generated by exchanging the SM gauge bosons with FC interactions. When vector bosons of the unbroken gauge symmetries, i.e., those of $SU(3)_C$ and $U(1)_{em}$ in the SM, are exchanged, such double-penguin contributions should vanish because of the gauge invariance. In fact, form factors of their FC penguin vertices should be proportional to q^2 , i.e., vanish in the limit of $q^2 \rightarrow 0$ for the gauge invariance, where q is the momentum transfer. Then, $\Delta F = 2$ double-penguin diagrams depend on $q^4 \times 1/q^2$, where $1/q^2$ represents the propagator of the unbroken gauge boson. Hence, they disappear in the limit of $q^2 \rightarrow 0$.

In our formula, this gauge invariance is confirmed by observing the cancellations among the Wilson coefficients. Once $\Delta F = 1$ operators (and $\Delta F = 2$ ones if necessary) are generated by the penguin diagrams at the NP scale, we will see that $\Delta F = 2$ contributions cancel out below the EWSB scale, if the diagrams are mediated by the gauge bosons of the unbroken gauge symmetries. Here, the one-loop matching conditions are necessary. These results justify our one-loop matching conditions in Sec. ??.

We will focus on the double-penguin diagrams with exchanging the gauge bosons associated with the unbroken gauge symmetries. At the NP scale, penguin-type $\Delta F = 1$ contributions are generated by exchanging them. The effective Lagrangian from the massless B , W^3 and gluon can be written as

$$\begin{aligned}
\mathcal{L}^B &= \frac{\alpha}{4\pi c_W^2} (C_{L,ij}^B \bar{d}_i \gamma^\mu P_L d_j + C_{R,ij}^B \bar{d}_i \gamma^\mu P_R d_j) (Y_{u_L} \bar{u}_k \gamma_\mu P_L u_k + Y_{u_R} \bar{u}_k \gamma_\mu P_R u_k) \\
&\quad + \frac{\alpha}{4\pi c_W^2} (C_{L,ij}^B \bar{d}_i \gamma^\mu P_L d_j + C_{R,ij}^B \bar{d}_i \gamma^\mu P_R d_j) (Y_{d_L} \bar{d}_k \gamma_\mu P_L d_k + Y_{d_R} \bar{d}_k \gamma_\mu P_R d_k) \\
&= \frac{\alpha}{4\pi} (C_{L,ij}^B \bar{d}_i \gamma^\mu P_L d_j + C_{R,ij}^B \bar{d}_i \gamma^\mu P_R d_j) Q_u \bar{u}_k \gamma_\mu u_k \\
&\quad - \frac{\alpha_Z}{4\pi} s_W^2 (C_{L,ij}^B \bar{d}_i \gamma^\mu P_L d_j + C_{R,ij}^B \bar{d}_i \gamma^\mu P_R d_j) (I_u^3 - Q_u s_W^2) \bar{u}_k \gamma_\mu u_k \\
&\quad + \frac{\alpha}{4\pi} (C_{L,ij}^B \bar{d}_i \gamma^\mu P_L d_j + C_{R,ij}^B \bar{d}_i \gamma^\mu P_R d_j) Q_d \bar{d}_k \gamma_\mu d_k \\
&\quad - \frac{\alpha_Z}{4\pi} s_W^2 (C_{L,ij}^B \bar{d}_i \gamma^\mu P_L d_j + C_{R,ij}^B \bar{d}_i \gamma^\mu P_R d_j) (I_d^3 - Q_d s_W^2) \bar{d}_k \gamma_\mu d_k, \tag{C.1}
\end{aligned}$$

$$\begin{aligned}
 \mathcal{L}^{W^3} &= \frac{\alpha}{4\pi s_W^2} C_{L,ij}^{W^3} (\bar{d}_i \gamma^\mu P_L d_j) (I_u^3 \bar{u}_k \gamma_\mu P_L u_k) + \frac{\alpha}{4\pi s_W^2} C_{L,ij}^{W^3} (\bar{d}_i \gamma^\mu P_L d_j) (I_d^3 \bar{d}_k \gamma_\mu P_L d_k) \\
 &= \frac{\alpha}{4\pi} C_{L,ij}^{W^3} (\bar{d}_i \gamma^\mu P_L d_j) Q_u \bar{u}_k \gamma_\mu u_k + \frac{\alpha_Z}{4\pi} c_W^2 C_{L,ij}^{W^3} (\bar{d}_i \gamma^\mu P_L d_j) (I_u^3 - Q_u s_W^2) \bar{u}_k \gamma_\mu u_k \\
 &\quad + \frac{\alpha}{4\pi} C_{L,ij}^{W^3} (\bar{d}_i \gamma^\mu P_L d_j) Q_d \bar{d}_k \gamma_\mu d_k + \frac{\alpha_Z}{4\pi} c_W^2 C_{L,ij}^{W^3} (\bar{d}_i \gamma^\mu P_L d_j) (I_d^3 - Q_d s_W^2) \bar{d}_k \gamma_\mu d_k, \quad (\text{C.2})
 \end{aligned}$$

$$\mathcal{L}^g = \frac{\alpha_s}{4\pi} \left(C_{L,ij}^g \bar{d}_i \gamma^\mu P_L T^A d_j + C_{R,ij}^g \bar{d}_i \gamma^\mu P_R T^A d_j \right) (\bar{u}_k \gamma_\mu T^A u_k + \bar{d}_k \gamma_\mu T^A d_k), \quad (\text{C.3})$$

where Y_f is the hypercharge, I_f^3 the $SU(2)_L$ charge, and Q_f the $U(1)_{em}$ charge. Also, α_s and α are the gauge couplings of $SU(3)_C$ and $U(1)_{em}$, respectively. The coefficients, $C_{c,ij}^V$ ($V = B, W^3, g$ and $c = L, R$), are generated by integrating out the NP particles. In the second lines of \mathcal{L}^B and \mathcal{L}^{W^3} , the effective Lagrangians are divided into the would-be γ - and Z -penguin contributions, which are proportional to αQ_f and $\alpha_Z (I_f^3 - Q_f s_W^2)$, respectively. Here, $\alpha_Z = \alpha / (c_W^2 s_W^2)$. In terms of the SMEFT operators, the above operators are represented as

$$\begin{aligned}
 (\mathcal{C}_{qq}^{(1)})_{ijkk} &= (\mathcal{C}_{qq}^{(1)})_{kkij} \\
 &= -\frac{\alpha_s}{16N_c\pi} C_{L,ij}^g + \frac{\alpha}{8\pi} Y_q \left(C_{L,ij}^B + C_{L,ij}^{W^3} \right) + \frac{\alpha_Z}{8\pi} s_W^2 Y_q \left(s_W^2 C_{L,ij}^B - c_W^2 C_{L,ij}^{W^3} \right), \quad (\text{C.4})
 \end{aligned}$$

$$(\mathcal{C}_{qq}^{(1)})_{ikkj} = (\mathcal{C}_{qq}^{(1)})_{kjik} = \frac{\alpha_s}{32N_c\pi} (N_c - 2) C_{L,ij}^g, \quad (\text{C.5})$$

$$\begin{aligned}
 (\mathcal{C}_{qq}^{(3)})_{ijkk} &= (\mathcal{C}_{qq}^{(3)})_{kkij} \\
 &= -\frac{\alpha}{16\pi} \left(C_{L,ij}^B + C_{L,ij}^{W^3} \right) + \frac{\alpha_Z}{16\pi} c_W^2 \left(s_W^2 C_{L,ij}^B - c_W^2 C_{L,ij}^{W^3} \right), \quad (\text{C.6})
 \end{aligned}$$

$$(\mathcal{C}_{qq}^{(3)})_{ikkj} = (\mathcal{C}_{qq}^{(3)})_{kjik} = \frac{\alpha_s}{32\pi} C_{L,ij}^g, \quad (\text{C.7})$$

$$(\mathcal{C}_{ud}^{(1)})_{kkij} = \frac{\alpha}{4\pi} Q_u C_{R,ij}^B - \frac{\alpha_Z}{4\pi} s_W^2 C_{R,ij}^B (-s_W^2 Q_u), \quad (\text{C.8})$$

$$(\mathcal{C}_{ud}^{(8)})_{kkij} = \frac{\alpha_s}{4\pi} C_{R,ij}^g, \quad (\text{C.9})$$

$$(\mathcal{C}_{qu}^{(1)})_{ijkk} = \frac{\alpha}{4\pi} Q_u \left(C_{L,ij}^B + C_{L,ij}^{W^3} \right) - \frac{\alpha_Z}{4\pi} \left(s_W^2 C_{L,ij}^B - c_W^2 C_{L,ij}^{W^3} \right) (-s_W^2 Q_u), \quad (\text{C.10})$$

$$(\mathcal{C}_{qu}^{(8)})_{ijkk} = \frac{\alpha_s}{4\pi} C_{L,ij}^g, \quad (\text{C.11})$$

$$(\mathcal{C}_{qd}^{(1)})_{kkij} = \frac{\alpha}{4\pi} Q_q C_{R,ij}^B - \frac{\alpha_Z}{4\pi} s_W^2 C_{R,ij}^B (I_q^3 - s_W^2 Q_q), \quad (\text{C.12})$$

$$(\mathcal{C}_{qd}^{(8)})_{ijkk} = \frac{\alpha_s}{4\pi} C_{L,ij}^g, \quad (\text{C.13})$$

$$(\mathcal{C}_{qd}^{(8)})_{kkij} = \frac{\alpha_s}{4\pi} C_{R,ij}^g. \quad (\text{C.14})$$

In addition, one has to include $\Delta F = 2$ contributions which come from the diagram in Fig. C.1. They are generated at the NP scale. The $d_i \rightarrow d_j$ transitions are induced by the penguin vertices of the NP contribution in one side and those of the SM contribution in another side, where the up-type quarks, especially the top quark, and the W boson are exchanged. The Wilson coefficients of the SMEFT operators are represented as

$$\begin{aligned}
 (\mathcal{C}_{qq}^{(1)})_{ijij} &= (\mathcal{C}_{qq}^{(3)})_{ijij} \\
 &= -\frac{\alpha^2 \lambda_t^{ij}}{8\pi^2 s_W^2} \left(C_{L,ij}^B + C_{L,ij}^{W^3} \right) \left\{ Q_{G^+} \frac{x_t}{8} L(x_t, \mu_W) + Q_{G^+} \frac{1}{4} M(x_t) - \frac{1}{8} [2 - 6L(x_t, \mu_W)] \right\}
 \end{aligned}$$

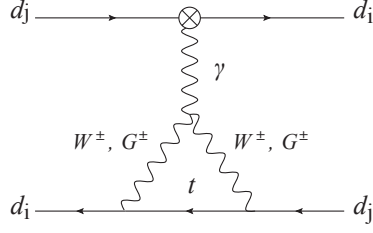


Figure C.1: Feynman diagram for the one-loop contribution to $\Delta F = 2$ operators at the NP scale.

$$\begin{aligned}
& + \frac{\alpha\alpha_Z\lambda_t^{ij}}{8\pi^2 s_W^2} \left(s_W^2 C_{L,ij}^B - c_W^2 C_{L,ij}^{W^3} \right) \left\{ (I^{G^+} - s_W^2 Q^{G^+}) \frac{x_t}{8} L(x_t, \mu_W) \right. \\
& \left. + (-s_W^2 Q_{G^+}) \frac{1}{4} M(x_t) - \frac{1}{8} c_W^2 [2 - 6L(x_t, \mu_W)] \right\} \quad (C.15)
\end{aligned}$$

$$\begin{aligned}
& = -\frac{\alpha^2 \lambda_t^{ij}}{8\pi^2 s_W^2} \left(C_{L,ij}^B + C_{L,ij}^{W^3} \right) K(x_t, \mu_W) \\
& - \frac{\alpha\alpha_Z\lambda_t^{ij}}{8\pi^2 s_W^2} \left(s_W^2 C_{L,ij}^B - c_W^2 C_{L,ij}^{W^3} \right) \left[\frac{x_t}{16} L(x_t, \mu_W) + \frac{1}{4} M(x_t) - c_W^2 K(x_t, \mu_W) \right], \quad (C.16)
\end{aligned}$$

$$\begin{aligned}
(C_{qd}^{(1)})_{ijij} & = -\frac{\alpha^2 \lambda_t^{ij}}{4\pi^2 s_W^2} C_{R,ij}^B \left\{ Q_{G^+} \frac{x_t}{8} L(x_t, \mu_W) + Q_{G^+} \frac{1}{4} M(x_t) - \frac{1}{8} [2 - 6L(x_t, \mu_W)] \right\} \\
& + \frac{\alpha\alpha_Z\lambda_t^{ij}}{4\pi^2 s_W^2} \left(s_W^2 C_{R,ij}^B \right) \left\{ (I^{G^+} - s_W^2 Q^{G^+}) \frac{x_t}{8} L(x_t, \mu_W) + (-s_W^2 Q_{G^+}) \frac{1}{4} M(x_t) \right. \\
& \left. - \frac{1}{8} c_W^2 [2 - 6L(x_t, \mu_W)] \right\} \quad (C.17)
\end{aligned}$$

$$\begin{aligned}
& = -\frac{\alpha^2 \lambda_t^{ij}}{4\pi^2 s_W^2} C_{R,ij}^B K(x_t, \mu_W) \\
& - \frac{\alpha\alpha_Z\lambda_t^{ij}}{4\pi^2} C_{R,ij}^B \left[\frac{x_t}{16} L(x_t, \mu_W) + \frac{1}{4} M(x_t) - c_W^2 K(x_t, \mu_W) \right], \quad (C.18)
\end{aligned}$$

where $Q_{G^+} = 1$ and $I^{G^+} = 1/2$. Here, the GIM mechanism is used to reduce the results, and the loop functions are given as

$$L(x, \mu) = \ln \frac{\mu}{M_W} + \frac{3x-1}{4(x-1)} - \frac{x^2 \ln x}{2(1-x)^2}, \quad (C.19)$$

$$M(x) = \frac{x}{1-x} + \frac{x^2 \ln x}{(1-x)^2}. \quad (C.20)$$

For the gluon double-penguin contributions, one obtains the low-scale $\Delta F = 2$ operators through the one-loop matching conditions, Eqs. (3.16)–(3.18), from the SMEFT $\Delta F = 1$ operators in Eqs. (C.4)–(C.14) as

$$(C_1)_{ij} = (C_1)_{ij}^{1\text{-loop}}$$

$$\begin{aligned}
 &= -\frac{\alpha\lambda_t^{ij}}{4\pi s_W^2} \frac{\alpha_s}{4\pi} \frac{2(N_c - 1)}{N_c} C_{L,ij}^g [I_1(x_t, \mu_W) + 2J(x_t) - K(x_t, \mu_W)] \\
 &= 0,
 \end{aligned} \tag{C.21}$$

$$\begin{aligned}
 (C_4)_{ij} &= (C_4)_{ij}^{1\text{-loop}} \\
 &= \frac{\alpha\lambda_t^{ij}}{\pi s_W^2} \frac{\alpha_s}{4\pi} C_{R,ij}^g [I_1(x_t, \mu_W) + 2J(x_t) - K(x_t, \mu_W)] \\
 &= 0,
 \end{aligned} \tag{C.22}$$

$$\begin{aligned}
 (C_5)_{ij} &= (C_5)_{ij}^{1\text{-loop}} \\
 &= -\frac{\alpha\lambda_t^{ij}}{\pi s_W^2} \frac{\alpha_s}{4\pi} \frac{1}{N_c} C_{R,ij}^g [I_1(x_t, \mu_W) + 2J(x_t) - K(x_t, \mu_W)] \\
 &= 0.
 \end{aligned} \tag{C.23}$$

Since all these Wilson coefficients are proportional to the function, $I_1(x_t, \mu_W) + 2J(x_t) - K(x_t, \mu_W)$, which is identical to zero, there are no contributions to the $\Delta F = 2$ operators. Hence, the gluon double-penguin contributions vanish, as expected from the gauge invariance.

Next, for the γ double-penguin contributions, the low-scale $\Delta F = 2$ operators are generated from the SMEFT $\Delta F = 2$ operators in Eqs. (C.16) and (C.18) through the tree-level matching as well as the $\Delta F = 1$ ones in Eqs. (C.4)–(C.14) through the one-loop matching conditions, Eqs. (3.16)–(3.18). In total, the low-scale $\Delta F = 2$ coefficients are

$$\begin{aligned}
 (C_1)_{ij} &= (C_1)_{ij}^{\text{tree}} + (C_1)_{ij}^{1\text{-loop}} \\
 &= \frac{\alpha\lambda_t^{ij}}{\pi s_W^2} \frac{\alpha}{4\pi} \left(C_{L,ij}^B + C_{L,ij}^{W^3} \right) K(x_t, \mu_W) \\
 &\quad - \frac{\alpha\lambda_t^{ij}}{\pi s_W^2} \frac{\alpha}{4\pi} \left(C_{L,ij}^B + C_{L,ij}^{W^3} \right) \left\{ Q_u [I_1(x_t, \mu_W) + 2J(x_t)] - Q_d K(x_t, \mu_W) \right\} \\
 &= 0,
 \end{aligned} \tag{C.24}$$

$$\begin{aligned}
 (C_5)_{ij} &= (C_5)_{ij}^{\text{tree}} + (C_5)_{ij}^{1\text{-loop}} \\
 &= -\frac{2\alpha\lambda_t^{ij}}{\pi s_W^2} \frac{\alpha}{4\pi} C_{R,ij}^B K(x_t, \mu_W) \\
 &\quad + \frac{2\alpha\lambda_t^{ij}}{\pi s_W^2} \frac{\alpha}{4\pi} C_{R,ij}^B \left\{ Q_u [I_1(x_t, \mu_W) + 2J(x_t)] - Q_d K(x_t, \mu_W) \right\} \\
 &= 0,
 \end{aligned} \tag{C.25}$$

and other Wilson coefficients do not receive contributions. It is noticed that $(C_1)_{ij}$ and $(C_5)_{ij}$ are proportional to the function which is identical to zero, because $Q_d = Q_u - 1$. Hence, the γ double-penguin contributions also vanish, as expected from the gauge invariance, and it guarantees our one-loop matching conditions.^{#1}

^{#1} The Z double-penguin contributions also vanish in the limit of the gauge invariance of the $SU(2)_L \times U(1)_Y$ symmetry. Non-zero contributions due to the $SU(2)_L \times U(1)_Y$ breaking are encoded into the $\Delta F = 1$ effective op-

erators, $(\mathcal{O}_{Hq}^{(1)})_{ij}$, $(\mathcal{O}_{Hq}^{(3)})_{ij}$ and $(\mathcal{O}_{Hd})_{ij}$, in a gauge-invariant manner [20,21] (see also Ref. [81] for a supersymmetric study).

$b \rightarrow d\gamma$ and $b \rightarrow s\gamma$

In this section, we consider flavor-violations in the scalar trilinear couplings. They contribute to the decays of $b \rightarrow d_i\gamma$ ($d_i = d, s$) at the one-loop level.^{#1} The decays are described by the effective Hamiltonian,

$$\mathcal{H}_{\text{eff}} = -\frac{4G_F}{\sqrt{2}}[\lambda_t]_{i3} \left[\mathcal{C}_{7\gamma} \mathcal{O}_{7\gamma} + \mathcal{C}_{8g} \mathcal{O}_{8g} \right] + (L \leftrightarrow R), \quad (\text{D.1})$$

where the effective operators are defined as

$$\mathcal{O}_{7\gamma} = \frac{e}{16\pi^2} m_b \bar{d}_i \sigma^{\mu\nu} P_R b F_{\mu\nu}, \quad \mathcal{O}_{8g} = \frac{g_3}{16\pi^2} m_b \bar{d}_i \sigma^{\mu\nu} T^a P_R b G_{\mu\nu}^a, \quad (\text{D.2})$$

where $e > 0$ and $g_3 > 0$, and the covariant derivatives for the quark and squark follow the same sign convention as Eq. (??). At the one-loop level, the gluino contributions are obtained as

$$\mathcal{C}_{7\gamma} = \frac{\sqrt{2}\pi\alpha_s}{4G_F[\lambda_t]_{i3}m_{\tilde{g}}^2} \left[\mathcal{R}_{ri}^{d*} \mathcal{R}_{r3}^d \left(\frac{8}{9} D_1(x_r) \right) - \frac{m_{\tilde{g}}}{m_b} \mathcal{R}_{ri}^{d*} \mathcal{R}_{r6}^d \left(\frac{8}{9} D_2(x_r) \right) \right], \quad (\text{D.3})$$

$$\begin{aligned} \mathcal{C}_{8g} = \frac{\sqrt{2}\pi\alpha_s}{4G_F[\lambda_t]_{i3}m_{\tilde{g}}^2} & \left[\mathcal{R}_{ri}^{d*} \mathcal{R}_{r3}^d \left(\frac{1}{3} D_1(x_r) - 3D_3(x_r) \right) \right. \\ & \left. - \frac{m_{\tilde{g}}}{m_b} \mathcal{R}_{ri}^{d*} \mathcal{R}_{r6}^d \left(\frac{1}{3} D_2(x_r) - 3D_4(x_r) \right) \right], \end{aligned} \quad (\text{D.4})$$

where $x_r = m_{\tilde{d}_r}^2/m_{\tilde{g}}^2$, and the loop functions are defined to be

$$D_1(x) = \frac{-x^3 + 6x^2 - 3x - 2 - 6x \ln x}{6(1-x)^4}, \quad (\text{D.5})$$

$$D_2(x) = \frac{x^2 - 1 - 2x \ln x}{(1-x)^3}, \quad (\text{D.6})$$

$$D_3(x) = \frac{2x^3 + 3x^2 - 6x + 1 - 6x^2 \ln x}{6(1-x)^4}, \quad (\text{D.7})$$

^{#1} They also contribute to the (CP -violating) $B_{d,s}$ mixings. In the parameter regions of our interest, gluino box contributions to them are smaller than the current experimental and theoretical uncertainties. Also, the CP -violating scalar trilinear couplings can contribute to the electric dipole moments (EDMs) e.g., of the neutron. Since the CP phases are introduced in the flavor off-diagonal components, the gluino contributions to the EDMs satisfy the experimental limits.

$$D_4(x) = \frac{3x^2 - 4x + 1 - 2x^2 \ln x}{(1-x)^3}. \quad (\text{D.8})$$

Also, $\mathcal{C}'_{7\gamma}$ and \mathcal{C}'_{8g} are obtained by flipping the chirality of $\mathcal{R}_{ri}^{d(*)}$ in $\mathcal{C}_{7\gamma}$ and \mathcal{C}_{8g} , respectively.

In the analysis, an approximation formula in Ref. [?] is used to estimate the SUSY contributions to the branching ratio of $b \rightarrow s\gamma$, where the Wilson coefficients are set at $\mu_b = 4.8 \text{ GeV}$. For $\mathcal{B}(\bar{B} \rightarrow X_d\gamma)$, the formula in Refs. [?, ?] is used, where the SUSY contributions to the Wilson coefficients at the top-mass scale are needed. The latest results of the SM values are [?]

$$\mathcal{B}(\bar{B} \rightarrow X_s\gamma)^{\text{SM}} = (3.36 \pm 0.23) \times 10^{-4}, \quad (\text{D.9})$$

$$\mathcal{B}(\bar{B} \rightarrow X_d\gamma)^{\text{SM}} = (1.73^{+0.12}_{-0.22}) \times 10^{-5}, \quad (\text{D.10})$$

for $E_\gamma > 1.6 \text{ GeV}$. On the other hand, the experimental results are [?, ?, ?]

$$\mathcal{B}(\bar{B} \rightarrow X_s\gamma)^{\text{exp}} = (3.32 \pm 0.15) \times 10^{-4}, \quad (\text{D.11})$$

$$\mathcal{B}(\bar{B} \rightarrow X_d\gamma)^{\text{exp}} = (1.41 \pm 0.57) \times 10^{-5}, \quad (\text{D.12})$$

for $E_\gamma > 1.6 \text{ GeV}$. In the analysis, the theoretical prediction including the SM and SUSY contributions is required to be consistent with the experimental result at the 2σ level.

Vacuum stability

The Wilson coefficients in Eqs. (6.39)–(6.41) are enhanced by large off-diagonal trilinear couplings, $(T_D)_{i3}$ and $(T_D)_{3i}$ ($i = 1, 2$). Such large trilinear couplings tend to generate dangerous charge and color breaking (CCB) global minima in the scalar potential [119]. Hence, they are limited by the vacuum (meta-)stability condition: the lifetime of the EW vacuum must be longer than the age of the Universe. In this section, we will investigate the vacuum stability conditions of $(T_D)_{i3}$ and $(T_D)_{3i}$.

The vacuum decay rate per unit volume is represented by $\Gamma/V = A \exp(-S_E)$, where S_E is the Euclidean action of the bounce solution [120]. CosmoTransition 2.0.2 [121] is used to estimate S_E at the semiclassical level. The prefactor A cannot be determined unless radiative corrections are taken into account [122, 123]. We adopt an order-of-magnitude estimation, $A \sim (100 \text{ GeV})^4$. By requiring $(\Gamma/V)^{1/4}$ to be smaller than the current Hubble parameter, the lifetime of the EW vacuum becomes longer than the age of the Universe. The condition corresponds to $S_E \gtrsim 400$. In this paper, thermal effects and radiative corrections to the vacuum transitions are discarded.

The bounce solution and S_E are determined by the scalar potential. The potential relevant for the vacuum decay generated by $(T_D)_{13}$ and/or $(T_D)_{31}$ is

$$\begin{aligned}
V = & \frac{1}{2}m_{11}^2 h_d^2 + \frac{1}{2}m_{22}^2 h_u^2 - m_{12}^2 h_d h_u \\
& + \frac{1}{2}m_{\tilde{Q},1}^2 \tilde{d}_L^2 + \frac{1}{2}m_{\tilde{Q},3}^2 \tilde{b}_L^2 + \frac{1}{2}m_{\tilde{D},1}^2 \tilde{d}_R^2 + \frac{1}{2}m_{\tilde{D},3}^2 \tilde{b}_R^2 \\
& + \frac{1}{\sqrt{2}} [(T_D)_{33} h_d - y_b \mu h_u] \tilde{b}_L \tilde{b}_R + \frac{1}{\sqrt{2}} (T_D)_{13} h_d \tilde{d}_L \tilde{b}_R + \frac{1}{\sqrt{2}} (T_D)_{31} h_d \tilde{b}_L \tilde{d}_R \\
& + \frac{1}{4}y_b^2 (\tilde{b}_L^2 \tilde{b}_R^2 + \tilde{b}_L^2 h_d^2 + \tilde{b}_R^2 h_d^2) \\
& + \frac{1}{24}g_3^2 (\tilde{d}_L^2 + \tilde{b}_L^2 - \tilde{d}_R^2 - \tilde{b}_R^2)^2 + \frac{1}{32}g_2^2 (h_u^2 - h_d^2 + \tilde{d}_L^2 + \tilde{b}_L^2)^2 \\
& + \frac{1}{32}g_Y^2 \left(h_u^2 - h_d^2 + \frac{1}{3}\tilde{d}_L^2 + \frac{1}{3}\tilde{b}_L^2 + \frac{2}{3}\tilde{d}_R^2 + \frac{2}{3}\tilde{b}_R^2 \right)^2, \tag{E.1}
\end{aligned}$$

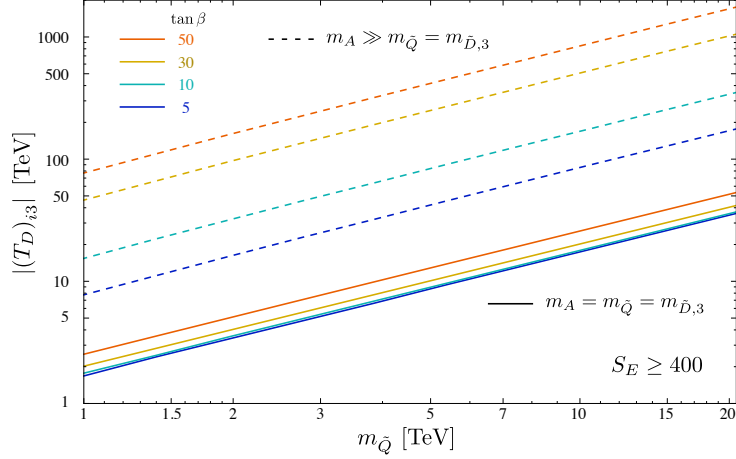


Figure E.1: The upper bound on $|(T_D)_{i3}|$ for $i = 1, 2$ from the vacuum stability condition as a function of $m_{\tilde{Q}}$. Here, $\tan\beta = 5, 10, 30, 50$ are taken. The solid lines are in the case of $m_A = m_{\tilde{Q},i} = m_{\tilde{D},3} \equiv m_{\tilde{Q}}$, while the dashed lines represent the decoupling limit of the heavy Higgs multiplets, $m_A \gg m_{\tilde{Q},i} = m_{\tilde{D},3} \equiv m_{\tilde{Q}}$.

where the coefficients are

$$m_{11}^2 = m_A^2 \sin^2 \beta - \frac{1}{2} m_Z^2 \cos 2\beta, \quad (\text{E.2})$$

$$m_{22}^2 = m_A^2 \cos^2 \beta + \frac{1}{2} m_Z^2 \cos 2\beta, \quad (\text{E.3})$$

$$m_{12}^2 = \frac{1}{2} m_A^2 \sin 2\beta. \quad (\text{E.4})$$

Here, $h_d, h_u, \tilde{d}_L, \tilde{b}_L, \tilde{d}_R, \tilde{b}_R$ are real scalar fields with $\langle h_d \rangle = v \cos \beta$ and $\langle h_u \rangle = v \sin \beta$ at the EW vacuum. In this potential, all coefficients can be rotated to be real by rephasing the fields. The terms proportional to light flavor Yukawas are discarded, because those contributions are negligible. The scalar potential for \tilde{s}_L, \tilde{s}_R is obtained by substituting $\tilde{d}_{L,R} \rightarrow \tilde{s}_{L,R}$, $(T_D)_{13} \rightarrow (T_D)_{23}$, and $(T_D)_{31} \rightarrow (T_D)_{32}$.

Let us first consider the vacuum stability condition when only $(T_D)_{13}$ is large. The scalar potential is simplified to be

$$V = \frac{1}{2} m_{11}^2 h_d^2 + \frac{1}{2} m_{22}^2 h_u^2 - m_{12}^2 h_d h_u + \frac{1}{2} m_{\tilde{Q},1}^2 \tilde{d}_L^2 + \frac{1}{2} m_{\tilde{D},3}^2 \tilde{b}_R^2 + \frac{1}{\sqrt{2}} (T_D)_{13} h_d \tilde{d}_L \tilde{b}_R \quad (\text{E.5})$$

$$+ \frac{1}{4} y_b^2 \tilde{b}_R^2 h_d^2 + \frac{1}{24} g_3^2 (\tilde{d}_L^2 - \tilde{b}_R^2)^2 + \frac{1}{32} g_2^2 (h_u^2 - h_d^2 + \tilde{d}_L^2)^2 + \frac{1}{32} g_Y^2 \left(h_u^2 - h_d^2 + \frac{1}{3} \tilde{d}_L^2 + \frac{2}{3} \tilde{b}_R^2 \right)^2.$$

When $m_A \sim m_{\tilde{Q},1} \sim m_{\tilde{D},3}$, CCB vacua appear around a $h_d - \tilde{d}_L - \tilde{b}_R$ plane. In Fig. E.1, the solid lines show upper bounds on $|(T_D)_{13}|$ for $\tan\beta = 5, 10, 30$, and 50 . We assumed $m_A = m_{\tilde{Q},1} = m_{\tilde{D},3}$. It is shown that the upper bounds are proportional to $m_{\tilde{Q}}$. Also, the results depend on $\tan\beta$ slightly. This is because the scalar potential is stabilized by a quartic coupling $y_b^2 \tilde{b}_R^2 h_d^2 \sim (2m_b^2/v^2) \tan^2 \beta \tilde{b}_R^2 h_d^2$, when $\tan\beta$ is large.

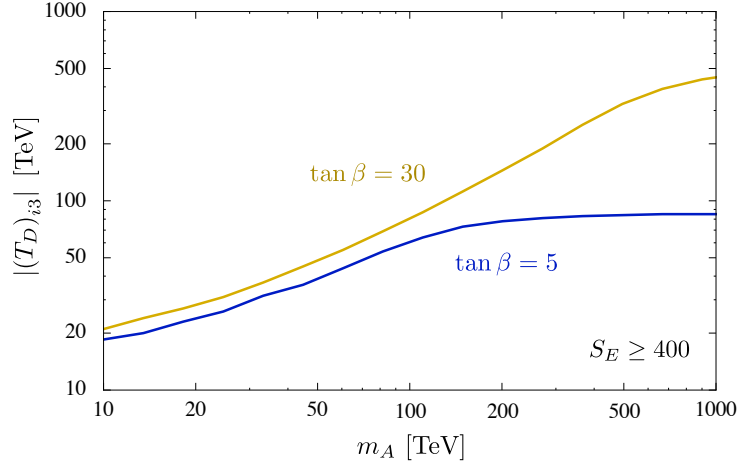


Figure E.2: The vacuum stability condition of $|(T_D)_{i3}|$ for $i = 1, 2$ as a function of m_A . Here, $m_{\tilde{Q},i} = m_{\tilde{D},3} = 10$ TeV, and $\tan \beta = 5$ and 30 are taken.

When m_A is larger than $m_{\tilde{Q},1} \sim m_{\tilde{D},3}$, the position of the CCB vacuum approaches to a H - \tilde{d}_L - \tilde{b}_R plane, where H includes the SM-like Higgs boson, $H = h_{\text{SM}} + v$. In Fig. E.2, the m_A dependence of the upper bound is shown. Here, $\tan \beta = 5$ and 30 are taken. We found that the vacuum stability condition is relaxed for large m_A .

In the decoupling limit of the heavy Higgs bosons ($m_A^2 \gg m_Z^2, \alpha \rightarrow \beta - \pi/2$), the scalar potential can be expressed by H , \tilde{d}_L , and \tilde{b}_R as

$$\begin{aligned}
V = & -\frac{1}{4}m_Z^2 \cos^2 2\beta H^2 + \frac{1}{2}m_{\tilde{Q},1}^2 \tilde{d}_L^2 + \frac{1}{2}m_{\tilde{D},3}^2 \tilde{b}_R^2 + \frac{1}{\sqrt{2}}(T_D)_{13} \cos \beta H \tilde{d}_L \tilde{b}_R \\
& + \frac{1}{4}y_b^2 \tilde{b}_R^2 H^2 \cos^2 \beta + \frac{1}{24}g_3^2(\tilde{d}_L^2 - \tilde{b}_R^2)^2 + \frac{1}{32}g_2^2(H^2 \cos 2\beta - \tilde{d}_L^2)^2 \\
& + \frac{1}{32}g_Y^2 \left(H^2 \cos 2\beta - \frac{1}{3}\tilde{d}_L^2 - \frac{2}{3}\tilde{b}_R^2 \right)^2.
\end{aligned} \tag{E.6}$$

The upper bounds on $|(T_D)_{13}|$ are shown by the dashed lines in Fig. E.1.^{#1} Again, they are proportional to $m_{\tilde{Q}}$. In contrast to the case of $m_A \sim m_{\tilde{Q}}$, the result is almost proportional to $\tan \beta$. This is understood by $\cos \beta$ associated to $(T_D)_{13}$. A fitting formula of the vacuum stability condition in the large m_A limit with $m_{\tilde{Q},1} = m_{\tilde{D},3} \equiv m_{\tilde{Q}}$ is derived as

$$\frac{|(T_D)_{13}|}{\tan \beta} \lesssim -0.186 \text{ TeV} + 1.675 m_{\tilde{Q}}, \tag{E.7}$$

where the phase of $(T_D)_{i3}$ is taken into account. This formula works well for $m_{\tilde{Q}} > 1$ TeV.

^{#1} In this scalar potential, the SM-like Higgs boson is lighter than 125 GeV. The vacuum stability condition can be evaluated naively by adding top-stop radiative corrections, $(g_2^2 + g_Y^2) \delta_H^{(t)} \sin^4 \beta H^4 / 8$, [124–127] to Eq. (E.6) in order to achieve the 125 GeV SM-like Higgs boson at the EW vacuum. We found that Eq. (E.7) is barely changed. Dedicated studies are needed to fully include the radiative corrections (see Ref. [123]).

Let us next turn on $(T_D)_{23}$ in addition to $(T_D)_{13}$. The scalar trilinear term becomes

$$V \supset \frac{1}{\sqrt{2}} \left[(T_D)_{13} \tilde{d}_L + (T_D)_{23} \tilde{s}_L \right] \tilde{b}_R h_d. \quad (\text{E.8})$$

Here, $(T_D)_{13,23}$ are taken to be real by rephasing the scalar fields. By mixing \tilde{d}_L and \tilde{s}_L , one can obtain

$$V \supset \frac{1}{\sqrt{2}} \left[(T_D)_{13}^2 + (T_D)_{23}^2 \right]^{1/2} \tilde{d}'_L \tilde{b}_R h_d, \quad (\text{E.9})$$

where $\tilde{d}_L = \tilde{d}'_L \cos \theta - \tilde{s}'_L \sin \theta$ and $\tilde{s}_L = \tilde{d}'_L \sin \theta + \tilde{s}'_L \cos \theta$ with $\tan \theta = (T_D)_{23} / (T_D)_{13}$. When $m_{\tilde{Q},1}^2 = m_{\tilde{Q},2}^2 \equiv m_{\tilde{Q}}^2$, the scalar potential of \tilde{d}'_L is obtained from that of \tilde{d}_L by substituting $(T_D)_{13} \rightarrow \left[(T_D)_{13}^2 + (T_D)_{23}^2 \right]^{1/2}$ as well as $\tilde{d}_L \rightarrow \tilde{d}'_L$. Therefore, the vacuum stability condition (E.7) is extended to be

$$\frac{\sqrt{|(T_D)_{13}|^2 + |(T_D)_{23}|^2}}{\tan \beta} \lesssim -0.186 \text{ TeV} + 1.675 m_{\tilde{Q}}, \quad (\text{E.10})$$

where the phases of $(T_D)_{13,23}$ are taken into account appropriately. The formula is valid when $m_{\tilde{Q}} \equiv m_{\tilde{Q},1} = m_{\tilde{Q},2} = m_{\tilde{D},3} > 1 \text{ TeV}$ and m_A is decoupled.^{#2}

When only $(T_D)_{31}$ is large, the potential becomes

$$\begin{aligned} V = & \frac{1}{2} m_{11}^2 h_d^2 + \frac{1}{2} m_{22}^2 h_u^2 - m_{12}^2 h_d h_u + \frac{1}{2} m_{\tilde{Q},3}^2 \tilde{b}_L^2 + \frac{1}{2} m_{\tilde{D},1}^2 \tilde{d}_R^2 + \frac{1}{\sqrt{2}} (T_D)_{31} h_d \tilde{b}_L \tilde{d}_R \quad (\text{E.11}) \\ & + \frac{1}{4} y_b^2 \tilde{b}_L^2 h_d^2 + \frac{1}{24} g_3^2 (\tilde{b}_L^2 - \tilde{d}_R^2)^2 + \frac{1}{32} g_2^2 (h_u^2 - h_d^2 + \tilde{b}_L^2)^2 + \frac{1}{32} g_Y^2 \left(h_u^2 - h_d^2 + \frac{1}{3} \tilde{b}_L^2 + \frac{2}{3} \tilde{d}_R^2 \right)^2. \end{aligned}$$

By repeating the above procedure, one can obtain quantitatively the same fitting formula for $(T_D)_{3i}$ as Eq. (E.10),

$$\frac{\sqrt{|(T_D)_{31}|^2 + |(T_D)_{32}|^2}}{\tan \beta} \lesssim -0.186 \text{ TeV} + 1.675 m_{\tilde{Q}}, \quad (\text{E.12})$$

where $m_{\tilde{Q}} \equiv m_{\tilde{Q},3} = m_{\tilde{D},1} = m_{\tilde{D},2} > 1 \text{ TeV}$ and m_A is decoupled.

^{#2} We have validated the formula (E.10) explicitly by analyzing the bounce action of the scalar potential of H , \tilde{d}_L , \tilde{s}_L , and \tilde{b}_R .

Neutron and proton EDM with chiral Lagrangian technique

In this section, we provide contributions of four-quark operators to the neutron and proton EDM with the chiral Lagrangian technique through a procedure in [106]. We focus on CP violating interactions through meson condensation by four-quark operators $\tilde{\mathcal{O}}_1^{q'q}$.

At parton level, CP violating interactions with $\tilde{\mathcal{O}}_1^{q'q}$ are rewritten as

$$\begin{aligned} \mathcal{L}_{\text{CPV}} \supset & \sum_{q' \neq q, q, q' = u, d, s} \tilde{C}_1^{q'q} \tilde{\mathcal{O}}_1^{q'q} \\ & = \sum_{i, j, k, l = u, d, s} \left[i C_{ijkl}^{LRLR} (\bar{q}_i P_R q_j) (\bar{q}_k P_R q_l) + i C_{ijkl}^{RLLR} (\bar{q}_i P_L q_j) (\bar{q}_k P_R q_l) \right] - (L \leftrightarrow R), \end{aligned} \quad (\text{F.1})$$

where the coefficients are defined as

$$C_{ijkl}^{LRLR} = C_{ijkl}^{RLLR} \equiv \sum_{q \neq q'} \tilde{C}_1^{q'q} \delta_{i, q'} \delta_{j, q'} \delta_{k, q} \delta_{l, q}. \quad (\text{F.2})$$

Under rotations, $U(3)_L \times U(3)_R$, we impose a following transformation:

$$P_L q_i \rightarrow (L)_{ij} P_L q_j, \quad (\text{F.3})$$

$$P_R q_i \rightarrow (R)_{ij} P_R q_j, \quad (\text{F.4})$$

$$C_{ijkl}^{LRLR} \rightarrow \sum_{m, n, o, p} (L)_{im} (L)_{ko} C_{mnop}^{LRLR} (R^\dagger)_{nj} (R^\dagger)_{pl}, \quad (\text{F.5})$$

$$C_{ijkl}^{RLLR} \rightarrow \sum_{m, n, o, p} (R)_{im} (L)_{ko} C_{mnop}^{RLLR} (L^\dagger)_{nj} (R^\dagger)_{pl}, \quad (\text{F.6})$$

where $L \in U(3)_L$ and $R \in U(3)_R$. Then, right-hand side of Eq. (F.1) is invariant under the above transformation. Reflecting this symmetry in the meson chiral Lagrangian at order $\mathcal{O}(p^2)$, CP violating terms is written as

$$\begin{aligned} \mathcal{L}_{\text{CPV}}^{\text{meson}} = & \frac{F_\pi^2}{4} \text{Tr} \left[(D_\mu U)^\dagger D^\mu U + \chi (U + U^\dagger) \right] + \frac{F_0^2 - F_\pi^2}{12} \text{Tr} \left[U D_\mu U^\dagger \right] \text{Tr} \left[U^\dagger D^\mu U \right] \\ & + a_0 \text{Tr} \left[\ln U - \ln U^\dagger \right]^2 \end{aligned}$$

$$\begin{aligned}
 & + \sum_{i,j,k,l=u,d,s} \left[iC_{ijkl}^{LRLR} \left(c_1[U]_{ji}[U]_{lk} - c_1[U^\dagger]_{ji}[U^\dagger]_{lk} + c_2[U]_{li}[U]_{jk} - c_2[U^\dagger]_{li}[U^\dagger]_{jk} \right) \right. \\
 & \left. + iC_{ijkl}^{RLLR} \left(c_3[U^\dagger]_{ji}[U]_{lk} - c_3[U]_{ji}[U^\dagger]_{lk} \right) \right],
 \end{aligned} \tag{F.7}$$

where U and χ are given by

$$U = \exp \left[\frac{2i}{\sqrt{6}} \eta_0 I_3 + \frac{2i}{F_\pi} \Pi \right], \quad \Pi \equiv \begin{pmatrix} \frac{1}{2}\pi^0 + \frac{1}{2\sqrt{3}}\eta_8 & & \\ & \frac{1}{\sqrt{2}}\pi^- & \\ & & \frac{1}{\sqrt{2}}K^- \end{pmatrix}, \quad \begin{pmatrix} \frac{1}{\sqrt{2}}\pi^+ & & \\ -\frac{1}{2}\pi^0 + \frac{1}{2\sqrt{3}}\eta_8 & & \\ & & \frac{1}{\sqrt{2}}K^0 \end{pmatrix} \begin{pmatrix} \frac{1}{\sqrt{2}}K^+ \\ \frac{1}{\sqrt{2}}K^0 \\ -\frac{1}{\sqrt{3}}\eta_8 \end{pmatrix} \tag{F.8}$$

$$I_3 \equiv \text{diag}(1, 1, 1), \tag{F.9}$$

$$\chi = 2B_0 \text{diag}(m_u, m_d, m_s). \tag{F.10}$$

Here, the mesons matrix-valued field transforms as $U \rightarrow RUL^\dagger$ under $U(3)_L \times U(3)_R$, F_π is the pion decay constant, F_0 is the decay constant for η_0 . We approximate as $F_0 \simeq F_\pi$, $B_0 \simeq m_\pi^2/(m_u + m_d)$ and $48a_0/F_0^2 \simeq m_\eta^2 + m_{\eta'}^2 - 2m_K^2$. Besides, by naive dimensional analysis, we estimate unknown low energy constants, c_1, c_2 and c_3 as

$$c_1 \sim c_2 \sim c_3 \sim \frac{(4\pi F_\pi)^6}{(4\pi)^4}. \tag{F.11}$$

Scalar potential with neutral mesons π^0, η_8 and η_0 in Eq. (F.8) is extracted as

$$\begin{aligned}
 V(\pi^0, \eta_8, \eta_0) = & F_\pi^2 B_0 \left(m_u \cos \left(\frac{\pi^0}{F_\pi} + \frac{\eta_8}{\sqrt{3}F_\pi} + \frac{2\eta_0}{\sqrt{6}F_0} \right) + m_d \cos \left(-\frac{\pi^0}{F_\pi} + \frac{\eta_8}{\sqrt{3}F_\pi} + \frac{2\eta_0}{\sqrt{6}F_0} \right) \right. \\
 & \left. + m_s \cos \left(-\frac{2\eta_8}{\sqrt{3}F_\pi} + \frac{2\eta_0}{\sqrt{6}F_0} \right) \right) - 24 \frac{a_0}{F_0^2} (\eta_0)^2 \\
 & + 2c_1 \left(\left(\tilde{C}_1^{ud} + \tilde{C}_1^{du} \right) \sin \left(\frac{2\eta_8}{\sqrt{3}F_\pi} + \frac{4\eta_0}{\sqrt{6}F_0} \right) + \left(\tilde{C}_1^{us} + \tilde{C}_1^{su} \right) \sin \left(\frac{\pi^0}{F_\pi} - \frac{\eta_8}{\sqrt{3}F_\pi} + \frac{4\eta_0}{\sqrt{6}F_0} \right) \right. \\
 & \left. + \left(\tilde{C}_1^{ds} + \tilde{C}_1^{sd} \right) \sin \left(-\frac{\pi^0}{F_\pi} - \frac{\eta_8}{\sqrt{3}F_\pi} + \frac{4\eta_0}{\sqrt{6}} \right) \right) \\
 & + 2c_3 \left(\left(\tilde{C}_1^{ud} - \tilde{C}_1^{du} \right) \sin \left(-\frac{2\pi^0}{F_\pi} \right) + \left(\tilde{C}_1^{us} - \tilde{C}_1^{su} \right) \sin \left(-\frac{\pi^0}{F_\pi} - \frac{\sqrt{3}\eta_8}{F_\pi} \right) \right. \\
 & \left. + \left(\tilde{C}_1^{ds} - \tilde{C}_1^{sd} \right) \sin \left(\frac{\pi^0}{F_\pi} - \frac{\sqrt{3}\eta_8}{F_\pi} \right) \right).
 \end{aligned} \tag{F.12}$$

If $\tilde{C}_1^{ud}, \tilde{C}_1^{du}, \tilde{C}_1^{us}$ and \tilde{C}_1^{su} takes zero, non-zero small meson VEVs coming from \tilde{C}_1^{ds} and \tilde{C}_1^{sd} , $\langle \pi^0 \rangle, \langle \eta_8 \rangle$ and $\langle \eta_0 \rangle$ of the above potential Eq. (F.12) are given as

$$\frac{\langle \pi^0 \rangle}{F_\pi} \simeq - \left(\tilde{C}_1^{ds} + \tilde{C}_1^{sd} \right) \frac{c_1}{B_0 F_\pi^2} \frac{B_0 F_\pi^2 m_u m_s + 8a_0(m_d + 2m_s)}{B_0 F_\pi^2 m_u m_d m_s + 8a_0(m_u m_d + m_d m_s + m_s m_u)}$$

$$+ \left(\tilde{C}_1^{ds} - \tilde{C}_1^{sd} \right) \frac{c_3}{B_0 F_\pi^2} \frac{B_0 F_\pi^2 m_s m_u - 8a_0(m_d - 2(m_u + m_s))}{B_0 F_\pi^2 m_u m_d m_s + 8a_0(m_u m_d + m_d m_s + m_s m_u)}, \quad (\text{F.13})$$

$$\begin{aligned} \frac{\langle \eta_8 \rangle}{F_\pi} &\simeq - \left(\tilde{C}_1^{ds} + \tilde{C}_1^{sd} \right) \frac{c_1}{\sqrt{3} B_0 F_\pi^2} \frac{B_0 F_\pi^2 m_u (2m_d - m_s) + 24a_0 m_d}{B_0 F_\pi^2 m_u m_d m_s + 8a_0(m_u m_d + m_d m_s + m_s m_u)} \\ &- \left(\tilde{C}_1^{ds} - \tilde{C}_1^{sd} \right) \frac{c_3}{\sqrt{3} B_0 F_\pi^2} \frac{B_0 F_\pi^2 (2m_d + m_s) m_u + 24a_0(m_d + 2m_u)}{B_0 F_\pi^2 m_u m_d m_s + 8a_0(m_u m_d + m_d m_s + m_s m_u)}, \end{aligned} \quad (\text{F.14})$$

$$\begin{aligned} \frac{\langle \eta_0 \rangle}{F_0} &\simeq \left(\tilde{C}_1^{ds} + \tilde{C}_1^{sd} \right) \frac{\sqrt{2} c_1}{\sqrt{3} B_0 F_\pi^2} \frac{B_0 F_\pi^2 (m_d + m_s) m_u}{B_0 F_\pi^2 m_u m_d m_s + 8a_0(m_u m_d + m_d m_s + m_s m_u)} \\ &+ \left(\tilde{C}_1^{ds} - \tilde{C}_1^{sd} \right) \frac{\sqrt{2} c_3}{\sqrt{3} B_0 F_\pi^2} \frac{B_0 F_\pi^2 (m_d - m_s) m_u}{B_0 F_\pi^2 m_u m_d m_s + 8a_0(m_u m_d + m_d m_s + m_s m_u)}. \end{aligned} \quad (\text{F.15})$$

By the meson condensations, CP violating interactions are generated by the baryon chiral Lagrangian at $\mathcal{O}(p^2)$:

$$\begin{aligned} \mathcal{L}_{\text{baryons}} &= \text{Tr} \left[\bar{B} i \gamma^\mu (\partial_\mu B + [\Gamma_\mu, B]) - M_B \bar{B} B \right] \\ &- \frac{D}{2} \text{Tr} \left[\bar{B} \gamma^\mu \gamma_5 \{ \xi_\mu, B \} \right] - \frac{F}{2} \text{Tr} \left[\bar{B} \gamma^\mu \gamma_5 [\xi_\mu, B] \right] - \frac{\lambda}{2} \text{Tr} [\xi_\mu] \text{Tr} [\bar{B} \gamma^\mu \gamma_5 B] \\ &+ b_D \text{Tr} [\bar{B} \{ \chi_+, B \}] + b_F \text{Tr} [\bar{B} [\chi_+, B]] + b_0 \text{Tr} [\chi_+] \text{Tr} [\bar{B} B] + \dots, \end{aligned} \quad (\text{F.16})$$

where baryons matrix-valued field B is defined as

$$B = \begin{pmatrix} \frac{1}{\sqrt{2}} \Sigma^0 + \frac{1}{\sqrt{6}} \Lambda^0 & \Sigma^+ & p \\ \Sigma^- & -\frac{1}{\sqrt{2}} \Sigma^0 + \frac{1}{\sqrt{6}} \Lambda^0 & n \\ \Xi^- & \Xi^0 & -\frac{2}{\sqrt{6}} \Lambda^0 \end{pmatrix}, \quad (\text{F.17})$$

$\xi_{L,R}$ are defined as $U = \xi_R \xi_L^\dagger$, where $\xi_R = \xi_L^\dagger$.

Besides, M_B is the baryon mass, a covariant derivative for baryons Γ_μ , fields consisting mesons ξ_μ and χ_+ consisting quark masses are defined as

$$\Gamma_\mu \equiv \frac{1}{2} \xi_R^\dagger (\partial_\mu - i r_\mu) \xi_R + \frac{1}{2} \xi_L^\dagger (\partial_\mu - i l_\mu) \xi_L, \quad (\text{F.18})$$

$$\xi_\mu \equiv i \xi_R^\dagger (\partial_\mu - r_\mu) \xi_R - i \xi_L^\dagger (\partial_\mu - l_\mu) \xi_L, \quad (\text{F.19})$$

$$\chi_+ \equiv 2B_0 \xi_L^\dagger \text{diag} (m_u, m_d, m_s) \xi_R + 2B_0 \xi_R^\dagger \text{diag} (m_u, m_d, m_s) \xi_L. \quad (\text{F.20})$$

By inserting meson VEVs $\langle \pi^0 \rangle$, $\langle \eta_8 \rangle$ and $\langle \eta_0 \rangle$ into the baryon chiral Lagrangian Eq. (F.16), CP violating interactions are given as

$$\begin{aligned} \mathcal{L}_{\text{baryons}} &\supset \bar{g}_{np\pi} \bar{n} p \pi^- + \bar{g}_{n\Sigma K} \bar{\Sigma}^+ p K^+ \\ &+ \bar{g}_{\pi^+ np} \bar{p} n \pi^+ + \bar{g}_{K^+ \Lambda p} \bar{p} \Lambda K^+ + \bar{g}_{K^+ \Sigma^0 p} \bar{p} \Sigma^0 K^+, \end{aligned} \quad (\text{F.21})$$

where the coupling constants are given by

$$\bar{g}_{n\Sigma K^+} = \frac{B_0}{F_\pi} (b_D - b_F) \left[-\frac{1}{\sqrt{2}} (3m_u + m_s) \frac{\langle \pi^0 \rangle}{F_\pi} + \frac{1}{\sqrt{6}} (-m_u + 5m_s) \frac{\langle \eta_8 \rangle}{F_\pi} - \frac{4}{\sqrt{3}} (m_u + m_s) \frac{\langle \eta_0 \rangle}{F_0} \right], \quad (\text{F.22})$$

$$\bar{g}_{\pi^+np} = \frac{B_0}{F_\pi}(b_D + b_F) \left[\sqrt{2}(m_d - m_u) \frac{\langle \pi^0 \rangle}{F_\pi} - \frac{2\sqrt{2}}{\sqrt{3}}(m_u + m_d) \frac{\langle \eta_8 \rangle}{F_\pi} - \frac{4}{\sqrt{3}}(m_u + m_d) \frac{\langle \eta^0 \rangle}{F_0} \right], \quad (\text{F.23})$$

$$\bar{g}_{K^+\Lambda p} = \frac{B_0}{F_\pi}(b_D + 3b_F) \left[\frac{1}{2\sqrt{3}}(m_s + 3m_u) \frac{\langle \pi^0 \rangle}{F_\pi} + \frac{1}{6}(m_u - 5m_s) \frac{\langle \eta_8 \rangle}{F_\pi} + \frac{2\sqrt{2}}{3}(m_u + m_s) \frac{\langle \eta^0 \rangle}{F_0} \right], \quad (\text{F.24})$$

$$\bar{g}_{K^+\Sigma^0 p} = \frac{B_0}{F_\pi}(b_D - b_F) \left[-\frac{1}{2}(m_s + 3m_u) \frac{\langle \pi^0 \rangle}{F_\pi} - \frac{1}{2\sqrt{3}}(m_u - 5m_s) \frac{\langle \eta_8 \rangle}{F_\pi} - 2\sqrt{\frac{2}{3}}(m_u + m_s) \frac{\langle \eta^0 \rangle}{F_0} \right]. \quad (\text{F.25})$$

These couplings contribute to the neutron and proton EDMs through baryon-meson loop diagram as followings [115]:

$$d_n \sim -\frac{e}{8\pi^2 F_\pi} \left[\frac{\bar{g}_{np\pi^-}}{\sqrt{2}}(D + F) \left(1 + \ln \frac{m_\pi^2}{m_N^2} \right) - \frac{\bar{g}_{n\Sigma K^+}}{\sqrt{2}}(D - F) \left(1 + \ln \frac{m_{K^+}^2}{m_N^2} + \frac{\pi(m_{\Sigma^-} - m_n)}{m_{K^+}} \right) \right], \quad (\text{F.26})$$

$$d_p \sim -\frac{e}{8\pi^2 F_\pi} \left[-\frac{\bar{g}_{np\pi^-}}{\sqrt{2}}(D + F) \left(1 + \ln \frac{m_\pi^2}{m_N^2} \right) + \frac{\bar{g}_{K^+\Lambda p}}{2\sqrt{3}}(D + 3F) \left(1 + \ln \frac{m_{K^+}^2}{m_N^2} + \frac{\pi(m_\Lambda - m_n)}{m_{K^+}} \right) - \frac{\bar{g}_{K^+\Sigma^0 p}}{2}(D - F) \left(1 + \ln \frac{m_{K^+}^2}{m_N^2} + \frac{\pi(m_{\Sigma^0} - m_n)}{m_{K^+}} \right) \right], \quad (\text{F.27})$$

where we include only leading order terms of the baryon-meson loops. Divergent terms and a mass scale coming from the dimensional regularization are set as zero-value and the nucleon mass m_N , respectively.

By substituting the meson VEVs into Eq. (F.26) and Eq. (F.27), and using the pion decay constant $F_\pi = 86.8$ MeV [116], measured meson-baryon couplings from hyperon β decays $D = 0.804$ and $F = 0.463$ [117], low-energy-constants (LECs) determined from the baryon octet mass splittings $b_D = 0.161$ GeV $^{-1}$ and $b_F = -0.502$ GeV $^{-1}$ [118] and the quark masses $m_u(1 \text{ GeV}) = 2.699$ MeV, $m_d(1 \text{ GeV}) = 5.868$ MeV and $m_s(1 \text{ GeV}) = 117$ MeV which are evaluated by the QCD four-loop RGEs [80], $m_{ud}(2 \text{ GeV}) = 3.373$ MeV and $m_s(2 \text{ GeV}) = 92.0$ MeV, the neutron and proton EDMs are approximated as

$$d_n \sim e \cdot \left[-0.026\tilde{C}_1^{ds} + 0.169\tilde{C}_1^{sd} \right] \text{ GeV}^{-1}, \quad (\text{F.28})$$

$$d_p \sim e \cdot \left[0.023\tilde{C}_1^{ds} - 0.149\tilde{C}_1^{sd} \right] \text{ GeV}^{-1}. \quad (\text{F.29})$$

Bibliography

- [1] G. Aad *et al.* [ATLAS Collaboration], Phys. Lett. B **716**, 1 (2012) doi:10.1016/j.physletb.2012.08.020 [arXiv:1207.7214 [hep-ex]].
- [2] S. Chatrchyan *et al.* [CMS Collaboration], Phys. Lett. B **716**, 30 (2012) doi:10.1016/j.physletb.2012.08.021 [arXiv:1207.7235 [hep-ex]].
- [3] P. A. R. Ade *et al.* [Planck Collaboration], Astron. Astrophys. **594**, A13 (2016) doi:10.1051/0004-6361/201525830 [arXiv:1502.01589 [astro-ph.CO]].
- [4] ATLAS results summarized in [webpage](#); and CMS results in [webpage](#).
- [5] A. Cerri *et al.*, arXiv:1812.07638 [hep-ph].
- [6] E. Kou *et al.* [Belle-II Collaboration], arXiv:1808.10567 [hep-ex].
- [7] Richard Keith Ellis *et al.*, “Physics Briefing Book : Input for the European Strategy for Particle Physics Update 2020,” arXiv:1910.11775 [hep-ex].
- [8] D. Wurm *et al.*, “The PanEDM Neutron Electric Dipole Moment Experiment at the ILL,” arXiv:1911.09161 [physics.ins-det].
- [9] V. Anastassopoulos *et al.*, “A Storage Ring Experiment to Detect a Proton Electric Dipole Moment,” Rev. Sci. Instrum. **87**, no. 11, 115116 (2016) doi:10.1063/1.4967465 [arXiv:1502.04317 [physics.acc-ph]].
- [10] W. Buchmuller and D. Wyler, Nucl. Phys. B **268**, 621 (1986). doi:10.1016/0550-3213(86)90262-2
- [11] B. Grzadkowski, M. Iskrzynski, M. Misiak and J. Rosiek, JHEP **1010**, 085 (2010) doi:10.1007/JHEP10(2010)085 [arXiv:1008.4884 [hep-ph]].
- [12] A. Dedes, W. Materkowska, M. Paraskevas, J. Rosiek and K. Suxho, JHEP **1706**, 143 (2017) doi:10.1007/JHEP06(2017)143 [arXiv:1704.03888 [hep-ph]].
- [13] E. E. Jenkins, A. V. Manohar and M. Trott, JHEP **1310**, 087 (2013) doi:10.1007/JHEP10(2013)087 [arXiv:1308.2627 [hep-ph]].
- [14] E. E. Jenkins, A. V. Manohar and M. Trott, JHEP **1401**, 035 (2014) doi:10.1007/JHEP01(2014)035 [arXiv:1310.4838 [hep-ph]].
- [15] R. Alonso, E. E. Jenkins, A. V. Manohar and M. Trott, JHEP **1404**, 159 (2014) doi:10.1007/JHEP04(2014)159 [arXiv:1312.2014 [hep-ph]].

BIBLIOGRAPHY

- [16] M. Endo, T. Kitahara and D. Ueda, *JHEP* **1907**, 182 (2019) doi:10.1007/JHEP07(2019)182 [arXiv:1811.04961 [hep-ph]].
- [17] M. Endo and D. Ueda, arXiv:1911.10805 [hep-ph].
- [18] J. Aebischer, A. Crivellin, M. Fael and C. Greub, *JHEP* **1605**, 037 (2016) doi:10.1007/JHEP05(2016)037 [arXiv:1512.02830 [hep-ph]].
- [19] J. Aebischer, A. Crivellin and M. Fael, private communication.
- [20] C. Bobeth, A. J. Buras, A. Celis and M. Jung, *JHEP* **1707**, 124 (2017) doi:10.1007/JHEP07(2017)124 [arXiv:1703.04753 [hep-ph]].
- [21] M. Endo, T. Kitahara, S. Mishima and K. Yamamoto, *Phys. Lett. B* **771**, 37 (2017) doi:10.1016/j.physletb.2017.05.026 [arXiv:1612.08839 [hep-ph]].
- [22] CKMfitter Group (J. Charles et al.), *Eur. Phys. J. C* **41**, 1-131 (2005) [hep-ph/0406184], updated results and plots available at: [webpage](#)
- [23] S. L. Glashow, J. Iliopoulos and L. Maiani, *Phys. Rev. D* **2**, 1285 (1970). doi:10.1103/PhysRevD.2.1285
- [24] A. V. Manohar, “Effective Theories for Precision Higgs and Flavor Physics,” talk given at [Higgs and Effective Field Theory-HEFT 2019](#), April 15-18, Louvain, Belgium (2019).
- [25] S. Weinberg, *Phys. Rev. Lett.* **43**, 1566 (1979). doi:10.1103/PhysRevLett.43.1566
- [26] F. Gabbiani, E. Gabrielli, A. Masiero and L. Silvestrini, *Nucl. Phys. B* **477**, 321 (1996) doi:10.1016/0550-3213(96)00390-2 [hep-ph/9604387].
- [27] J. A. Bailey, S. Lee, W. Lee, J. Leem and S. Park, *Phys. Rev. D* **98**, no. 9, 094505 (2018) doi:10.1103/PhysRevD.98.094505 [arXiv:1808.09657 [hep-lat]].
- [28] A. J. Buras and D. Guadagnoli, *Phys. Rev. D* **78**, 033005 (2008) doi:10.1103/PhysRevD.78.033005 [arXiv:0805.3887 [hep-ph]].
- [29] A. J. Buras, D. Guadagnoli and G. Isidori, *Phys. Lett. B* **688**, 309 (2010) doi:10.1016/j.physletb.2010.04.017 [arXiv:1002.3612 [hep-ph]].
- [30] M. Tanabashi *et al.* [Particle Data Group], *Phys. Rev. D* **98**, no. 3, 030001 (2018). doi:10.1103/PhysRevD.98.030001
- [31] A. J. Buras, S. Jager and J. Urban, *Nucl. Phys. B* **605**, 600 (2001) doi:10.1016/S0550-3213(01)00207-3 [hep-ph/0102316].

-
-
- [32] N. Garron *et al.* [RBC/UKQCD Collaboration], JHEP **1611**, 001 (2016) doi:10.1007/JHEP11(2016)001 [arXiv:1609.03334 [hep-lat]].
- [33] A. Bazavov *et al.* [Fermilab Lattice and MILC Collaborations], [arXiv:1602.03560 [hep-lat]].
- [34] J. de Vries, E. Mereghetti, R. G. E. Timmermans and U. van Kolck, Annals Phys. **338**, 50 (2013) doi:10.1016/j.aop.2013.05.022 [arXiv:1212.0990 [hep-ph]].
- [35] J. Bijnens and E. Pallante, Phys. Lett. B **387**, 207 (1996) doi:10.1016/0370-2693(96)00982-3 [hep-ph/9606285].
- [36] D. A. Demir, M. Pospelov and A. Ritz, Phys. Rev. D **67**, 015007 (2003) doi:10.1103/PhysRevD.67.015007 [hep-ph/0208257].
- [37] D. A. Demir, O. Lebedev, K. A. Olive, M. Pospelov and A. Ritz, Nucl. Phys. B **680**, 339 (2004) doi:10.1016/j.nuclphysb.2003.12.026 [hep-ph/0311314].
- [38] U. Haisch and A. Hala, JHEP **1911**, 154 (2019) doi:10.1007/JHEP11(2019)154 [arXiv:1909.08955 [hep-ph]].
- [39] J. M. Pendlebury *et al.*, Phys. Rev. D **92**, no. 9, 092003 (2015) doi:10.1103/PhysRevD.92.092003 [arXiv:1509.04411 [hep-ex]].
- [40] B. K. Sahoo, Phys. Rev. D **95**, no. 1, 013002 (2017) doi:10.1103/PhysRevD.95.013002 [arXiv:1612.09371 [hep-ph]].
- [41] A. J. Buras, JHEP **1604**, 071 (2016) doi:10.1007/JHEP04(2016)071 [arXiv:1601.00005 [hep-ph]].
- [42] T. Blum *et al.*, Phys. Rev. Lett. **108**, 141601 (2012) doi:10.1103/PhysRevLett.108.141601 [arXiv:1111.1699 [hep-lat]].
- [43] T. Blum *et al.*, Phys. Rev. D **86**, 074513 (2012) doi:10.1103/PhysRevD.86.074513 [arXiv:1206.5142 [hep-lat]].
- [44] T. Blum *et al.*, Phys. Rev. D **91**, no. 7, 074502 (2015) doi:10.1103/PhysRevD.91.074502 [arXiv:1502.00263 [hep-lat]].
- [45] A. J. Buras, M. Gorbahn, S. Jager and M. Jamin, JHEP **1511**, 202 (2015) doi:10.1007/JHEP11(2015)202 [arXiv:1507.06345 [hep-ph]].
- [46] A. J. Buras, D. Buttazzo, J. Girrbach-Noe and R. Knegjens, JHEP **1511**, 033 (2015) doi:10.1007/JHEP11(2015)033 [arXiv:1503.02693 [hep-ph]].

BIBLIOGRAPHY

- [47] T. Kitahara, U. Nierste and P. Tremper, *JHEP* **1612**, 078 (2016) doi:10.1007/JHEP12(2016)078 [arXiv:1607.06727 [hep-ph]].
- [48] F. Brizioli, “Status and prospects for the NA62 experiment at CERN SOS,” talk given at [2nd Workshop on Hadronic Contributions to New Physics Searches](#), Sept 23-28, Tenerife (2019).
- [49] N. Lurkin [NA62 Collaboration], arXiv:1907.12955 [hep-ex].
- [50] J. K. Ahn *et al.* [KOTO Collaboration], *Phys. Rev. Lett.* **122**, no. 2, 021802 (2019) doi:10.1103/PhysRevLett.122.021802 [arXiv:1810.09655 [hep-ex]].
- [51] E. Cortina Gil *et al.* [NA62 Collaboration], *JINST* **12**, no. 05, P05025 (2017) doi:10.1088/1748-0221/12/05/P05025 [arXiv:1703.08501 [physics.ins-det]].
- [52] Talk by H. Nanjo on “KOTO and KOTO step2 to search for the rare kaon decay, $K_L \rightarrow \pi^0 \nu \bar{\nu}$ ” in *International workshop on physics at the extended hadron experimental facility of J-PARC*, KEK Tokai, Japan, 5-6 March 2016.
- [53] Talk by G. Ruggiero on “Recent results from kaon physics” in *EPS Conference on High Energy Physics*, Venice, Italy, 5-12 July 2017.
- [54] G. Ecker and A. Pich, *Nucl. Phys. B* **366**, 189 (1991). doi:10.1016/0550-3213(91)90056-4
- [55] F. Mescia, C. Smith and S. Trine, *JHEP* **0608**, 088 (2006) doi:10.1088/1126-6708/2006/08/088 [hep-ph/0606081].
- [56] G. D’Ambrosio and T. Kitahara, *Phys. Rev. Lett.* **119**, no. 20, 201802 (2017) doi:10.1103/PhysRevLett.119.201802 [arXiv:1707.06999 [hep-ph]].
- [57] G. Isidori and R. Unterdorfer, *JHEP* **0401**, 009 (2004) doi:10.1088/1126-6708/2004/01/009 [hep-ph/0311084].
- [58] V. Cirigliano, G. Ecker, H. Neufeld, A. Pich and J. Portoles, *Rev. Mod. Phys.* **84**, 399 (2012) doi:10.1103/RevModPhys.84.399 [arXiv:1107.6001 [hep-ph]].
- [59] R. Aaij *et al.* [LHCb Collaboration], *Eur. Phys. J. C* **77**, no. 10, 678 (2017) doi:10.1140/epjc/s10052-017-5230-x [arXiv:1706.00758 [hep-ex]].
- [60] Talk by D. M. Santos on “Physics of LHCb Upgrade(s)” in *FPCP 2017 - Flavor Physics & CP Violation*, Prague, Czech Republic, 5-9 June 2017.
- [61] J. C. Pati and A. Salam, *Phys. Rev. D* **10**, 275 (1974) Erratum: [*Phys. Rev. D* **11**, 703 (1975)]. doi:10.1103/PhysRevD.10.275, 10.1103/PhysRevD.11.703.2

-
-
- [62] R. N. Mohapatra and J. C. Pati, Phys. Rev. D **11**, 566 (1975). doi:10.1103/PhysRevD.11.566
- [63] R. N. Mohapatra and J. C. Pati, Phys. Rev. D **11**, 2558 (1975). doi:10.1103/PhysRevD.11.2558
- [64] G. Senjanovic and R. N. Mohapatra, Phys. Rev. D **12**, 1502 (1975). doi:10.1103/PhysRevD.12.1502
- [65] G. Senjanovic, Nucl. Phys. B **153**, 334 (1979). doi:10.1016/0550-3213(79)90604-7
- [66] J. F. Gunion, J. Grifols, A. Mendez, B. Kayser and F. I. Olness, Phys. Rev. D **40**, 1546 (1989). doi:10.1103/PhysRevD.40.1546
- [67] N. G. Deshpande, J. F. Gunion, B. Kayser and F. I. Olness, Phys. Rev. D **44**, 837 (1991). doi:10.1103/PhysRevD.44.837
- [68] A. Maiezza and M. Nemevsek, Phys. Rev. D **90**, no. 9, 095002 (2014) doi:10.1103/PhysRevD.90.095002 [arXiv:1407.3678 [hep-ph]].
- [69] R. N. Mohapatra and G. Senjanovic, Phys. Lett. **79B**, 283 (1978). doi:10.1016/0370-2693(78)90243-5
- [70] K. S. Babu and R. N. Mohapatra, Phys. Rev. D **41**, 1286 (1990). doi:10.1103/PhysRevD.41.1286
- [71] S. M. Barr, D. Chang and G. Senjanovic, Phys. Rev. Lett. **67**, 2765 (1991). doi:10.1103/PhysRevLett.67.2765
- [72] G. Beall, M. Bander and A. Soni, Phys. Rev. Lett. **48**, 848 (1982). doi:10.1103/PhysRevLett.48.848
- [73] R. N. Mohapatra, G. Senjanovic and M. D. Tran, Phys. Rev. D **28**, 546 (1983). doi:10.1103/PhysRevD.28.546
- [74] J. Basecq, L. F. Li and P. B. Pal, Phys. Rev. D **32**, 175 (1985).
- [75] S. Bertolini, A. Maiezza and F. Nesti, Phys. Rev. D **89**, no. 9, 095028 (2014) [arXiv:1403.7112 [hep-ph]].
- [76] D. Chang, J. Basecq, L. F. Li and P. B. Pal, Phys. Rev. D **30**, 1601 (1984).
- [77] W. S. Hou and A. Soni, Phys. Rev. D **32**, 163 (1985).
- [78] G. Ecker and W. Grimus, Nucl. Phys. B **258**, 328 (1985).

BIBLIOGRAPHY

- [79] A. Maiezza, M. Nemevsek, F. Nesti and G. Senjanovic, Phys. Rev. D **82**, 055022 (2010) [arXiv:1005.5160 [hep-ph]].
- [80] K. G. Chetyrkin, J. H. Kuhn and M. Steinhauser, Comput. Phys. Commun. **133**, 43 (2000) [hep-ph/0004189].
- [81] M. Endo, T. Goto, T. Kitahara, S. Mishima, D. Ueda and K. Yamamoto, JHEP **1804**, 019 (2018) doi:10.1007/JHEP04(2018)019 [arXiv:1712.04959 [hep-ph]].
- [82] A. J. Buras, F. De Fazio and J. Girrbach, Eur. Phys. J. C **74**, no. 7, 2950 (2014) doi:10.1140/epjc/s10052-014-2950-z [arXiv:1404.3824 [hep-ph]].
- [83] A. J. Buras, D. Buttazzo and R. Knegjens, JHEP **1511**, 166 (2015) doi:10.1007/JHEP11(2015)166 [arXiv:1507.08672 [hep-ph]].
- [84] A. J. Buras, F. De Fazio, J. Girrbach, R. Knegjens and M. Nagai, JHEP **1306**, 111 (2013) doi:10.1007/JHEP06(2013)111 [arXiv:1303.3723 [hep-ph]].
- [85] P. Z. Skands *et al.*, JHEP **0407**, 036 (2004) doi:10.1088/1126-6708/2004/07/036 [hep-ph/0311123].
- [86] B. C. Allanach *et al.*, Comput. Phys. Commun. **180**, 8 (2009) doi:10.1016/j.cpc.2008.08.004 [arXiv:0801.0045 [hep-ph]].
- [87] J. S. Hagelin, S. Kelley and T. Tanaka, Nucl. Phys. B **415**, 293 (1994). doi:10.1016/0550-3213(94)90113-9
- [88] W. C. Griffith, M. D. Swallows, T. H. Loftus, M. V. Romalis, B. R. Heckel and E. N. Fortson, Phys. Rev. Lett. **102**, 101601 (2009) doi:10.1103/PhysRevLett.102.101601 [arXiv:0901.2328 [physics.atom-ph]].
- [89] B. Graner, Y. Chen, E. G. Lindahl and B. R. Heckel, Phys. Rev. Lett. **116**, no. 16, 161601 (2016) Erratum: [Phys. Rev. Lett. **119**, no. 11, 119901 (2017)] doi:10.1103/PhysRevLett.119.119901, 10.1103/PhysRevLett.116.161601 [arXiv:1601.04339 [physics.atom-ph]].
- [90] I. Brivio and M. Trott, Phys. Rept. **793**, 1 (2019) doi:10.1016/j.physrep.2018.11.002 [arXiv:1706.08945 [hep-ph]].
- [91] J. Aebischer, C. Bobeth, A. J. Buras and D. M. Straub, Eur. Phys. J. C **79**, no. 3, 219 (2019) doi:10.1140/epjc/s10052-019-6715-6 [arXiv:1808.00466 [hep-ph]].
- [92] M. A. Shifman, A. I. Vainshtein and V. I. Zakharov, Phys. Rev. D **18**, 2583 (1978) Erratum: [Phys. Rev. D **19**, 2815 (1979)]. doi:10.1103/PhysRevD.18.2583, 10.1103/PhysRevD.19.2815

-
-
- [93] J. Dai and H. Dykstra, Phys. Lett. B **237**, 256 (1990). doi:10.1016/0370-2693(90)91439-I
- [94] E. Braaten, C. S. Li and T. C. Yuan, Phys. Rev. D **42**, 276 (1990). doi:10.1103/PhysRevD.42.276
- [95] G. Boyd, A. K. Gupta, S. P. Trivedi and M. B. Wise, Phys. Lett. B **241**, 584 (1990). doi:10.1016/0370-2693(90)91874-B
- [96] J. Hisano, K. Tsumura and M. J. S. Yang, Phys. Lett. B **713**, 473 (2012) doi:10.1016/j.physletb.2012.06.038 [arXiv:1205.2212 [hep-ph]].
- [97] G. Degrassi, E. Franco, S. Marchetti and L. Silvestrini, JHEP **0511**, 044 (2005) doi:10.1088/1126-6708/2005/11/044 [hep-ph/0510137].
- [98] J. Brod and E. Stamou, arXiv:1810.12303 [hep-ph].
- [99] J. de Vries, G. Falcioni, F. Herzog and B. Ruijl, arXiv:1907.04923 [hep-ph].
- [100] M. Gorbahn and U. Haisch, Phys. Rev. Lett. **97**, 122002 (2006) doi:10.1103/PhysRevLett.97.122002 [hep-ph/0605203].
- [101] C. Bobeth, M. Gorbahn and E. Stamou, Phys. Rev. D **89**, no. 3, 034023 (2014) doi:10.1103/PhysRevD.89.034023 [arXiv:1311.1348 [hep-ph]].
- [102] G. Passarino and M. J. G. Veltman, Nucl. Phys. B **160**, 151 (1979).
- [103] H. H. Patel, Comput. Phys. Commun. **197**, 276 (2015) [arXiv:1503.01469 [hep-ph]].
- [104] H. H. Patel, Comput. Phys. Commun. **218**, 66 (2017) [arXiv:1612.00009 [hep-ph]].
- [105] J. Hisano, K. Tsumura and M. J. S. Yan, Phys. Lett. **713 B**, 473 (2012). [arXiv:1205.2212 [hep-ph]].
- [106] N. Haba, H. Umeeda and T. Yamada, JHEP **1805**, 052 (2018) [arXiv:1802.09903 [hep-ph]].
- [107] J. Bijnens and E. Pallante, Phys. Lett. **387 B**, 207 (1996). [arXiv:9606285 [hep-ph]].
- [108] D. Demir, O. Lebedev, K. A. Olive, M. Pospelov, and A. Ritz, Nucl. Phys. B **680**, 1 (2004) [arXiv:0311314 [hep-ph]].
- [109] J. L. Hewett *et al.*, [arXiv:1205.2671 [hep-ex]].
- [110] K. Kumar, Z-T. Lu and M. J. Ramsey-Musolf, [arXiv:1312.5416 [hep-ph]].
- [111] A. Lehrach, B. Lorentz, W. Morse, N. Nikolaev and F. Rathmann, [arXiv:1201.5773 [hep-ex]].

BIBLIOGRAPHY

- [112] Y. K. Semertzidis, [arXiv:1110.3378 [physics.acc-ph]].
- [113] M. Tanabashi *et al.* [Particle Data Group Collaboration], Phys. Rev. D **98**, 010001 (2018).
- [114] J. A. Bailey, S. Lee, W. Lee, J. Leem, and S. Park, Phys. Rev. D **98**, no. 9, 094505 (2018) [arXiv:1808.09657 [hep-lat]].
- [115] F-K. Guo and U-G. Meißner, JHEP **1212**, 097 (2012) [arXiv:1210.5887 [hep-ph]].
- [116] S. Borsányi *et al.*, Phys. Rev. D **88**, no. 1, 014513 (2013) [arXiv:1205.0788 [hep-lat]].
- [117] H. Abele and D. Mund, [arXiv:0312124 [hep-ph]].
- [118] J. M. Alarcon, L. S. Geng, J. Martin Camalich and J. A. Oller, Phys. Lett. **730 B**, 342 (20014). [arXiv:1209.2870 [hep-ph]].
- [119] J. h. Park, Phys. Rev. D **83**, 055015 (2011) doi:10.1103/PhysRevD.83.055015 [arXiv:1011.4939 [hep-ph]].
- [120] S. R. Coleman, Phys. Rev. D **15**, 2929 (1977) Erratum: [Phys. Rev. D **16**, 1248 (1977)]. doi:10.1103/PhysRevD.15.2929, 10.1103/PhysRevD.16.1248
- [121] C. L. Wainwright, Comput. Phys. Commun. **183**, 2006 (2012) doi:10.1016/j.cpc.2012.04.004 [arXiv:1109.4189 [hep-ph]].
- [122] C. G. Callan, Jr. and S. R. Coleman, Phys. Rev. D **16**, 1762 (1977). doi:10.1103/PhysRevD.16.1762
- [123] M. Endo, T. Moroi, M. M. Nojiri and Y. Shoji, JHEP **1601**, 031 (2016) doi:10.1007/JHEP01(2016)031 [arXiv:1511.04860 [hep-ph]].
- [124] J. Hisano and S. Sugiyama, Phys. Lett. B **696**, 92 (2011) Erratum: [Phys. Lett. B **719**, 472 (2013)] doi:10.1016/j.physletb.2010.12.013, 10.1016/j.physletb.2013.01.018 [arXiv:1011.0260 [hep-ph]].
- [125] T. Kitahara, JHEP **1211**, 021 (2012) doi:10.1007/JHEP11(2012)021 [arXiv:1208.4792 [hep-ph]].
- [126] T. Kitahara and T. Yoshinaga, JHEP **1305**, 035 (2013) doi:10.1007/JHEP05(2013)035 [arXiv:1303.0461 [hep-ph]].
- [127] M. Carena, S. Gori, I. Low, N. R. Shah and C. E. M. Wagner, JHEP **1302**, 114 (2013) doi:10.1007/JHEP02(2013)114 [arXiv:1211.6136 [hep-ph]].